

UNIVERSITY OF LEEDS

Identifying muscle activity patterns in static and dynamic activities of daily living

Rafael de Castro Aguiar

Submitted in accordance with the requirements for the degree of

Doctor of Philosophy

The University of Leeds

Faculty of Biological Sciences

School of Biomedical Sciences

February 2023

Intellectual Property

The candidate confirms that the work submitted is his own, except where work which has formed part of jointly authored publications has been included. The contribution of the candidate and the other authors to this work has been explicitly indicated below. The candidate confirms that appropriate credit has been given within the thesis where reference has been made to the work of others. The following list presents the articles generated by the author and collaborators, contained in this alternative style thesis:

- Rafael Castro Aguiar, Elijah Chisala, and Samit Chakrabarty ."Multiple muscle activation patterns in a static motor task". (Working Title; Final drafting stages). Presented in Chapter 3.
- Rafael Castro Aguiar, Edward Jero, and Samit Chakrabarty. "Simplified markerless stride detection pipeline (sMaSDP) for surface EMG segmentation." arXiv.2302.04243 (Under Peer Review; MDPI Sensors). Presented in Chapter 4
- Figueredo, Luis FC, Rafael De Castro Aguiar, Lipeng Chen, Thomas C. Richards, Samit Chakrabarty, and Mehmet Dogar. "Planning to minimize the human muscular effort during forceful human-robot collaboration." ACM Transactions on Human-Robot Interaction (THRI) 11, no. 1 (2021): 1-27. (Joint first author; Published). Presented in Chapter 5
- Figueredo, Luis FC, Rafael Castro Aguiar, Lipeng Chen, Samit Chakrabarty, Mehmet R. Dogar, and Anthony G. Cohn. "Human comfortability: Integrating ergonomics and muscular-informed metrics for manipulability analysis during human-robot collaboration." IEEE Robotics and Automation Letters 6, no. 2 (2020): 351-358. (Published)

Jointly authored publications stem from a 2 year collaboration project with Dr. Mehmet Dogar and Dr. Luis Figueredo (School of Computing). This project explored human-robot collabora-

tive tasks, employing kinematic/kinetic estimation tools and physiological recordings to maximise human efficacy during laborious motor tasks. The team of Dr. Dogar was in charge of supplying the robot and kinematic recording equipment, as well as the initially designed efficacy optimisation algorithms for two human motor task (i.e. drilling and cutting tasks). My first work, under the supervision of Dr. Samit Chakrabarty (School of Biomedical Sciences), was the collection of human physiological data and collaborative design of the experiment protocol. I have then processed and explored the physiological recordings of the executed tasks, in a biological setting, and designed an assessment protocol to define task efficacy in terms of physiological variables. Dr. Figueredo explored the robotic kinematic/kinetic variables collected during the executed tasks and compared the estimated efficacy kinematics with the recorded subject kinematics. With the results provided by my physiological processing pipeline, we adapted the optimisation algorithm and validated the estimated efficacy kinematic protocols with the recorded human data. Article work is then separated into the robotic/kinematic optimisation algorithm (Dr. Luis Figueredo) and the physiological recording, processing and validation (myself), in equal parts. The remainder of the authors aided in supervision and secondary task completions.

This copy has been supplied on the understanding that it is copyright material and that no quotation from the thesis may be published without proper acknowledgement.

© 2023 The University of Leeds, Rafael de Castro Aguiar



Signed

Acknowledgements

Being born on an island, I grew up knowing that a ship can only travel a great distance if a safe harbour is maintained at home, guarding the ship against any rough storms that may arise. To reach this moment I have stood on the warm, caring, broad shoulders of my amazing parents, Daniel and Susete, my amazing brothers, Paulo and Ricardo, and my loving significant other, Carolina. No words can describe the help you have provided me, the courage you have given me to face any challenge and the appreciation I have for you.

To Thomas Richards, Luis Figueredo, Mehmet Dogar and Christopher Russell, thank you for your incredible help, mentorship, exciting collaborations and training throughout my program.

To Josh Bolam and the other "Lunch Lads" students of Garstang 5.55, thank you for the laughs, the late nights, the shared desperation and survival, and the incredible times we had together.

To James Whitehouse, thank you for Leeds, for home and for a PhD brother I will cherish for life.

To the many undergraduate and Masters students I had the pleasure of mentoring and supervising, of special note Abisola, Carlie, Bowen and Kabir, thank you for teaching me how to teach. Our time, experiments, learning and fun together created some of best memories of my PhD.

To Ioannis (Yannis) Delis, thank you for your supervision, for the great mentorship and advice at the start of the program.

Last but not least, to you Samit Chakrabarty, thank you for everything. For the challenges, for the sleepless nights, for your amazing guidance, for our agreements and disagreements, for your impeccable supervision and for your friendship.

Abstract

Human motor control is primarily studied inside labs or clinics, through analysis of predefined, constrained motor tasks. In these studies subjects conduct experimental tasks with biomechanical constraints, in ways potentially unrealistic for the individual. We propose that to better understand the mechanisms of motor control, subjects and tasks need to be analysed in daily life unconstrained scenarios, and produce tools to highlight the inter-subject variability and tailor the analysis to the uniqueness of the individual. Shared motor control strategies across populations require investigation but importance should be equally given to the individuality and personal muscle recruitment strategies. Muscle activity patterns (MAPs) were identified in three motor experiments based on daily living (ADLs) tasks, assessing static and dynamic scenarios. Using non-invasive methods, algorithms were designed to identify MAPs from electromyography (EMG) recordings in each ADLs, establishing relationships with recorded biomechanics and generated forces. Active structures of the central nervous systems (CNS) for motor coordination, were predicted through spectral analysis of the EMG signals. These findings highlight inter-subject variability and need for individualised assessment of motor control strategies, along with shared features in the MAPs (Article 3). Active neural pathways were teased for healthy individuals, exhibiting an oscillatory behaviour throughout the tasks (Articles 3 and 4). To address the need for ADLs recordings, a novel method is presented for sEMG segmentation, in unconstrained gait scenarios, in Article 4. Lastly, results of a human-robot-interaction study link MAPs with biomechanics to provide a biomarker for personalised optimal muscle recruitment, minimising effort (Article 5). The overall study comprises a series of novel tools, able to characterise motor tasks in terms of MAPs, biomechanics and generated forces, with higher versatility for studies outside of the lab or clinic. These findings may greatly improve current motor control diagnosis by providing quantitative measurements and biomakers for individually-tailored neurorehabilitation.

General Abbreviations

ADLs	Activities of Daily Living
AgCl	Silver-chloride
BG	Basal Ganglia
Cb	Cerebellum
CNS	Central nervous system
CST	Corticospinal tract
DoF	Degrees-of-freedom
EEG	Electroencephalography
EMG	Electromyography
Hz	Hertz
IMU	Inertial Measurement Unit
KIN	Kinematics
KMEA	Kinematic Minimum-Effort Assumption
MAPs	Muscle activity patterns
MC	Motor Cortex
MDF	Median frequency

MNs	Motoneurone pools
MNF	Mean frequency
ms	Milliseconds
MU	Motor unit
MUAP	Motor unit action potential
MVC	Maximum-voluntary-contraction
MVF	Maximum-voluntary-force
NNMF	Non-negative Matrix Factorisation
PCA	Principal Component Analysis
PD	Parkinson's Disease
RMS	Root-mean-square
RST	Reticulospinal tract
sEMG	Surface EMG
sMaSDP	Simplified markerless stride detection pipeline
SPN	Spinal
TMS	Transcranial magnetic stimulation
V	Volts

Contents

1 General Introduction **1**

1.1 Motor Control in daily living 1

1.2 Hierarchy in the human motor control architecture 3

1.3 Modularity in motor control 5

1.3.1 Muscle Activity Patterns in the literature 6

1.3.2 MAPs: tools and processes 8

1.4 Project Aims 11

1.5 Document Structure 13

2 General Methods **16**

2.1 sEMG as a diagnostic tool 16

2.1.1 Principles of surface Electromyography 16

2.1.2 Recording and processing pipeline for sEMG data 18

2.2 Biomechanics of motor tasks 21

2.2.1 Motor task characterisation through kinematics and forces 21

2.2.2 Kinematics and force analysis pipeline 23

3 Healthy MAPs for static upper-limb ADLs **28**

3.1 Short Introduction 28

3.2 Article 29

3.2.1 Metadata 29

3.2.2 Abstract 30

3.2.3 Introduction 31

3.2.4 Methods 32

3.2.5 Results . . . 37
3.2.6 Discussion . . . 42
3.2.7 Conclusion . . . 46
3.2.8 References . . . 47
3.3 Short Summary . . . 48

4 Markerless sEMG segmentation in ADL locomotion 50
4.1 Short Introduction . . . 50
4.2 Article . . . 51
4.2.1 Metadata . . . 51
4.2.2 Abstract . . . 51
4.2.3 Introduction . . . 52
4.2.4 Methodology . . . 57
4.2.5 Results . . . 64
4.2.6 Discussion and Conclusions . . . 67
4.2.7 Abbreviations . . . 69
4.2.8 References . . . 70
4.3 Short Summary . . . 75

5 MAPs and biomechanics in dynamic ADLs 76
5.1 Short Introduction . . . 76
5.2 Article . . . 77
5.2.1 Metadata . . . 77
5.2.2 Abstract . . . 78
5.2.3 Introduction . . . 79
5.2.4 Problem Formulation . . . 84
5.2.5 Predicting the Muscle Effort: Task- to Muscle-Space Mapping . . . 87
5.2.6 Predicting the Human Kinematic Configuration: The Kinematic Minimum-Effort Assumption . . . 92
5.2.7 Ensuring Grasp and Robot Stability . . . 94
5.2.8 Planning – Quantitative Analysis . . . 95
5.2.9 Human-Robot Experiments . . . 99
5.2.10 Comfort Performance from EMGs Biofeedback . . . 102

5.2.11 Participants' perception of comfort . . . 106
5.2.12 Quantitative Analysis of KMEA . . . 108
5.2.13 Individual Muscle Selection and Assessment . . . 109
5.2.14 Conclusion and Future-Work . . . 111
5.2.15 Acknowledgements . . . 112
5.2.16 References . . . 113
5.3 Appendix . . . 120
5.3.1 Potential Application Towards Rehabilitation Assistive Technologies . . . 120
5.4 Short Summary . . . 120

6 General Discussions 122
6.1 Identifying MAPs in ADLs . . . 122
6.1.1 Significant inter-subject variability . . . 123
6.1.2 sEMG spectral features for neural pathway discrimination . . . 126
6.2 MAPs and Biomechanics in Motor Control . . . 127
6.2.1 Kinematics or Force for motor event detection . . . 127
6.2.2 Linking MAPs, Force and Kinematics: creating a biomarker . . . 129
6.3 Summary of study outcomes . . . 130

7 General Conclusions 132
7.1 Concluding Remarks and Applications . . . 132
7.2 Future Work . . . 134
7.3 Reflective Summary . . . 135

References 138

List of Figures

1.1 Duality between human and robot motor control schemes 2
1.2 Simplified structures and pathways diagram 5
1.3 Relationships between motor task variables 12

2.1 sEMG recording system diagram 17
2.2 Processing pipeline for sEMG signals 18
2.3 Processing pipeline for kinematics 24
2.4 Simplified forces, torques and kinematics diagram for an upper-limb static task . 27

3.1 Summary diagram for "Multiple muscle activation patterns in a static motor task" article 28
3.2 Experiment methodology 34
3.3 Force profiles for each subject 38
3.4 Individual MAPs per subject 38
3.5 Correlation matrices for each muscle pair, per subject 39
3.6 MAPs and Force profile in entire trial set 40
3.7 Force, MAPs and computed pathway information 41
3.8 Mean coefficient of variation of active pathways 42

4.1 Summary diagram for "Simplified markerless stride detection pipeline (sMaSDP) for surface EMG segmentation" article 50
4.2 Simplified stages of a typical gait cycle 53
4.3 Schematic of the sEMG and IMU sensor placement locations 58
4.4 Summary of method architecture 59
4.5 Summary diagram illustrating the different stages of the method 62

4.6 Segmented sEMG from a single extracted gait cycle 65
4.7 Observations with mean and standard deviation of muscle activity extracted . . . 66
4.8 HS detection on unconstrained Parkinson gait 67

5.1 Summary diagram for "Planning to Minimize the Human Muscular Effort during Forceful Human-Robot Collaboration" article 77
5.2 Example forceful human-robot collaborative tasks and configurations 79
5.3 Overview of the comfort-based forceful human-robot collaborative planning . . . 85
5.4 Human-joints kinematics used in Subsection 5.2.5.3 88
5.5 Muscle effort variation within human's kinematic redundancy 93
5.6 Experiments showing forceful human-robot collaborative puncturing and cutting and robot configurations 99
5.7 Measured summed muscle activity and respective task-space force values 102
5.8 Predicted muscle forces from musculoskeletal model and corresponding task-space forces 106
5.9 Average response from participants according to questions in Subsection 5.2.11 . 107
5.10 Norm of the kinematics error between predicted KMEA and measured joints . . 108
5.11 Puncturing task dataset for the comfort-planner 111

List of Tables

1.1 Factorisation algorithms 9

2.1 Influencing factors of sEMG 17

3.1 Muscles recorded through sEMG and respective functions 33

4.1 Summary of advantages and disadvantages of presented gait event detection solutions, in terms of applicability, interface, robustness and cost. 57

5.1 Average muscular activity effort 96

5.2 Muscular activity effort for min-max optimization 98

5.3 Summed Muscle Activity of each subject presented as the Mean ± Standard Deviation for both Puncturing and Cutting tasks 103

5.4 Selection of muscles and their respective functions associated with the upper-limb 109

5.5 Ratio between the predicted least summed muscular force 110

Chapter 1

General Introduction

1.1 Motor Control in daily living

Human movement encompasses a rich repertoire of dexterous, coordinated and adaptive motor tasks. By combining organised motor actions we are able to walk through different environments, reach and grasp objects and even hold loads of varied weights. We are able to generate volitional movement through the interaction of our biomechanical system with our physiological control system. The biomechanical system encompasses the several joints and the muscles that interact with them, while the physiological control system is responsible for issuing different activation levels to each muscle via neural signals.

To understand and even replicate human movement, several disciplines have created models to explain the different systems involved in the generation of motor tasks: biology and neuroscience look at the physiology, the central nervous system and the neural signal that elicits muscle contractions; biomechanics studies the kinematics and kinetics of human anatomy and the varied physical properties involved; control engineering and robotics explore the motor control mechanisms that link the anatomy with the physiology, and in some cases, attempt to replicate these in anthropomorphic robots.

In Figure 1.1 we present a diagram linking the biology and robotic mechanics with the respective motor control systems that coordinate and issue activation commands to the muscles or actuators. Due to the high complexity of human motor control, we face an over-actuated biomechanical system, that presents more actuators or muscles than joints to control. This generates

redundancy, which endows our system with a multitude of joint and muscle activity pattern solutions to solve a certain motor task. At this time, robotics still hasn't reached the level of dexterity or control of the human system. The complexity of the biomechanical joints, the redundancy issue and the coordinated recruitment of the different actuators are all challenges that need to be addressed. This is especially relevant when considering the field of neuroprosthetics, where robotic limbs are still poorly controlled by the human physiological signals, due this discrepancy and poor understanding of the control mechanisms in the human counterpart.

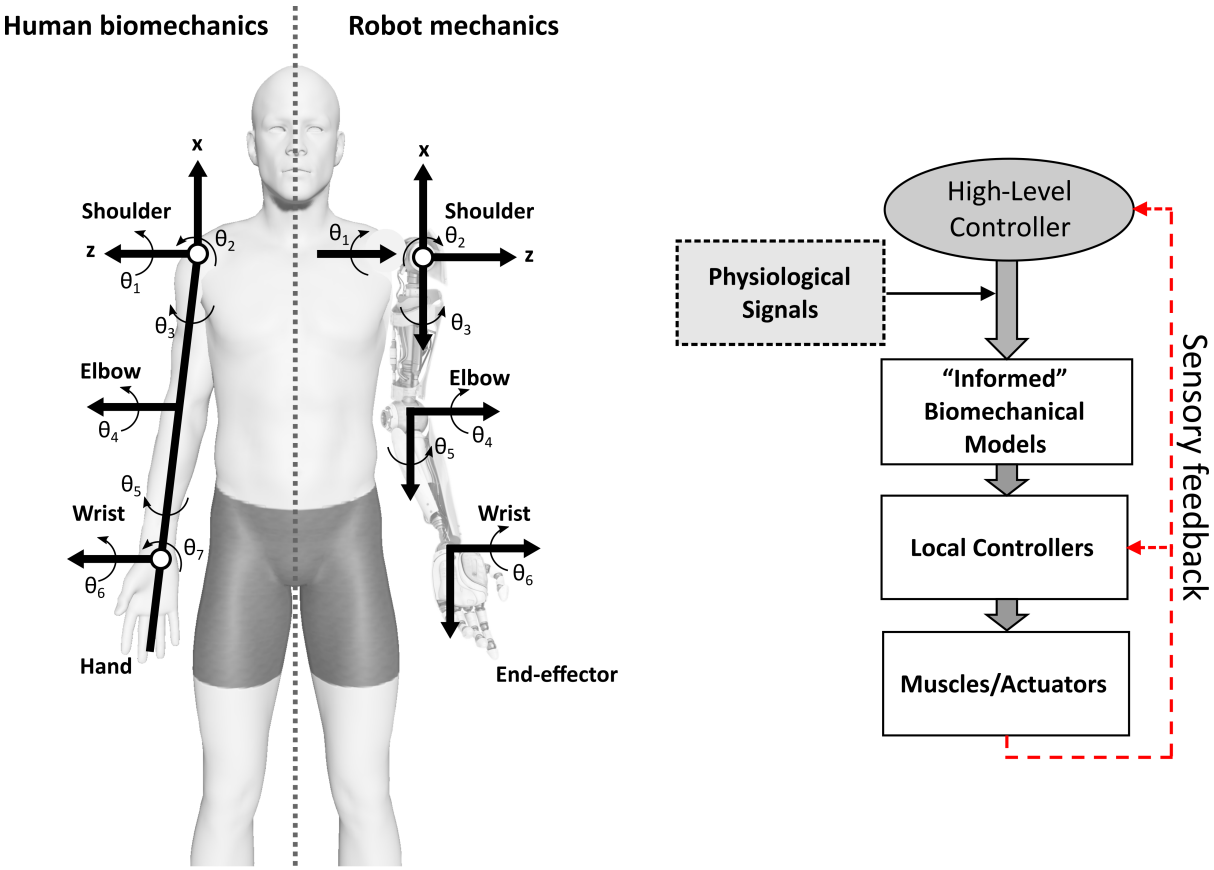


Figure 1.1: **Duality between human and robot motor control schemes**, considering an anthropomorphic upper limb (based on Ficuciello et al. 2014). On the left we present the several mechanical degrees-of-freedom (θ), for a human arm (disregarding the hand) and the equivalent in an anthropomorphic robotic arm. On the right, we present a possible control architecture, with comparable structures between the biological and the robotic system.

To investigate human motor control, we need to take into account the findings of these different disciplines. The dexterity witnessed when we perform motor tasks suggests a system that is both quick to respond to stimuli and adaptable in different environments and motion constraints. To generate such a complex multitude of motor actions, with real time error corrections and adaptability, the CNS is organised in a distributed hierarchical control architecture.

1.2 Hierarchy in the human motor control architecture

The human motor control system spans hundreds of muscles, controlled via a dense network of neural structures, pathways and neural circuitry. The witnessed complexity, dexterity and adaptability of human movement suggests a hierarchical distribution, with different CNS structures responsible for the initiation, coordination and execution of motor tasks. Based on the current literature we present an overview of the human motor control hierarchy and respective components in the summary diagram of Figure 1.2.

Human movement is made possible through the interaction of key supraspinal structures, as the Motor Cortex (MC), Basal Ganglia (BG) and Cerebellum (Cb) (Scott 2004; Merel et al. 2019; Houk and Wise 1995), with spinal interneuron and motoneuron populations, via descending pathways involved in volitional motor control (Corticopsinal and Reticulospinal tracts) (Lemon 2008). Each of these supraspinal structures has specific roles in the initiation, motor coordination, drive regulation and sensory interpretation (Houk 1989; Merel et al. 2019) of neural motor commands during the execution of a motor task. The output of this motor control architecture is the coordinated activation of skeletal muscles, executing a series of muscle contractions that will accomplish the desired motor task. To ensure adaptation and correct completion of a motor task, the human motor control architecture requires a closed loop, with sensory information arising from muscles (Ia and Ib afferents), and other local afferents, to constantly inform each hierarchy structure of the current state of the biological system and of the task completion (Dehghani and Bahrami 2020; Eberle et al. 2021; Shadmehr and Krakauer 2008).

Several studies have explored in detail the different suprapsinal structures (MC, BG and Cb) and analysed their respective roles and functions, creating solid models for the higher levels of motor control, primarily in different mammals (e.g. cats (Armstrong 1988) and primates (Oya et al. 2020)). In humans, investigation of supraspinal structures is only possible in isolated cases, through research of neurological disorders, indirect stimulation (e.g. Transcranial Magnetic Stimulation - TMS), or via approximations to the animal models, due to the typical invasive nature of this type of research. Similarly, investigation of the neural descending pathways is mainly possible through the research of pathological scenarios (e.g. stroke, spinal cord injury), to better understand the impacts on the neural signal if alterations in CST or RST occur. The next best approach is, as mentioned, approximation of studied animal models, linking these to pathological human cases, and creating estimation models of different complexities for the

different levels of the human motor control architecture (e.g. De Kamps et al. 2008; Osborne et al. 2021; York et al. 2022).

To validate and explore the previous models we require direct information of the neural signal passing through the control architecture. In an ideal scenario, we would have an architecture receiving a known input, information on the structures and their roles over this input signal and the respective transformation into an observable output or, in this case, a motor action. For the case of human studies, it is only possible to record the final outputs of this neural motor command: the muscle activity levels, recorded through Electromyography (EMG), the joint movements associated to the completed motor task and the produced limb forces. All these outputs are encoded in the neural signal and can be used to estimate the active mechanisms of motor control, gathering information on the activity of the spinal and supraspinal structures, through non-invasive manners.

As the recordable final outcome of the neural signal, an EMG signal contains a multitude of features of the neural command that can be used to identify active structures and mechanisms. Used currently as a basic diagnostic tool, the true potential of EMG is not yet fully explored in the clinical setting. Through the analysis of time-domain features, EMG can provide direct muscle contraction amplitudes and timings, as well as defined relationships between active muscles through correlation. Even further, studies like Oya et al. 2020; Frère 2017 and Richards 2018 have started to explore the spectral features of the EMG signal. Through coherence and power spectrum analysis studies demonstrate that different CNS pathways operate on the neural signal at different frequency bands. By isolating said bands in the EMG signal, through filtering and processing, we may be able to estimate which structures are active in different time windows, and investigate their impact and role on the motor task.

In Figure 1.2 a simplified architecture of the active neural circuitry in an upper-limb motor task summarises the previously presented concepts. Three core levels are explored, corresponding to the Initiation, Coordination and Execution of a motor task, and what information can be extracted to infer on the activity of each level.

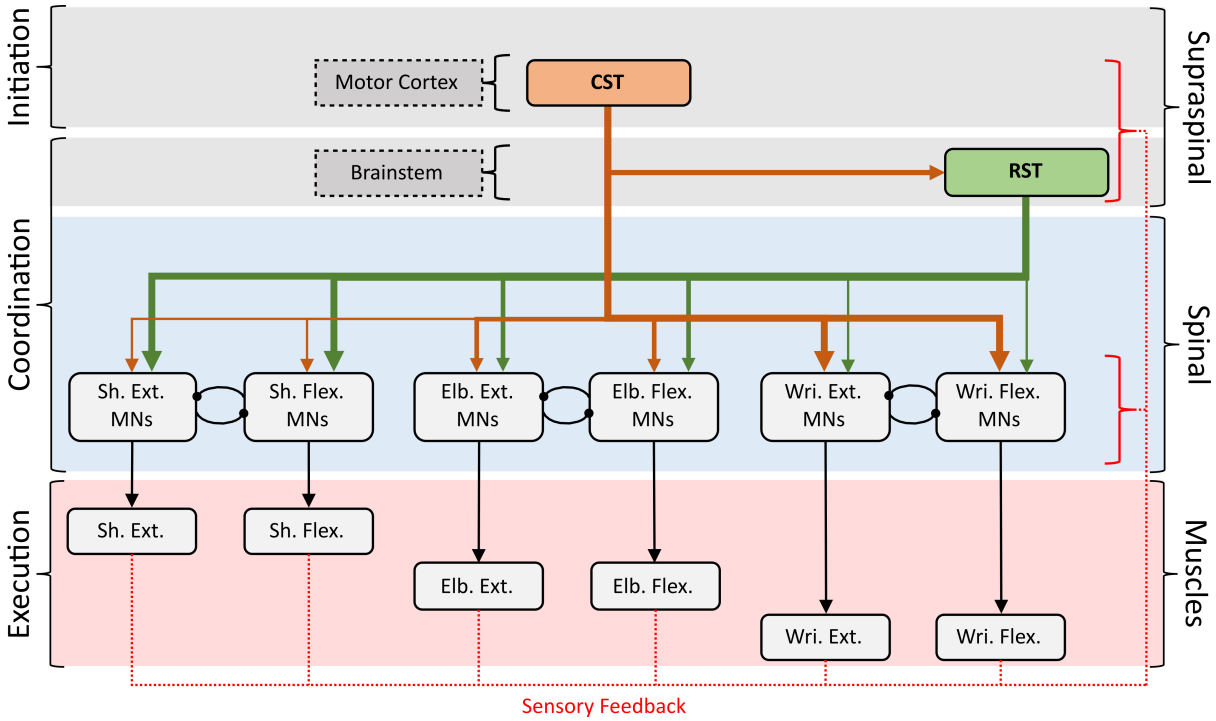


Figure 1.2: **Simplified structures and pathways diagram** for an upper limb motor task, based on Carpenter and Reddi 2012; Pierrot-Deseilligny and Burke 2005, and applicable to the study of Chapter 3. In this diagram, human motor control is comparable to a typical control architecture with: a high-level controller responsible for **Initiation**, decision and task supervision; mid/low level controllers for task variable **Coordination** and organisation, dependent on the Supraspinal structures processing of the sensory feedback throughout the task; and an actuator level, where the muscles **Execute** the contractions encoded in the neural signals. Each of these levels may be associated with different regions of the CNS. The core two pathways studied, linked to volitional motor control, are the Corticospinal Tract (CST), arising from the Motor Cortex, and the Reticulospinal Tract (RST), arising from the Reticular Formation in the Brainstem. In this diagram, connections between structures are represented as lines, and higher thickness indicates stronger connections. Both CST and RST interact with the spinal interneuron circuits, and transmit the encoded neural signals to the motoneuron pools (MNs) of the different muscle groups presented: Shoulder (Sh.), Elbow (Elb.) and Wrist (Wri.) extensors (Ext.) and flexors (Flex.). Sensory feedback from the muscles constantly informs each of the Supraspinal and Spinal levels and respective structures, closing the motor control loop.

1.3 Modularity in motor control

Our musculoskeletal system spans over 600 muscles, interacting with over 300 joints. To effectively complete a motor task, several muscles are issued neural commands and require simultaneous coordination and supervision, with constant sensory feedback. It is an extremely high energy and time taxing problem to individually control each muscle, coordinate these into different contraction levels and interactions (agonist and antagonist), and to constantly supervise and inform the different levels of the motor control system. Although beneficial in terms of dexterity and adaptation, redundancy becomes an issue here, as infinite solutions, with countless

different muscle and joint combinations, may solve a motor task at hand, without considering temporal and processing costs.

Alternatively, instead of a linear segmented control, studies theorised a modular control architecture, with distributed control over the previously motor structures and levels (Sherrington 1910). This further suggests that instead of individualised motor commands, muscles may commonly be recruited as groups or modules (Bernstein 1966), reducing the number of inputs the CNS needs to account for. A "module" then encodes the simultaneous activation parameters for a group of muscles, and can be recruited even when completing different tasks. When necessary, and only if a more dexterous task demands it, would the CNS then specify individualised fine-tuned motor commands for that specific muscle or small group of muscles. Succeeding this modular control theory new queries arose about the origin of the modularity, what information is encompassed within, and what mechanisms can be used to identify the modules.

1.3.1 Muscle Activity Patterns in the literature

Varied hypotheses explore the modularity of the CNS and respective mechanisms of muscle recruitment, querying the origin and coordination of muscle activity patterns, and how they are employed, leading researchers to different concepts, e.g., muscle synergies (d'Avella et al. 2003), force fields (Bizzi, d'Avella, et al. 2002), M modes (Latash et al. 2007), pre-motor drives (Kargo and Giszter 2008), among others. These varied concepts, sometimes exclusive in nature, generated a lack of consensus over the principles governing MAPs across disciplines.

The origin of modularity in MAPs is the first point to address. Research suggests that muscle groups acting on the same joint share an activity dependence, revealing patterns of activity, already previously studied as agonist, antagonist, and synergistic relations. Arising from this finding, some studies debate whether the origin of the MAPs is neural in nature or simply a by-product of the biomechanical properties of the musculoskeletal system (Kutch and Valero-Cuevas 2012; Tresch and Jarc 2009). Instead of shared neural commands, this line of research suggests that the natural biomechanical constraints of a joint would condition a pattern of activity for the muscles acting on the joint. Nevertheless, this biomechanical by-product justification for the MAPs alone is found lacking when explaining the witnessed variability in different subjects or repetitions of a motor task. A more extensive body of evidence from (Bizzi and V. C. K. Cheung 2013; Santello et al. 2013; Frère 2017; Takei et al. 2017) describes alternatively

a neurological origin to MAPs, supported by research on neurological disorders, e.g., post-stroke patients (Clark et al. 2010; Gizzi et al. 2011; Roh et al. 2013; V. C. K. Cheung et al. 2012; Hesam-Shariati et al. 2017). Although the biomechanical features of the musculoskeletal system remain unaffected, there is a noticeable deficiency in the movement of the stroke affected limb. Muscle activity analysis of these cases suggest issues in the neural commands transmitted to muscles, with potentially affected pathways or motor control structures. Results demonstrate scenarios of loss, fraction, merging of already existing MAPs, or even appearance of new MAPs altogether in the affected limb. In general, both these findings highlight the importance of the pathways involved and the roles of spinal and supra-spinal modulators in shaping and coordinating MAPs, but also considers a conditioning of the observed MAPs by the biomechanics of the musculoskeletal system.

To coordinate and employ MAPs, different CNS structures require task information to make an appropriate plan and pattern selection to complete a motor task. This suggests that MAPs may be task-dependant (Prochazka 1989) and have encoded task relevant information, as for example necessary end-point forces to stabilise limbs (Ting and Macpherson 2005; Torres-Oviedo 2006; Yakovenko, Sobinov, et al. 2018; Macpherson 1988), and kinematic (i.e., joint position, angle, and velocity) and kinetic (i.e., joint forces and torques) configurations (A. Georgopoulos et al. 1985; Ting and Macpherson 2005). In supraspinal levels, further evidence presents directional tuning information in some neuronal populations (Kalaska and Crammond 1992; A. P. Georgopoulos et al. 1986; Scott and Kalaska 1997), which is a possible selection element for different MAPs recruitment as well. This highlights the importance of establishing the relationship between the recorded muscle activity levels, the biomechanical properties of the individual (i.e., kinematics and generated forces) and the motor task being conducted, to appropriately identify relevant MAPs.

To investigate the responsible structures for coordinating MAPs, studies have looked at the frequency domain of the recordable EMG signals. As mentioned in the modularity introduction, neural pathways are hypothesised to operate at different frequency bands. Through the analysis of the spectral fingerprints of the recorded EMG signals, and calculation of inter-muscular coherence values among muscles conducting a motor task (Boonstra and Breakspear 2012; Kerkman et al. 2018; Jensen et al. 2019), we can tease out muscle groups with shared neural drive. Exploring how the neural drive changes across a motor task, and its impact on the extracted

MAPs provides insights into the coordination mechanisms of the motor control architecture, and the estimation of different roles of active CNS structures.

1.3.2 MAPs: tools and processes

As different disciplines explored muscle activity patterns, several tools were adapted and devised to extract patterns from a multitude of different motor tasks. The challenge remains in the dimensionality and the control of a widespread group of muscles to complete a motor task. To identify the individual MAPs, researchers turned to several different dimensionality reduction algorithms, in order to identify the shared inputs over a series of muscle activity levels. The following Table 1.1 presents the most dominant tools used in studies to extract MAPs:

Most of these presented tools weren't originally designed for the identification of MAPs or synergies herein, being adapted from different mathematical disciplines. As referenced in Table 1.1, these tools take assumptions over the neural commands extracted from the EMG signals and apply the different algorithms from the extraction of the MAPs. The works of Tresch, V. C. Cheung, et al. 2006 and Zhao et al. 2022 present reviews and comparisons over some of these methods and the results when extracting MAPs of both simulated and experimental datasets. Different dimensionality reduction algorithms presented in Tresch, V. C. Cheung, et al. 2006 share similarities in extracted MAPs for both simulated and experimental data, but are employed with differing assumptions that may lead to potentially conflicting results. For example, the consideration that each MAP for a task is a non-negative activation pattern, and may be independent or co-dependent to the remainder MAPs is conflicting between most the examined algorithms.

Associated with this issue of dependency among MAPs is the concern that commonly these dimensionality reduction algorithms often overlook the integration of assumed inter-muscle relationships. Agonist and antagonist interactions, that may arise from either a physiological or biomechanical nature, will influence the extracted MAPs. By neglecting these essential relationships, the complexity of muscle coordination patterns may be oversimplified, and highly dependent on the assumptions from the dimensionality reduction algorithm being used. Moreover, accounting for temporal progression coefficients, which describe the evolution of MAPs over time, is vital for capturing dynamic muscle coordination during movement. Neglecting this temporal aspect could result in incomplete insights into the complex interplay of muscles during

Table 1.1: **Factorisation algorithms** and alternative tools for synergy identification

Factorisation Algorithms	**Description**	**Used by:**
Principal Component Analysis	Seeks the orthogonal vectors that account for the majority of the signal's variability; assumes the outcome variables are linearly uncorrelated	Gentner and Classen 2006; Kutch and Valero-Cuevas 2012; Saltiel et al. 2001; Krishnamoorthy et al. 2003
Independent Component Analysis	Maximises statistical independence of extracted components; as PCA, assumes extracted components are independent, and uncorrelated	Gentner and Classen 2006; Artoni et al. 2016
Factor Analysis	Seeks lowest number of modules that can account for the correlation of a set of muscles; similar to PCA, but does not assume a linear combination, instead seeking measurements of latent variables	Kieliba et al. 2018; Merkle et al. 1998; Sabatini 2002
Non-negative Matrix Factorisation	Assumes a non-negative nature for the neural commands and muscle activations; unlike PCA, does not assume that components are uncorrelated, allowing for possible interdependent modules	Hesam-Shariati et al. 2017; Hu et al. 2018; Frère 2017; D'Avella 2014; Delis, Hilt, et al. 2018; Chvatal and Ting 2013; Alessandro et al. 2013; Semprini et al. 2017; Bizzi and V. C. K. Cheung 2013; Devarajan K. 2018; Amundsen Huffmaster et al. 2018; Takei et al. 2017; Antuvan et al. 2016
Cluster Analysis	Simpler look at a synergy, as a period of coextensive muscle activity; analysing relation between onset and offset EMG activity, and using associative clustering to extract possible synergies	Drew et al. 2008; Desrochers et al. 2018; Takei et al. 2017
Wavelet Decomposition	By defining a reference wavelet function, identifies similar components by using scaling and time translations; the summation of said components will amount to the original recorded signal	Yakovenko, Gritsenko, et al. 2018
Auto-encoders	Neural network with a single low-dimensional hidden layer (**m**-dimension); the input and output (encoder and decoder respectively, both with **n**-dimension), ensure that the low dimensional values of the hidden layer allow for an equal input and output, with **m** lower than **n**	Spuler and Sanz 2016

motor tasks, as this is not discussed at length in Tresch, V. C. Cheung, et al. 2006. The common assumption of the muscle synergy format as $WxC + e$ (MAPs times a temporal coefficient plus

an error coefficient) may not universally apply to all movements and individuals. The work of Delis, Panzeri, et al. 2014 for example considers alternative synergy formats that can reveal potential variations in muscle coordination across tasks and individuals, leading to a more nuanced understanding of motor control. Advancing MAPs studies require consideration and addressing of these complexities and challenges. By being transparent about assumptions, exploring alternative approaches, integrating inter-muscle relationships, considering alternative synergy formats, accounting for temporal progression coefficients, and acknowledging uncertainty and task-dependency, researchers can gain deeper insights into muscle coordination during human movement and contribute to the development of a more comprehensive understanding of motor control.

Lastly, a core issue that arises from these tools is the loss of information over the personal recruitment strategies. When the dimensionality reduction algorithms are applied in a population dataset, the commonalities of the motor control shared across those individuals are presented. Studies rely on a threshold of "variance accounted for" of 90% to define a sufficient level of detail over the extracted MAPs, discussed in detail in both Tresch, V. C. Cheung, et al. 2006 and Zhao et al. 2022. This is further escalated when considering the synergy models presented, especially when looking at sources of signal noise. A core difference between the simulated and experimental results of Tresch, V. C. Cheung, et al. 2006 is the existence of potentially different noise sources that may impact the performance of the dimensionality reduction algorithms. The concern here is that, while this issue is easily accounted for in the simulated data, when recording from human subjects the distinction between noise and potential individual subject variability is tenuous. The issue lies in the loss of the personal motor control strategies for each individual, potentially in the often discarded or unexplained variance of the data. This is further escalated due to the nature of the experiments where, to ensure consistency between trials and subjects, individual's are heavily constrained in their movements to ensure repetitiveness and consistency in the studied motor tasks. Even when conducting the same motor task repeatedly, no individual will recruit the exact same group of muscles, in the exact same level of activation, more than once. Several factors, including biomechanical (e.g., York et al. 2022), fatigue (e.g., Wærsted 2000), physiological (e.g., C. De Luca 2006) and even dietary (e.g., Kalmar and Cafarelli 1999), may influence an individual's performance and MAPs in motor tasks of their daily lives.

Nevertheless, understanding the shared control mechanisms is of key importance to identify a generalised structure for the human motor control architecture and its modularity. We here intend to add onto these findings further by introducing a new set of tools that allows for the investigation of the natural, individual recruitment strategies a person takes to conduct a series of natural tasks.

1.4 Project Aims

As discussed in the previous sections, the human motor control system is a highly complex, hierarchical and modular structure, that is still not fully understood. The investigated modularity suggests that motor control outputs consist primarily of patterns of activation for muscles, instead of individualised muscle commands. With this in mind, in order to better understand the MAPs and respective recruitment mechanisms in humans, the core aim of this study is to analyse EMG and biomechanics, through the use of non-invasive methods, in naturalistic scenarios. The goal is to design a tool-set, based on the investigated experiments, that links the recorded physiological and task variables. This tool-set improves our ability to characterise motor tasks, especially in unconstrained ADLs, and aims to reveal personal elements that cannot be picked up upon through typical recordings made in controlled lab or clinical settings.

Most research in this area focuses in the identification of shared mechanisms of neural motor control among individuals. The advantage we provide is the possibility to explore what makes motor control schemes unique, focusing instead on the individual and respective variability in MAPs, as an addition to just investigating the mean. This approach is critical to our understanding of the complex mechanisms that govern, coordinate and, most important, adapt motor control in different individuals, and in a variety of motor tasks.

In its simplest form, we assume that a motor task can be characterised using the following 3 variables: anatomy (biomechanics), physiology (through sEMG) and generated forces (joint torques and end-effector forces). We argue that a task can't sufficiently be described only as a combination of single or individual muscle activities, requiring instead the analysis of patterns of activity, witnessed over relevant muscles involved. Defining which muscles are relevant for the task and which ones to investigate should be initially based on the biomechanics/anatomy. Care should be taken in this selection as only two muscles are not sufficient to characterise a task isolated to a single joint, but selecting too many may lead to unexplained correlations over

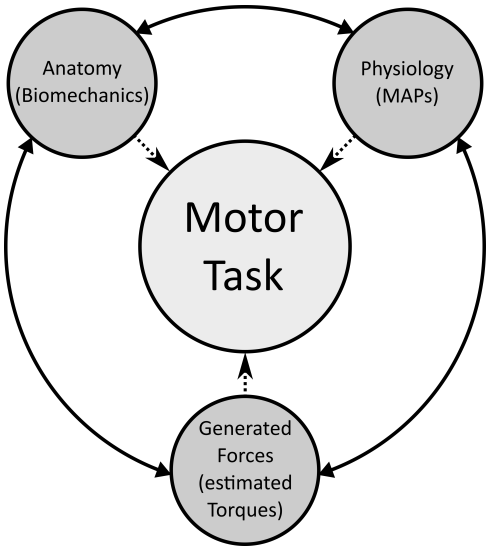


Figure 1.3: **Relationships between motor task variables**: to fully characterise a motor task, whether it is static or dynamic, the minimum information requirements are the activity patterns of the muscles involved (MAPs), the biomechanics of the limb and the produced forces. However, determining these variables is a complex process and establishing relationships between them can be even more challenging, due to the non-linearity of these connections. In human studies, especially in everyday activities (ADLs), any information gathered must be recorded using non-invasive methods. The first step then to determine the mechanisms of human control is the investigation of each of the different relationships among MAPs, biomechanics and forces, in isolated scenarios.

a large number of variables.

The motor task being conducted, be it static or dynamic, demonstrates adaptation or changes in the motor control mechanisms employed. The nature of the motor task being studied will then impact the selection of which of the 3 variables are relevant to record. At a first instance, we isolate two of the three variables being explored: maintaining a known constant force, within a range and known biomechanics configuration, allows for the extraction of MAPs, per subject, and highlights its variability for a static scenario. Following experiments subsequently isolate different variables to analyse each relationship and interactions. Figure 1.3 presents a reference diagram which will be used in each of the studies, highlighting the aimed relationships to be explored.

To summarise, we present in this study an alternative and complimentary muscle control investigation tool, that challenges the limitations of current methods. Unlike conventional approaches that rely on biased dimensionality reduction algorithms, our study emphasises the value of individual nuances in motor control. Through the different articles, we demonstrate the nuanced MAPs unique to each subject, and establish the need for person-tailored rehabilitation designs.

This study aligns seamlessly with the World Health Organization's (WHO) initiative for Rehabilitation 2030 (Organization 2020,Briggs and Dreinhöfer 2017), particularly in its pursuit of person-centered rehabilitation. By focusing on the individual nuances and muscle activity patterns of each subject, our study highlights the essence of person-centred care, a central tenet of the WHO's vision. The emphasis on person-tailored designs in rehabilitation reflects a strong commitment to understanding and addressing the specific needs and abilities of patients, a core principle of the Rehabilitation 2030 initiative.

Knowing the nuances of the individual's motor control structure and their physiological and biomechanical characteristics will improve the characterisation of motor tasks. By incorporating this individual variability into existing solutions, our study aims to usher in improved diagnosis and rehabilitation protocols, leading to quicker recovery times and enhanced outcomes for patients. Most notably, this study integrates motor assessment and diagnosis into daily-life scenarios, accounting for activities of daily living specific to each individual. It encompasses a range of technologies, from muscle activity recording and analysis to wearable sensor protocols, making it possible to extend the study of motor control beyond clinical settings and into the comfortable confines of a patient's home. Our approach thus pursues a new ideology for rehabilitative research and practice, with a core aim for individually tailored and effective rehabilitation methods.

1.5 Document Structure

As an alternative style thesis, each core chapter of this document will refer to a separate published study. Each of these studies tackled different ADLs experiments and tools, with the link between them building up the answer for the primary question of MAPs in ADLs. Through their combined findings, further steps are taken into understanding the variability of MAPs in inter-individuals, how MAPs are recruited and coordinated by different structures of the CNS, and how can they be applied, together with the other investigated task variables (kinematics and force), to improve personalised motor control schemes.

In Chapter 1, "General Introduction", the background of the project is presented. A motor control specific view of the CNS is introduced, backed by studies focusing of different modules of this control architecture. A brief outline of the current studies reveals the missing gap, specifically on the absence of investigation of "natural" movements, unconstricted by clinical of

lab environments. The hypothesis and project aims are then detailed at the end of the chapter.

In Chapter 2, "General Methods", an overview of tools and processes for the investigation of motor tasks is presented. Core focus is given in sEMG tools and processes, as one of three core output measures from the neural signals in motor control. Associated with sEMG, tools are presented for the investigation of biomechanics (kinematics) and the analysis of produced forces (estimation of joint torques). To further analyse the methods used, different cases of ADLs are presented, discussing differences in static and dynamic motor tasks and which tools are required for either scenario. This aids the reader in understanding in more detail each of the studies discussed thereafter, in which some or all of the methods discussed are employed.

In Chapter 3, "Healthy MAPs for static upper-limb ADLs", the first of three studies is presented. This study investigates an upper-limb Maximum Voluntary Force task, as a static motor task. Fifteen subjects were recruited to perform this experiment, exploring this motor task in a naturalistic way to the individual, and individual MAPs are recorded and compared. The relationship of MAPs and generated forces is established, and the spectral analysis of the sEMG signals is performed to identify active neural structures during this task. Findings indicate a varied combination of MAPs in different subjects, paired with variable active neural structures. These findings aid in designing a new way to investigate MAPs and characterise static motor tasks, with higher focus on the individual instead of the typically used expected mean subject activity.

In Chapter 4, "Markerless sEMG segmentation in ADL locomotion", the second of three studies is presented. In this chapter, an sEMG segmentation method is designed, based on a unconstrained gait dataset. The work of Brantley et al. 2018 provides a rich dataset of unconstrained, naturalistic gait in different walking modalities, with sEMG, kinematics and Electroencephalography (EEG) synchronised recordings. Using this dataset, we have designed a simplified method for gait event detection through recorded kinematics, and sEMG segmentation based on the extracted gait cycles. This methods study is written as a guide for gait analysis beginners, going into simple detail on how to analyse, process and use a single IMU (inertial measurement unit) data to identify heel-strike gait events, and relate this information with synchronised sEMG data. This study also explores the relationship with sEMG and biomechanics, transitioning from the previous static scenario from the previous study of Chapter 3, to a fully dynamic environment with more complex and varied MAPs.

In Chapter 5, "MAPs and biomechanics in dynamic ADLs", the last of the three studies is presented. Using the findings of the other studies, a fully dynamic upper-limb motor task experiment was designed, in collaboration with Dr.Dogar's Human-Robot-Interactions team (further author information presented in the **Intellectual Property** disclaimer). The produced article is divided into two core sections: the design and implementation of the task optimisation algorithms for the robot positioning, as well as the preliminary human-effort-estimation (led by the Human-Robot-Interaction team of Dr. Dogar and Dr. Figueredo); and the experimental design and collection, analysis, and validation of physiological data (myself). Three different task conditions were tested, based on different optimisation algorithms derived from MAPs and kinematics of the subjects. The motor task recordings are then analysed, and each task is characterised is terms of biomechanics, force and MAPs. With the intention of creating an ergonomic optimisation algorithm, we provide the physiological validation marker and a new approach to characterise a dynamic upper-limb task.

In Chapter 6, "General Discussions", we tie in the findings of the different studies, and link these to the explored literature of Chapters 1 and 2. From a static to dynamic exploration of motor tasks, we discuss the varied techniques employed and how these compare or improve upon existing studies.

In Chapter 7, "General Conclusions", a series of remarks are summarised, highlighting the benefits of this research, its shortcomings and future directions and applications. In addition, a reflective summary of the project and PhD program is discussed.

Chapter 2

General Methods

2.1 sEMG as a diagnostic tool

2.1.1 Principles of surface Electromyography

Motor commands are initiated, organised and transmitted throughout the CNS via electrical impulses relayed among neurons. The final output of this motor neural circuitry is the motor unit (MU), which comprises a bundle of muscle fibres and the motoneuron that innervates and excites them. When muscle fibres contract, dependent on the neural signal encoded, a motor unit action potential (MUAP) is generated and can be detected through electrodes. Located in muscles are also sensory structures (muscle spindles and Golgi Apparatus) that convey the current state of the muscle fibres and tendons back to the CNS through ascending neural signals. The combination of the descending and ascending signals can be recorded from a selected muscle, in a non-invasive manner, through surface Electromyography (sEMG). The principle of sEMG lies in the detection of the summed action potentials of muscle fibres, during a contraction, via an electrode configuration placed on the subject's skin above the muscle. An example of a differential electrode configuration, used in Chapters 3, 4 and 5, can be seen in Figure 2.1.

At rest, the electrical activity observed in the muscle is defined as a baseline. During a muscle contraction, the summation of the MUAP of the muscle is perceived and recorded as a voltage shift in the sEMG. Higher contraction amplitudes lead to higher amplitude of the sEMG. The intensity of the contraction, the firing rate of the MU, the electrode positioning and other important factors (summary in Table 2.1) will all affect the amplitude and spectral features of

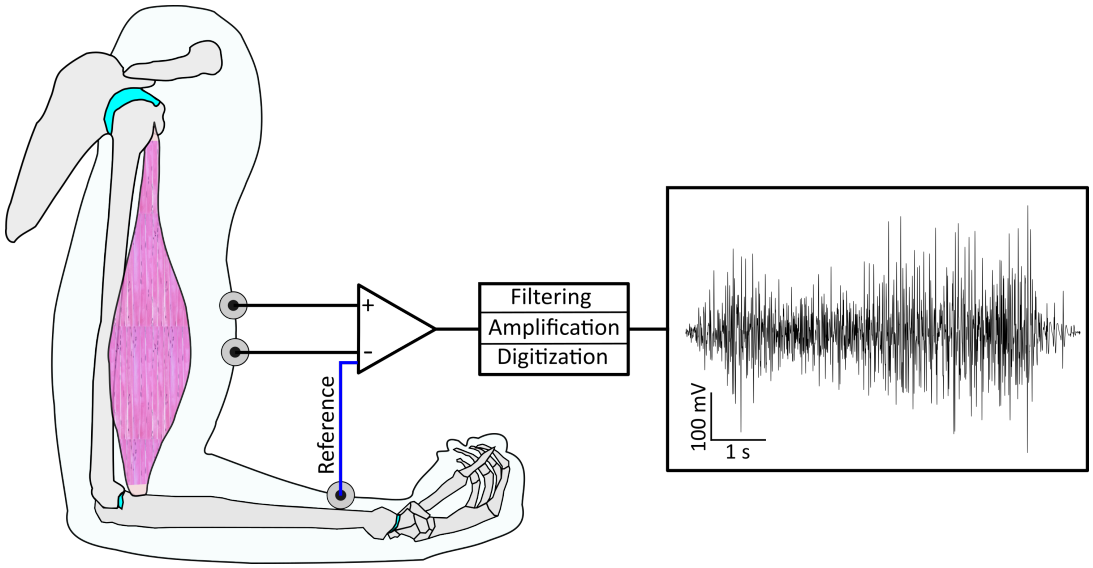


Figure 2.1: **sEMG recording system diagram**, with a bipolar electrode configuration. In this system, two separate electrodes are placed on the skin surface, over the selected muscle to measure from, in a standardised location (Hermens et al. 1999). A third reference electrode is placed in an electrically unrelated tissue, preferably an electrically neutral area as a bone surface. Using a differential amplifier and an acquisition system, the raw sEMG is then recorded, as seen at the far right display of the diagram.

the sEMG. Knowing how to identify, analyse, discriminate and isolate these factors provides us insights on features of the encoded neural signal. Through characterisation of temporal and spectral features of the sEMG signals, we can establish relationships between muscle activity patterns, generated movements and forces involved in a motor task, and infer on active neural circuitry.

Table 2.1: **Influencing factors of sEMG**, adapted from C. De Luca 2006

Factors influencing sEMG			
Causative		*Intermediate*	*Deterministic*
Intrinsic	Extrinsic		
Number of active MU	Electrode configuration	Differential electrode filters	Number of active MU
MU firing rate (synchronisation)	Motor point	Detection volume	MU force twitch
MU force twitch	Muscle edge	Superposition	Muscle fibre interaction
Fibre type	Fibre orientation	Conduction velocity	MU firing rate
Lactic acid	Tendon	Spatial filtering	Number of detected MU
Blood flow			MUAP amplitude, duration
Fibre diameter			Recruitment stability
Electrode fibre location			
Subcutaneous tissues			
Others...			

Due to the multiple factors presented in Table 2.1, sEMG signals are quite variable and subject dependent. The recording environment, equipment used and nature of the studied motor tasks will all heavily influence the sEMG recordings as well. To ensure the validity and replicability of sEMG recordings, sets of standards and practices for the equipment, data collection procedure and processing were created and are often under review (e.g. Tankisi et al. 2020,Stålberg et al. 2019,Merletti and Muceli 2019,Reaz et al. 2006). As sEMG is employed across varied disciplines, as clinical diagnostics and rehabilitation, neuroscience, sports sciences and engineering, the transferability of these standards is a must.

2.1.2 Recording and processing pipeline for sEMG data

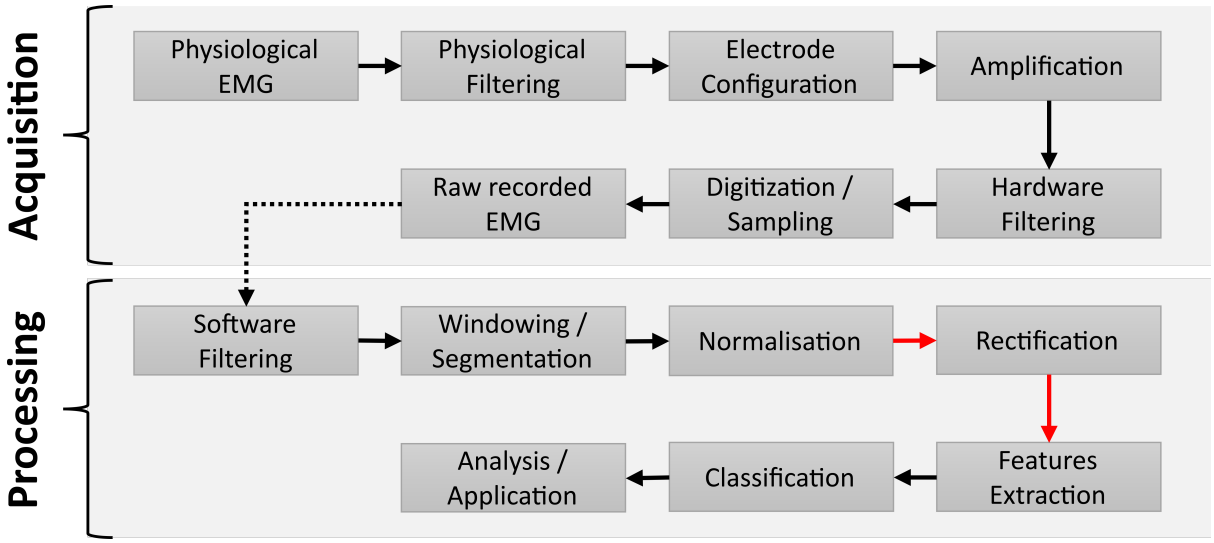


Figure 2.2: **Processing pipeline for sEMG signals**, separated into Acquisition and Processing stages. The "Physiological EMG" step, adapted from C. De Luca 2006, refers to the initial MUAP directly from the muscle fibres. Tissues surrounding the muscle fibres and skin has filtering effects over the MUAPs. The remainder of the steps refer to the acquisition, recording and processing of the EMG signal as seen at skin surface.

Knowing the principles of sEMG, we can now focus on its' acquisition and processing procedures. Figure 2.2 shows a diagram with all the steps of this pipeline, from muscle fibre until application of processed sEMG. This pipeline is used in each of the studies of Chapters 3, 4 and 5. The following list goes into detail over the individual steps presented in Figure 2.2:

- As mentioned in the Figure 2.2 caption, the **Physiological EMG** and **Physiological Filtering** sections are steps prior to the recording. Tissues surrounding the muscle fibres have a low-pass filtering effect on the electrical signal as it passes through. At the interface between skin and electrode surface, there is a high-pass filtering effect. These filters, due

to their nature, are subject and environment dependent, but this variability is taken into account by the recording equipment.

- Prior to placement, the skin location that would contact the electrodes was shaved, abraded with gel and disinfected, as per standard recommendation. This step increases signal-to-noise ratio in the recordings and removes possible sources of skin-electrode interface noise.

- The sEMG system used was a *Noraxon DTS EMG (Noraxon U.S.A. Inc.)* system, TeleMyo DTS Model 542 (Noraxon 2013). A bipolar **electrode configuration**, using AgCl (Silver Chloride) electrodes was selected, as seen on Figure 2.1. Each of our presented studies details how many sEMG channels were used, and which muscles were recorded.

- At skin surface, the sEMG signals are in the order of μV, so it requires amplification prior to recording. **Amplification** of the signal had an overall gain of 500, with measurement accuracy of $\pm 2\mu V_{RMS}$.

- The spectral band of sEMG signals has been studied between a broad band of 10 - 500 Hz. This system was configured with a first order high-pass **Hardware Filter** of 10 Hz, and a low-pass filter of 1500 Hz.

- To ensure that all the nuances of the sEMG signal are recorded, taking into consideration its' spectral band, a **sampling** frequency of 1500 Hz was selected (a sample at each 0.67 ms). The sEMG signal is then sampled and digitised with 16 bit resolution.

- At this stage we have an observable **raw recorded EMG**, and the end of the Acquisition stage. At this point, the signal is visually inspected for quality and consistency, with any data containing noise or signal drops to be flagged for removal. sEMG signals from the different recording sites are then prepared to export and processing.

- For the sEMG processing, algorithms handling each step of the Processing Stage were coded in *Matlab* (MATLAB 2020). The first step is **Software Filtering**. To ensure full removal of noise from the sEMG signals, a Butterworth (Butterworth et al. 1930) 4th order bandpass filter was designed (based on G. De Luca 2003), to isolate the signal within 10 - 150 Hz. A notch filter (see Hirano et al. 1974 for further information) was implemented at 50 Hz, to remove possible power-line contamination, also known as "mains hum", from the hardware power supply.

- **Segmentation** of the recorded sEMG signals was done in different methods across the presented studies. The core objective of each of these methods was to isolate the relevant sEMG activity during a controlled time window. As the example of Study 3, the synchronised force recordings were used to segment sEMG activity. In this case, time-points were force rose above a defined threshold were used to cut sEMG data into bins. Measures as signal energy contents and peak amplitude detection are other viable options that were considered.

- To ensure sEMG data can be comparable, among sEMG channels, trials and subjects, **Normalisation** is an important step. Typically, normalisation methods take the highest activity recorded from a selected muscle, during a maximum voluntary contraction, and use this value to establish the maximum of an activity ratio. As we will demonstrate, this approach may lead to biased results as activity values from subsequent maximum voluntary contractions may vary considerably, and may not be a good indicative for a ratio among distinct muscles. Instead, we present here an alternative normalisation method: the highest recorded sEMG amplitude, per subject, was used as a normalisation factor, establishing every other sEMG signal as a ratio of this factor:

$$NormEMG_{m,t} = \frac{EMG_{m,t}}{Max(EMG_{\forall m,\forall t}))} \tag{2.1}$$

  Where $\boldsymbol{m}$ is a single muscle, $\boldsymbol{t}$ is a single trial, $\forall m, \forall t$ is all muscles, in all trials.

- Here, the **Rectification** is presented as it is widely used in sEMG studies, with advantages when looking for single MU. This step has a non-linear effect on the spectral analysis of the sEMG data (Neto and Christou 2010,McClelland et al. 2012b,Negro et al. 2015,Boonstra and Breakspear 2012). Therefore in our analysis we do not include rectification, as it may alter our results in a non-comprehensible manner.

- Previously in Table 2.1, a large set of factors were discussed. All these factors embed the sEMG with a large quantity of information. In order to isolate meaningful information from such a complex signal, a series of relevant **features** need to be selected. The work of Phinyomark, Phukpattaranont, et al. 2012, Phinyomark, Quaine, et al. 2014 presents a comprehensive review over typical features used for sEMG analysis. In our studies, for time-domain features we extracted the root-mean-square (RMS) (in Britannica 2023b) of

the EMG signal (Equation 2.2), respective mean and standard deviation/error.

$$EMG_{RMS} = \sqrt{\frac{1}{N}\sum_{i=1}^{N} EMG_i^2} \tag{2.2}$$

Where $\boldsymbol{i}$ is the sample number and $\boldsymbol{N}$ is the maximum number of samples in the EMG segment. In regards to frequency domain, we computed the power spectrum of each signal, using a Hanning (Oppenheim, Schafer, and Buck 1999) window with a resolution of 1024 points, and extracted both mean (MNF) and median frequency (MDF) (in Phinyomark, Thongpanja, et al. 2012).

$$MNF = \sum_{j=1}^{M} f_j P_j / \sum_{j=1}^{M} P_j \tag{2.3}$$

$$\sum_{j=1}^{MDF} Pj = \sum_{j=MDF}^{M} P_j = \frac{1}{2}\sum_{j=1}^{M} P_j \tag{2.4}$$

Where f_j is frequency of the spectrum at frequency bin $\boldsymbol{j}$, P_j is the EMG power spectrum at frequency bin $\boldsymbol{j}$, and $\boldsymbol{M}$ is length of the frequency bin.

- The final steps of **classification** and **analysis** were dependent on each of the presented studies. For each case, we have used measures of RMS and spectral information to separate the experiment results and draw respective conclusions, detailed in the respective chapters.
- In each separate study, MAPs are, as discussed, obtained through processing and analysis of the normalised RMS of each muscle's sEMG recording. When dealing with spectral features and other frequency-domain operations, pre-normalised sEMG signals (filtered and segmented only) are used instead in these processing and analysis stages, as both normalisation and RMS operations impose undesired alterations in the frequency contents of sEMG.

2.2 Biomechanics of motor tasks

2.2.1 Motor task characterisation through kinematics and forces

Muscle activity levels alone are not sufficient to fully characterise a motor task. Study of the biomechanics is necessary to identify **joint kinematics**, **forces and torques**, and the **type of contractions** observed, linked to recorded sEMG. Though necessary for the characterisation of the task, each of these variables adds new layers of complexity to a study. We explore here joint

kinematics as the joint positions and angular displacements in a world reference frame, without delving into the more complex kinetics. Due to the non-invasive nature of the project, joint torques are estimates through a computational model in Chapter 5, and forces are recorded as the limb endpoint generated forces in Chapters 3 and 5.

When investigating motor tasks, typical studies and experiments over-constrain the subject's movement, often having the subject strapped in and limiting joint kinematics. This indeed isolates the variables of interest, and kinematics can be estimated a-priori but, in ADLs, subjects do not perform the same task always on the same manner. Adaptability is a key component of human movement, and no two subjects perform a motor task exactly alike. By subjecting individuals to follow a certain trajectory or constrain certain mechanical degrees of freedom, the naturalistic behaviour and their personal way of conducting the task is influenced.

Nevertheless, analysing all the biomechanical variables in par with sEMG, in a fully unconstrained ADL task, is an overly complex problem to solve. A compromise in using constraints in the research of natural movement is required but studies need to be tailored to each subjects' movement characteristics. To breakdown this complexity issue and take into consideration the ADLs and subject differences, our project was divided into stages, ranging from more constrained static ADLs, with fixed joint configurations, to fully dynamic movement to carry out a task.

The type of contraction and joint kinematics studied will define if a task is static or dynamic. Important to refer that, although clear distinction in kinematics exists between static and dynamic tasks, such distinction is not easily noticeable in sEMG (Christensen et al. 1995; Lehman 2002; Masuda et al. 1999; Sjøgaard et al. 2004). Without a-priori knowledge of the task, only by analysing the kinematics can we truly infer on the type of contraction. Consider then the following types of contraction, based on Reed and Bowen 2008:

- Isometric contraction: muscle fibres retain a constant length and there is an increase in muscle tone and tension. There is increased torque/force at the joints the muscle acts on, but joint kinematics remain constant, defining this as a static environment. The task conducted on Chapter 3 (Maximum Voluntary Force) is an upper-limb isometric contraction, where force is generated, sEMG increases but no movement occurs.
- Concentric and Eccentric contractions: in these contractions muscle length will decrease

or increase, respectively, at the same time as tension in muscle increases. These generate movement by displacement of the joints acted on, and shifts on the sEMG signal. Both contractions constitute the basis of a dynamic environment, with varying movements, and are studied in the tasks of Chapters 4 and 5.

The activity of skeletal muscles, acting under any joint configuration, produces a muscle force to counter a load, withstand gravity or to produce an external net force (e.g. limb interacting with an object or surface). To investigate individual muscle forces and respective joint torques, invasive methods are required, rendering these methods unfeasible for human studies. Instead, the external net force produced in a motor task can be recorded via force sensors. The relationship between the muscle activity and generated force is non-linear and may vary considerably among muscles and subjects (Bigland-Ritchie 1981; Woods and Bigland-Ritchie 1983; Disselhorst-Klug et al. 2009; Kuriki et al. 2012).

Studies continue to explore this relationship (Sidek and Haja Mohideen 2012; Borzelli et al. 2022) in attempts to map the activity of muscle groups into generated forces in different tasks, in a non-invasive manner. The best alternative is the use of human kinematic models, like *OpenSim* (Delp et al. 2007). Making use of these models and with cadaveric tissues and biomechanics information, studies (e.g. Saul et al. 2014) estimate individual muscle forces and joint configurations required to produce a certain net force at the limb.

2.2.2 Kinematics and force analysis pipeline

In each of the presented studies (Chapters 3, 4 and 5), kinematic and force analysis was conducted with a similar basis, even if using different technologies or sensors. One imperative step in recording motor task data is the **synchronisation** of all variables. A combination of hardware and software tools is used to ensure sEMG, kinematics and force recordings are synchronised in time, even if sampled at different time intervals. For studies presented herein, synchronisation was either achieved by a synchronisation unit, based on transistor-transistor logic (TTL Synchronisation), or via share data acquisition units, with embedded synchronised ports. Figure 2.3 presents a generalised pipeline, indicating how data acquired for both biomechanical and sEMG variables shapes the overall process.

The following list present in further detail each of the steps presented:

- Like sEMG, both kinematics and force recordings are susceptible to motion and electri-

cal noises, which require **filtering**. In the case of force sensors, filtering is conducted to remove any sudden, inexplicable acceleration spikes, or readings that do not involve force generated by the subject, which all contaminate the recordings. As for kinematics, the filtering stage is highly dependent on the technology used. Two specific cases are investigated here, in the studies of Chapters 4 and 5, respectively:

– Acceleration recordings, for example from an IMU, are easily influenced by motion

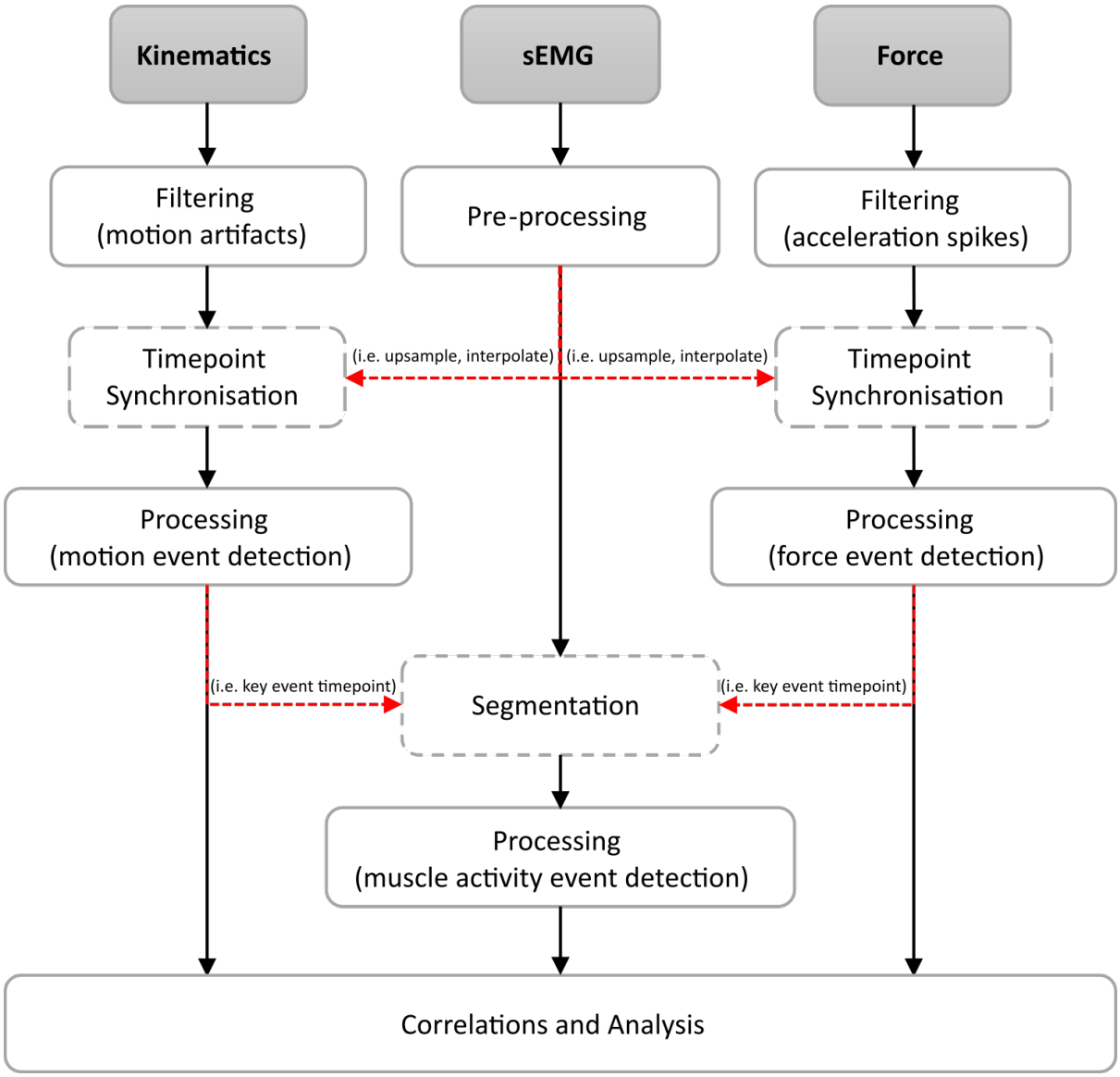


Figure 2.3: **Processing pipeline for kinematics**, force and sEMG synchronised recordings. Dashed lines indicate processing dependencies on other variables. A dependent stage (dashed box) requires a step or function (dashed red line) from an alternative variable. For example, in "Timepoint Synchronisation" from the Kinematics, the dataset is interpolated to sample match the same sample frequency from the sEMG dataset. In the "Segmentation" stage, the sEMG is segmented using the processed detected event timepoints from the Kinematics and/or Force recordings.

artefacts, sensor orientation, location and material sensor is applied to (e.g. issues if placed over loose clothing). A combination of high-pass filters to remove electrical noises, and low-pass, anti-aliasing filters are required to isolate the recording to only relevant captured motion.

  - Optical kinematic systems, where retro-reflective markers are used, commonly have noise associated to marker occlusion, erroneous marker placements (and associated estimation errors), or environmental noise (e.g. lighting conditions or reflective clothes/objects). Identification of outliers, and interpolation of data in cases of short marker occlusion are two of the techniques used in these studies to filter noisy recordings.

- Biomechanics and sEMG recordings are synchronous to ensure temporal matching of data. Though synchronised, the sampling frequencies for each variable may differ, leading to different sample numbers for the same temporal duration of the recorded task. Especially in the recording of kinematics with optical systems, recording a similar number of samples per second as sEMG (as mentioned earlier, 1500 Hz or samples per second) is unfeasible. To **timepoint synchronise** both variables, upsampling via linear interpolation (Davis 1975) (Equation 2.5) is used in the studies of Chapters 4 and 5:

$$y = y_1 + (x - x_1)\frac{(y_2 - y_1)}{(x_2 - x_1)} \tag{2.5}$$

  Where y is the interpolated value, x is the sample timepoint to perform interpolation, y_1 and y_2 are the first and second signal samples, and x_1 and x_2 are the first and second timepoints. An example of this method is presented in detail in Chapter 4, where sEMG had a sampling frequency of 1500 Hz, and the IMU a sampling frequency of 60 Hz (sEMG data had 25 times more samples than the IMU data). Note that interpolation may alter the frequency contents of a signal and is in fact estimating a sample, so this process, though useful for kinematics and force data, should not be applied to sEMG, especially if spectral analysis is involved. In the generalise case of Figure 2.3, the sampling frequency of the sEMG recording is then used to upsample the kinematics and/or force data.

- Both biomechanics and sEMG now have equal number of samples. Through **processing** of kinematics or force data, key events of the motor task are then identified. Each study

presents a different approach and the selection of different features to identify these key moments. For the case of the study of Chapter 3, force events were detected using gradients (in Britannica 2023a) (Equation 2.6) and thresholds, identifying the start and end of the static task.

$$gradient = \frac{y_2 - y_1}{x_2 - x_1} \tag{2.6}$$

Where y_1 and y_2 are the first and second signal samples, and x_1 and x_2 are the first and second timepoints. In the study of Chapter 4, a rolling window, threshold and signal energy (in Oppenheim and Schafer 1975) (Equation 2.7)analysis is used to identify moments of movement.

$$E_y = \sum_{n=-\infty}^{\infty} \left| y(x)^2 \right| \tag{2.7}$$

Where E_y is the energy of signal y, n is the sample number and x is the timepoint. A simplified method algorithm is then designed to identify specific gait event timings, and described as the core finding of the study.

- Using the timepoints provided by the processing stage of the kinematics and/or force pipelines, the sEMG and biomechanics data is **segmented** into relevant time windows of activity, and sEMG data proceeds to be processed according to the pipeline presented in Figure 2.2.

- In the final step, the relationship between the biomechanics variables and the sEMG is analysed, and is presented in detail in each study.

The following diagram in Figure 2.4 serves as a summary, exemplifying the intricate relationships between biomechanical and physiological variables. In a simplified manner, it demonstrates how a muscle contraction generates force on the muscle's insertion points, leading to torques in the affected joints. Despite extensive examination, accurately mapping muscle activity observed on sEMG to the specific force produced by the muscle remains a challenging task.

To illustrate this further, let's consider a static upper limb force generation task, similar to the motor task studied in Study 3. Figure 2.4's diagram showcases a basic 4-muscle model based on the shoulder and elbow joint. The model incorporates two antagonistic pairs: Anterior and Posterior Deltoid for the shoulder joint, and Biceps Brachii and Lateral Triceps for the elbow joint. This minimalist approach highlights the fundamental variables and dependencies necessary to explain force generation at the limb's endpoint.

The total net force generated in this model depends on the muscle forces (F_{muscle}) and their respective insertion points, with each muscle contributing to a joint torque (τ). Additionally, the limb's kinematics, such as segment length (L), mass (m), and joint angles (θ), are crucial to investigate moment arms and to infer on limb kinetics. Combining these factors, each joint torque (τ) influences the force produced at the limb's endpoint. Bear in mind this model only considers a static task, with joints operating only in a two-dimensional plane. Motor tasks in a three-dimensional dynamic environment will thus greatly increase the complexity of this analysis and relationships.

This interconnected relationship between biomechanics (kinematics and kinetics), physiology (muscle activity levels), and generated forces is effectively depicted through the inter-dependency of these three core variables in Figure 2.4. In addition, other factors as muscle mass, muscle fibres (Fitts et al. 1991), fatigue (Viitasalo and Komi 1981; Stevens and Cain 1970; Lee et al. 2022; Garcia-Aguilar et al. 2022; Wærsted 2000), among others, will directly impact the net force in a yet poorly understood manner. Understanding these complex interactions is vital for advancing our comprehension of human movement and optimising approaches to rehabilitation.

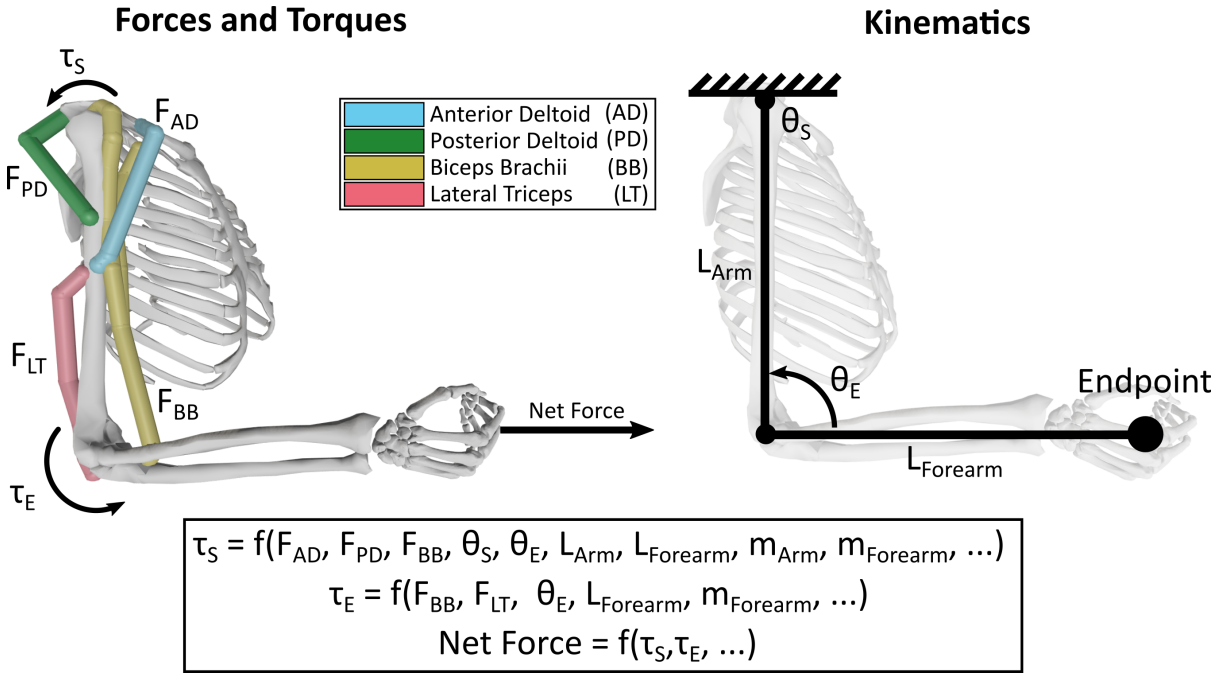


Figure 2.4: **Simplified forces, torques and kinematics diagram for an upper-limb static task**. Based on Saul Holzbaur et al. 2005; Chen et al. 2020, this diagram presents the basic generated net force dependencies, considering limb kinematics (segment lengths - L, for arm and forearm, and joint angles - θ, for shoulder - S, and elbow - E), the torques (τ) generated at the shoulder (S) and elbow (E) joint and the individual muscle forces (F_{muscle}) per muscle responsible for said torques. The generated *Net Force* at the limb endpoint is thus a direct function ($f()$) of the joint torques and, consequently, each represented variable.

Chapter 3

Healthy MAPs for static upper-limb ADLs

3.1 Short Introduction

A static task is a motor task that does not involve joint movement and is achieved through isometric contractions, meaning that there is no change in the length of muscle fibres during the task. This type of task is often used as the basis for Maximum Voluntary Contraction (MVC) studies, which are commonly used in clinical assessments.

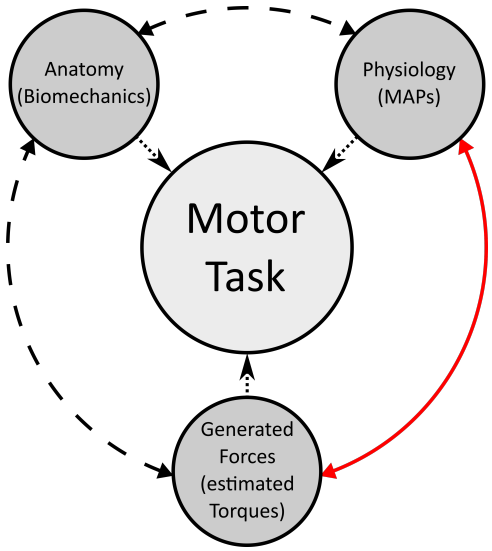


Figure 3.1: **Summary diagram for "Multiple muscle activation patterns in a static motor task" article**. Focus is on the relationship between the physiology and the generated forces in this isometric task.

In these MVC studies, a subject's limb is typically fixed or constrained in a certain configuration while performing the static task. This allows for the measurement of maximum muscle contraction of a focused muscle involved in the task, and provides information about the subject's force generation levels. However, it is important to note that every individual will have a different "natural" muscle and joint configuration to complete a given task. Therefore, in the article being presented, an adapted MVC study is proposed that takes into account these individual differences. Using an Maximum Voluntary Force (MVF) task, we shift the typical focus on the activity of a single muscle towards the muscle activity pattern that generates the highest possible net force. This way we ensure a less constrained experiment for the subject, minimising typical constraints to the limb, to better reflect the individual's natural joint and muscle configuration and considering a higher number of relevant muscles.

The aim of this experiment was to identify the MAPs recruited per subject and the corresponding relationship with the generated forces and force profiles. The limb configuration is visually inspected per trial, and the subject's elbow angle is minimally controlled to ensure the subject maintains a 90-degree angle within and between trials. In this case, the experiment limits the biomechanical variable to focus solely on the relationship between MAPs and Force.

3.2 Article

3.2.1 Metadata

Title: Multiple muscle activation patterns in a static motor task.

Authors: Rafael Castro Aguiar[1], Elijah Chisala[2], and Samit Chakrabarty [1]

Details:

- [1] R. Castro Aguiar and S. Chakrabarty are with the School of Biomedical Sciences, Faculty of Biological Sciences, University of Leeds, Leeds LS2 9JT, UK.
- [2] Elijah Chisala is with University Hospitals Birmingham NHS Foundation Trust, Birmingham, UK
- Correspondence: bsrdca@leeds.ac.uk.
- Current address: Faculty of Biological Sciences, University of Leeds, Leeds LS2 9JT, UK.

3.2.2 Abstract

In clinical settings, for most neuromuscular disorders, muscle activity is routinely used to assess a subject's ability to conduct volitional tasks. However, current measures and protocols to investigate muscle activity and performance are subjective and inconsistent. Here we present preliminary evidence to establish a quantifiable measure based on interaction between muscles and their control, for development of standardised protocol. Commonly, methods like Maximum Voluntary Contraction (MVC) at the elbow are used to assess neuromuscular function of the upper limb using recordings from one or two muscles, for example Biceps Brachii and Triceps. We predict that muscle interactions during a task are better characterised if multiple active muscles are recorded from. We improve upon this current limitation by identifying muscle activity patterns from the recordings of relevant upper-limb muscles, in an isometric task. A maximum voluntary force (MVF) task was performed by the subjects, producing sustained (5 seconds) maximal force (minimum of 4 trials). Subjects' elbow was held close to their body, forming a 90-degree angle between the arm and the forearm. Data was collected from 15 healthy subjects (1 female, 25 +/- 5 years). Muscle activity was recorded via surface Electromyography (sEMG), from 9 upper-limb muscles. The endpoint force generated was recorded and synchronised in time with sEMG. The root mean square (RMS) of both muscle activity and force was computed and an average of all the trials per subject generated. Correlations between all muscle pairs were computed for all subjects. The pairs of muscles exhibiting significant correlation are explained in terms of their anatomical organisation at the elbow. These natural muscle pairing groups will help stratification of patients, aiding in the choice of appropriate rehabilitation programs focusing on the needs of the individual. Through the investigation of spectral features of sEMG, in specific windows of the MVF, we are able to identify the activity of neural pathways as well. Results demonstrate the inter-variability among subjects, and the consistency of MAPs when investigating the individual nuances of motor control per subject. Increasing the number of subjects in this study will substantiate the presence of these patterns in healthy subjects, providing the foundation for future clinical assessment for normal and dysfunctional motor states. The presented protocol for MAPs identification and the protocol to analyse dynamic neural pathway changes may be integrated into a potential biomarker tool to assess and diagnose neurological disorders.

Keywords: sEMG, muscle control, smart therapy, daily-life tasks, neurorehabilitation.

3.2.3 Introduction

The ability to do the daily tasks necessary for personal care is the foundation for assessing function, and therefore the primary focus of rehabilitative therapies for individuals with neural deficits. Although this focus is outcome based, understanding the underlying control structures (namely, the numerous sensorimotor faculties of the central and peripheral nervous system, the neuromuscular junctions and the musculoskeletal system) will help improve the efficacy of neurorehabilitative therapies and ultimately restore function. Currently, there is a longstanding interest in Electromyography (EMG) as a measure and predictor of muscular activity. Surface Electromyography (sEMG), for example is widely used in prosthetic devices, particularly for the upper limb, where the need for fine control is necessary for acceptable levels of function. There have also been studies applying more invasive intramuscular EMG recordings in humans and animals to explore motoneuron behaviour in vivo. As a result, there are many examples in the literature of methods of interpreting, classifying and predicting the outcome of the activation patterns of skeletal muscle. This paper aims to present and demonstrate the limitations and areas for further research needed to fully comprehend the interactions and patterns that underpin the relationship between neuromuscular activity and force output. We explore this theory by observing and analysing the force output and muscle activity of 15 neurologically intact subjects during a force production task taken from current clinical practice settings. The task, a maximum voluntary contraction (MVC) is currently the standard for assessing the maximal force generating capacity of a muscle or group of muscles, assuming that all contributing muscles are maximally activated to produce the force; thus also assessing muscle strength. The theory presented in this paper is that the relationship between the activity of a muscle or a group of muscles and force output is non-linear and is influenced by numerous interactions, which will be explored in part and alluded to as a target for further work.

In our work, we explore and identify muscle activity patterns of healthy subjects, identifying the nuances of the individual's mechanism of control. By understanding the way the subjects neural systems encode the movement signals into muscle activity patterns, and relating these signal to biomechanical properties as the arm kinematics, we find a way to characterise a static motor task.

3.2.4 Methods

Activities of daily living (ADLs) involve a complexity of movements, where muscles are believed to be controlled and coordinated in patterns and not individually. These muscle activity patterns (MAPs) act on and incorporate muscles for multiple joints. Different individuals may display similar MAPs for a same motor task, and existent variability may reflect individual characteristics of the subject. These shared MAPs and variability can be extracted and used for improving analysis, diagnosis and used as a control signal for external devices.

The objective of this study was to identify typical MAPs in a static upper-limb force generation task using surface Electromyography (sEMG). The experiment designed has subjects conducting several trials of a maximum voluntary force (MVF) task with their upper-limb, in a defined and controlled configuration. sEMG sensors are placed on 9 key muscles, anatomically related to the task to be performed. Force produced during the MVF was recorded synchronously with the sEMG data. The physiological mechanism for muscle pattern recruitment in a static task can be discerned through these non-invasive recordings and their relationship. Experiments were conducted in accordance to the Ethics Committee Approval BIOSCI 21-007, from the University of Leeds, Leeds, UK, and in accordance with the Declaration of Helsinki. A pre-screening questionnaire ensured only healthy subjects were recruited, with no known history of neurological disorders or any current or past injuries that could affect the study or the subject. A total of 15 subjects were recruited: 7 biological females, 2 left-hand dominant, with an age range of 25 $\pm$ 5 years.

3.2.4.1 Material Specifications

To record sEMG signals, a Noraxon TeleMyo DTS EMG system was used. This system was configured to record at a sampling frequency of 1500 Hz, with an hardware high-pass filter at 10Hz. In total, 9 sEMG channels were configured for recording, each corresponding to a muscle from Table 1. Sensor locations were based on each respective muscle and corresponding guidelines from SENIAM. Skin over these intended muscles was prepared, with abrasive gel (NuPrep) and alcohol to maximise the signal-to-noise-ratio. To record force activity, a handle system was adapted and attached to a Noraxon Force Transducer (SML-500). Force was recorded and sampled synchronously with the sEMG channels, through the Noraxon acquisition board. Both sEMG and Force data was recorded, stored and processed in a desktop PC with the following

specifications: Intel(R) Core(TM) i5-4460 CPU @ 3.20 GHz, 8.00 GB RAM.

3.2.4.2 Experimental Protocol

When conducting the same motor task no two individuals recruit the exact same muscles in the exact same manner, even in a controlled environment. To verify this assumption a static motor task experiment was devised, to identify the different muscle activity patterns recruited by a set of healthy subjects.

Table 3.1: **Muscles recorded through sEMG and respective functions**. This muscle selection encompasses three main upper limb joints: shoulder, elbow, and wrist.

Muscle Code	Muscle Name	Main Functions	Relevant Joints Interacted
PM	Pectoralis Major	Arm adduction, internal rotation, and flexion	Shoulder
AD	Anterior Deltoid	Shoulder abduction and flexion	Shoulder
PD	Posterior Deltoid	Extension and external rotation of the arm	Shoulder
LD	Latissimus Dorsi	Extend, adduct and medially rotate shoulder	Shoulder
BB	Biceps Brachii	Flexion and supination of the forearm at the elbow joint	Elbow
LT	Lateral Triceps	Extension of elbow joint	Elbow
MT	Medial Triceps	Extension of elbow joint	Elbow
FCR	Flexor Carpi Radialis	Wrist flexion, wrist abduction	Wrist
ECR	Extensor Carpi Radialis	Wrist extension, wrist abduction	Wrist

With focus on an upper-limb maximum voluntary force (MVF), subjects are asked to pull a handle forward, with their elbow at a 90 degree angle between arm and forearm, with their arm close to their trunk, as demonstrated on Figure 3.2 (section a) and b)). During the task, the subjects generate a tensile force, in a forward direction in reference to the handle and subject

(Figure 3.2 section c)), recorded via a force sensor. This recorded tensile force corresponds to net force produced by the interaction of the upper-limb muscles and respective generated joint torques.

Subjects are initially fitted with the 9 sEMG sensors over the muscles described on Table 3.1, and the handle height is assessed in a pre-trial to ensure correct positioning of the subject. The subject's location on the ground and the height of the handle will be noted, ensuring repetitiveness of recordings between trials.

Three muscles listed (LD, FCR and ECR) act only as support structures for the shoulder and elbow joints, and are inspected not to participate in the force production. The analysis and main results therefore focuses on the main muscle group listed in Figure 3.2 b).

From a neutral position, the subject is given a start cue and proceeds to raise the handle until the desired arm configuration. The subjects then initiates the force production, maintaining it for at least 5 seconds, and ensuring their arm is static and no movement occurs. After concluding the trial, the subject is given a cue to return to a neutral arm position (down, next to body) and to hold the handle until asked to let go. At all times, an examiner is visually inspecting and controlling the subject's performance, and provides constructive feedback post trial if any leaning or deviation for the intended configuration is witnessed. This way, the examiner ensures the validity of trials and minimises deviations or errors on the data. A minimum of 6 trials are recorded per subject, allowing each subject a rest time of at least 2 minutes between trials to eliminate possible effects of fatigue (based on findings from Trossman and Li 1989; Green et al. 2014). Anonymous videos of each trial are recorded as well, to provide a posteriori performance assessment and control for incorrectly performed trials.

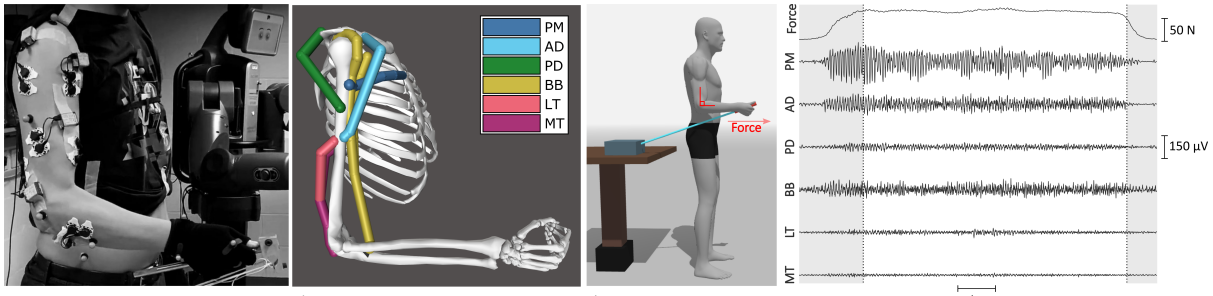


Figure 3.2: **Experiment methodology**: a) electrode placements and subject, b) OpenSim model of main recorded muscles, c) experiment diagram, d) sEMG and Force sample data for 1 subject, 1 trial, where grey area corresponds to loading and unloading response

3.2.4.3 Data Analysis Methodology

The following methodology is sub-divided into two separate sections, referring to the Pre-processing and Processing stages of data analysis. Here, pre-processing refers to the steps taken to filter and segment the dataset, prior to any feature extraction and analysis. In the processing section, we detail the steps and mathematical tools to normalise the data, compute the RMS of the signals, identify the MAPs, and identify active neural pathways through spectral analysis.

Pre-processing:

1. Hardware high-pass filter 10 Hz (removes noise coming from electrical sources and movement)
2. Software band-pass [10 - 150] Hz
3. Notch filter at 50Hz
4. Trial cutting, assisted by force signal information:
    - safety margin of 1 second (1500 data points) before and after force reaches 50% of maximum trial value, ensuring entirety of trial is maintained
    - reduces areas of noise and adjustments pre and post relevant task
5. Using gradients, segmentation of each trial into 3 separate sections (loading, hold, unloading):
    - loading: loading of the arm into the 90 degree angle at elbow, prior to the maximum force production section
    - hold: core section of trial, where subject is performing the MVF
    - unloading: force production segment finished and return to baseline, with arm close to the body at a neutral position

Processing:

1. Data normalisation techniques:
    - Force: find maximum value of force for all the trials of a singular subject; use this max_force value as a reference for normalisation: $current_force/max_force_all_trials =$

$norm_force$;

- sEMG: find muscle that exhibits highest activity out of all trials for subject X; use this maximum activity as a normalisation reference: $muscle_x/max_muscle_activity = norm_muscle_x$

2. Muscle activity value: using the root-mean-square ($\sqrt{norm_muscle_x^2}$), establish, for the duration of the hold segment (5 seconds), the general activity level of said muscle, out of the pre-process sEMG signal; this is done for all muscles, trials and subject
3. To analyse muscle activity, and muscle activity patterns, for all subjects, the mean and standard deviations of each muscle are computed, for all the trials of a single subject, and presented with all the subjects
4. Using non-normalised data, compute correlation between muscles, to validate possible patterns found at RMS stage; do so for all trials, averaging the results per subject
5. Spectral analysis:
   - sub-divide hold segments into 3 equal sized sub-segments, representing the early, mid and late stages of the MVF
   - investigate the power spectrum of each muscle individually
   - through filtering, isolate known pathways:
     - Corticospinal (CST): bandpass filter [10 - 35] Hz
     - Reticulospinal (RST): bandpass filter [35 - 60] Hz
     - Spinal loops (SPN): bandpass filter [60 - 100] Hz
   - compute power spectrum per isolated pathway, normalising the results for the maximum magnitude computed in the overall power spectrum (prior to isolating pathways); do so per muscle
   - considering any values below 10Hz and above 100Hz as negligible (or non-relevant activity)
   - to create an activity ratio for the pathways, all values per sub-segment are summed up, and the following formula is used to define individual pathway contribution:

  - $CST/(CST + RST + SPN) * 100$
  - $RST/(CST + RST + SPN) * 100$
  - $SPN/(CST + RST + SPN) * 100$

- to assess how much variation occurs throughout a single trial, per pathway, the coefficient of variation (Walters et al. 2021) was used:

$$CV = \frac{SD}{Mean} * 100 \tag{3.1}$$

  Where CV is the coefficient of variation, as a percentage value, along with the SD (standard deviation) and $Mean$ of the pathway spectral features observed per muscle and individual.

- due to the lack of data points, a traditional statistical method of variance is not applicable, but this equation gives, in its simplicity, a easy assessment of how much a pathway changes across the trial;

- this value is then averaged per pathway, for each respective muscle, and for the whole number of trials of a subject; variation above 5% is considered significant

3.2.5 Results

For the exact same motor task, in a minimally controlled environment, different subjects will present significant variation and individuality in the strategies employed to complete the task. Upper-limb configurations in the 90 degrees elbow angle and position next to the trunk, posture and stance, and manner to approach the task was kept under control and consistent among trials and participants. From recruitment strategies, to biomechanical configurations of their limbs, no two subjects present the exact same MAPs when completing the MVF.

In Figure 3.3 we present the mean and standard deviation of the generated force profiles of all trial, separated by subject. Three characteristic patterns are witnessed: an early overshoot of the force level, creating initial ripple, until stabilisation towards the end of the "hold" phase (e.g., subjects AE, AI, AJ, AM and AN); a slowly increasing force level throughout the trial, without plateauing (e.g., subjects AD, AF and AG); a stable performance, with reduced oscillations and standard deviation across trials, with a quick plateau effect early on the "hold" phase (e.g.,

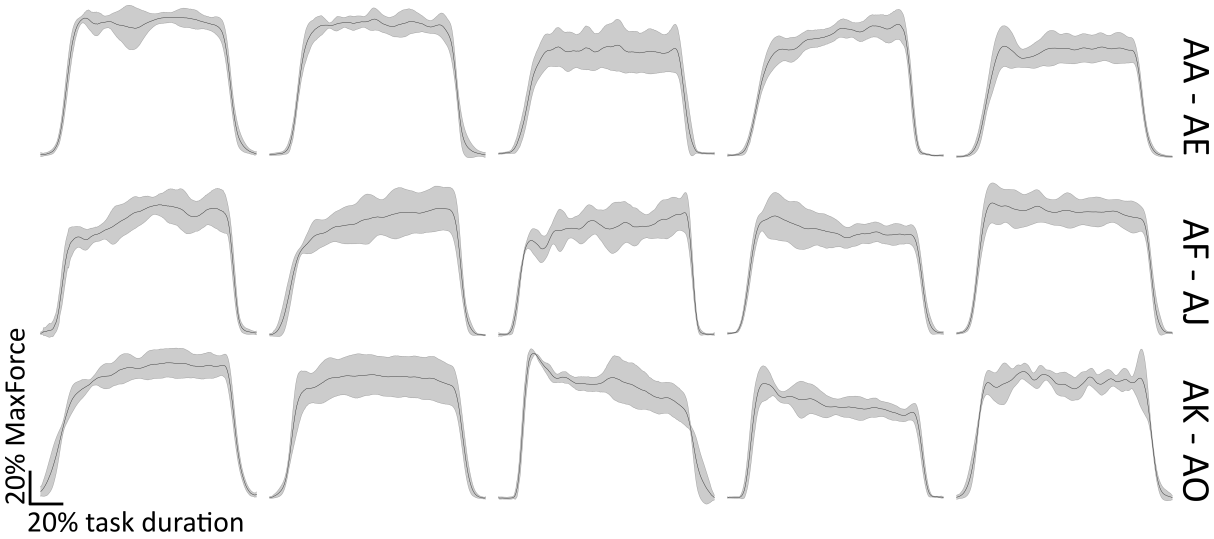


Figure 3.3: **Force profiles for each subject**, presenting the mean force and respective standard deviation as a shaded area around the mean. Values are normalised per subject, with percentage values referring to individual maximal forces and mean task duration. These profiles exhibit the entirety of the trial, including the mentioned "Loading", "Hold" and "Unloading" stages. For analysis purposes, focus is on the static stage in "Hold".

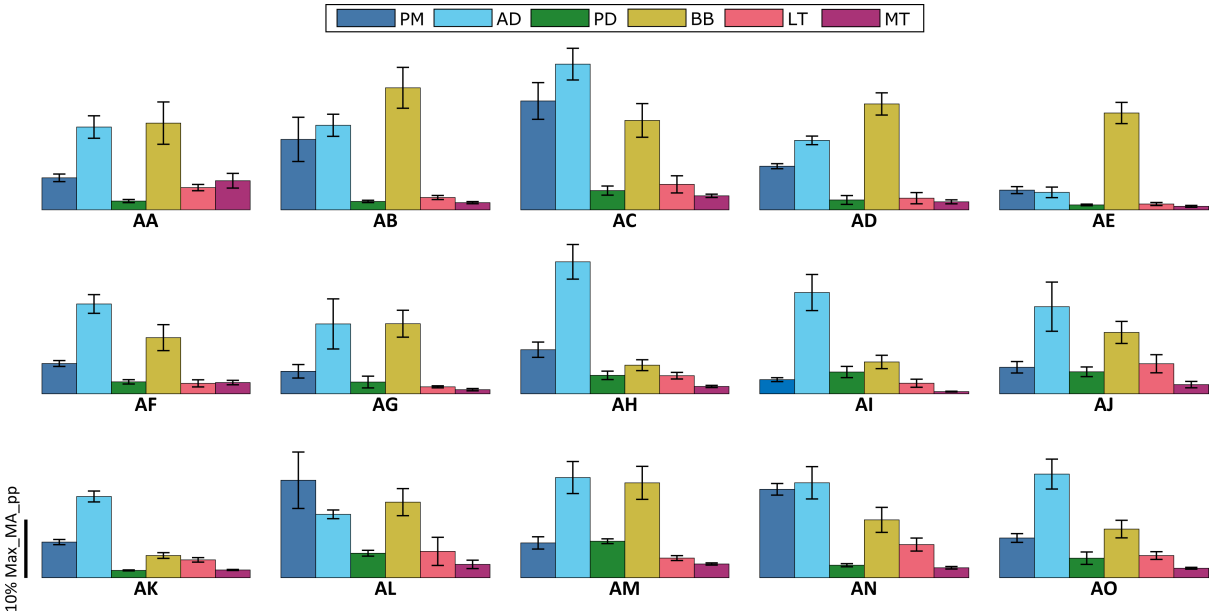


Figure 3.4: **Individual MAPs per subject**, presenting the respective mean and standard deviation from the normalised sEMG RMS of each muscle, for the entire set of trials of the subject. Scale is normalised per subject, using the highest active muscle in the entirety of trials of said subject, where Max_MA_pp: maximum muscle activation per subject. Noticeable variation in which is the highest active muscle, suggesting a different employed control mechanism per subject.

subjects AA, AB, AK, AL and AO). These results suggest a control mechanism at play, akin to an engineering PID (Proportional, Integrative, Derivative) controller, to fine-tune control an outcome variable, in this case, force level.

For the extracted force profiles of Figure 3.3, the corresponding MAPS were extracted by subject, and are presented in Figure 3.4. The computed means and standard deviations of the RMS values of each trial are here presented per subject. Clear variability is immediately detect on the different most active muscles and muscles groups between subjects. The distinction in muscle groups suggests a bias towards a certain joint. Subjects AA, AD and AE have higher activity levels in their BB muscle, suggesting a focus on the elbow joint. Subjects AC, AF, AI, AJ, AL, AN and AO, alternatively suggest a higher focus on muscles related to the shoulder joint. The remainder of subjects present a combination of similarly active muscle groups for both shoulder and elbow.

Correlations between muscles throughout trials were computed per subject, to validate the existence of patterns of activity. Antagonist and agonist relationships are shown in Figure 3.5. Interestingly, as with the witnessed variability in force profiles (Figure 3.3) and MAPs (Figure 3.4), in different subjects we find clear distinction in individual muscle pair correlations: of notice, the relationship between LT and MT, elbow extensors, is not always agonistic. These correlations allow us to explore which muscles may received shared control, recruited in groups,

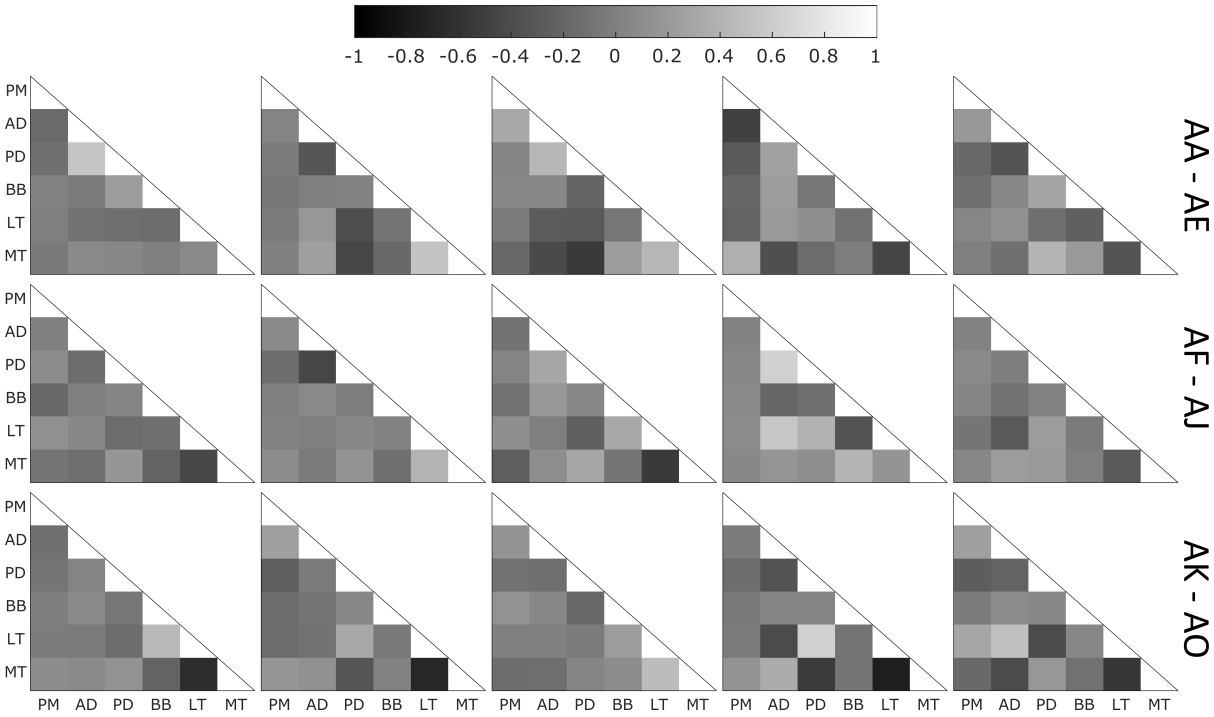


Figure 3.5: **Correlation matrices for each muscle pair, per subject**, computed from the processed sEMG signals over the trial duration. Scale indicates both positive and negative correlations, and teases agonist and antagonist behaviours between muscle pairs. Paired with MAPs, correlations validate the presence of a shared control or "synergy", involving different muscles.

indicating the presence of MAPs.

Based on the inter-subject variability demonstrated in Figure 3.4 and the witnessed correlations Figure 3.6, the following analysis focuses on the intra-trial and subject variability. The following results shown in Figure 3.6 explore this individual variability, in terms of generated forces and MAPs, within a subjects' recorded trials. Clear consistency in MAPs is witnessed across the randomly selected subject's trials. Variation below 5% is witnessed across the trials, associated with AD, BB and LT muscles. Interestingly, a considerably higher variation, above 10%, is witnessed in the force levels. This further highlights the non-linearity of the MAPs to force relation.

To explore the shared neural drive changes in the identified MAPs, and clarify the relationship between MAPs and force detected in 3.6, a spectral analysis and neural pathway identification is presented in Figure 3.7. These results, computed from a single randomly selected subject and trial, show the evolution of the MAPs and force throughout a trial, accompanied by the computed pathway activity. Apart from core muscles PM and AD, there is little variation (below 5%) in the MAPs. A small increase in the generated force is witnessed towards the end

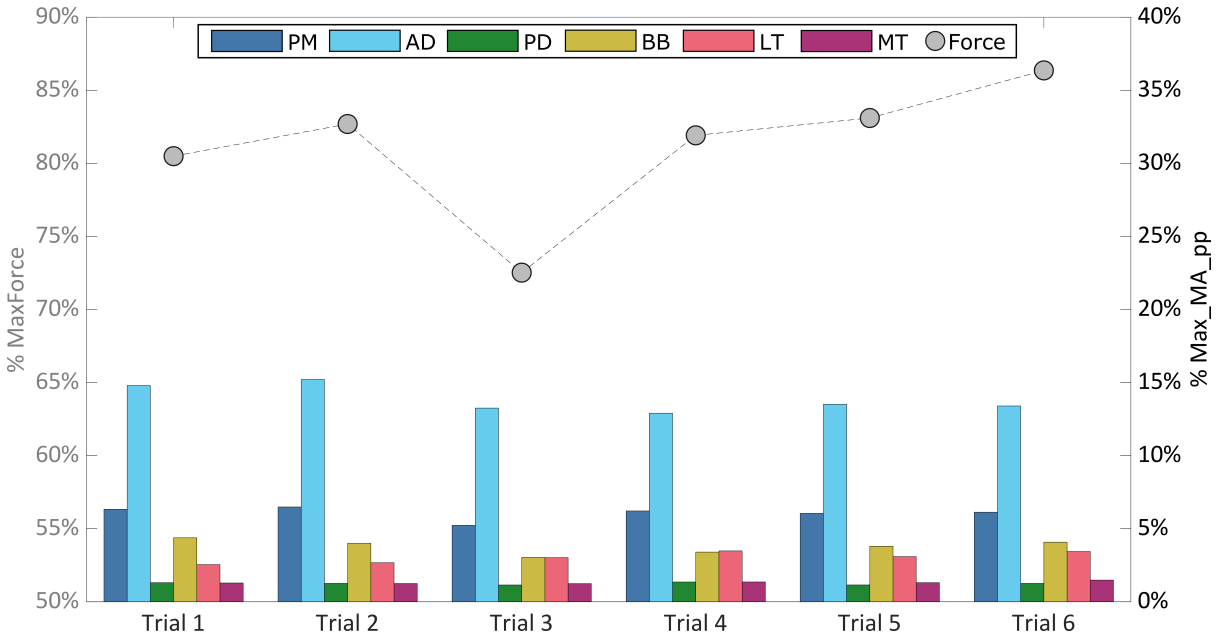


Figure 3.6: **MAPs and Force profile in entire trial set** of randomly selected subject (AK). Although a gradual increase in the generated force can be witnessed (over 5% increase over set of trials), no such variation is witnessed in the MAPs, validating the non-linear relationship between force and MAPs. Small MAPs variation (under 5%) can be witnessed in AD, BB and LT muscles alone. Values presented for both force and MAPs are computed as the RMS of each signal over the 5 seconds of MVF.

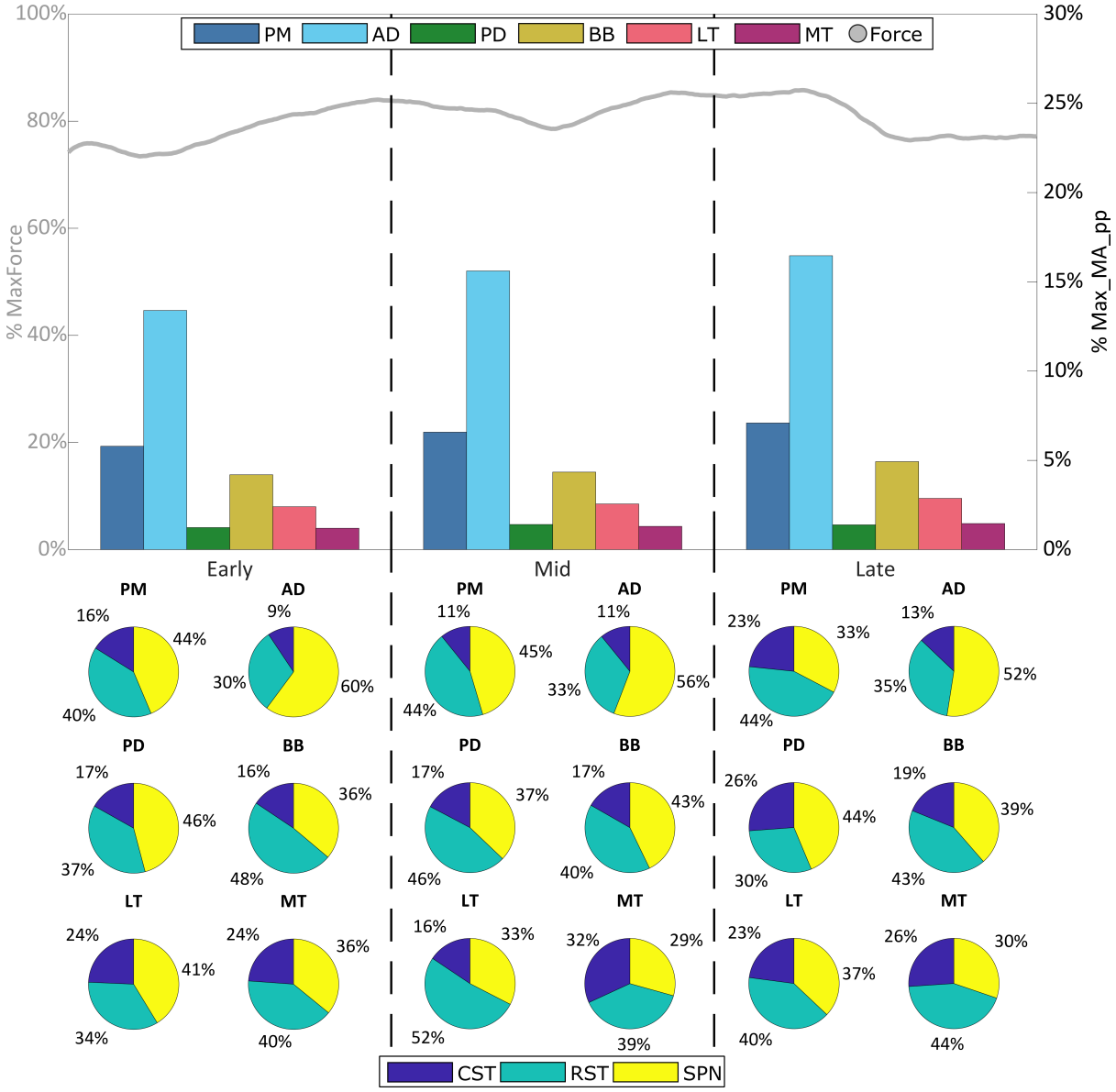


Figure 3.7: **Force, MAPs and computed pathway information**, considering a 3 phase segmentation of a randomly selected trial (AK Trial 1). Segmenting a trial into 3 equal parts: early, mid and late stage; reveals little variation over the MAPs, but some variation on the force profile and noticeable differences in each active pathway per muscle. An isometric task may suggest static behaviour from the CNS, when analysing only the MAPs, but sufficient variation in neural activity suggests a signal reinforcement and adaptation at different task stages.

of the trial. Muscles exhibit clear variation though in regards to active pathways, teasing a constant neural signal adaptation, throughout the task.

Similar oscillations in the activity of the pathways are found across all trials and subjects. Figure 3.8 presents the mean % of variation, per muscle and hypothesised active pathway throughout the entirety of a trial, averaged within individual muscles, per subject. Significant variation was found in each muscle and pathway, across trials and subjects, based on the criteria that a

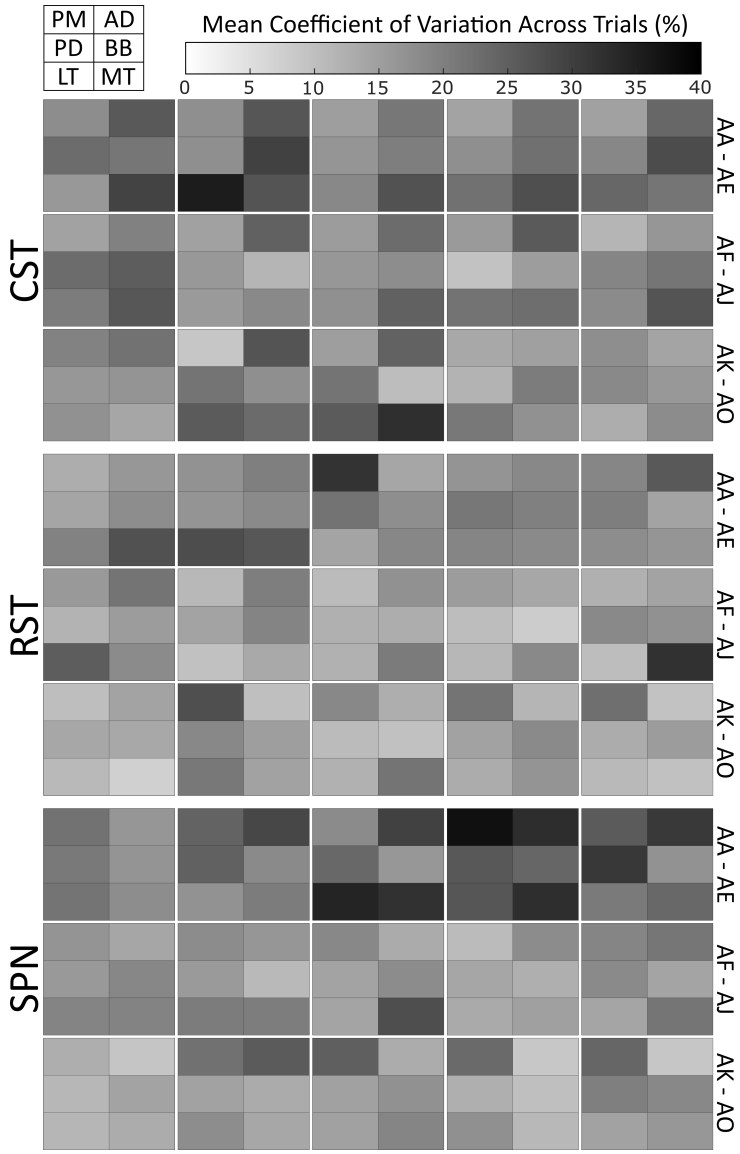


Figure 3.8: **Mean coefficient of variation of active pathways**, throughout trials and for every subject, with each pathway in a separate section for individual analysis; when considering a criteria of 5% variation (based on Walters et al. 2021 for significance, all the presented mean coefficients of variation are deemed significant, indicating a constant adaptation of each of the investigated pathways throughout the subjects and muscles.

mean coefficient of variation over 5% represents sufficient variability (based on Walters et al. 2021), with the smallest variation encountered being 7.4%. This variation is witnessed in all cases across subjects, muscles and pathways, confirming the neural adaptation (and possibly reinforcement), even when conducting a static motor task.

3.2.6 Discussion

In this study we explore the relationship between muscle activation patterns and forces generated during a static task. The identification of MAPs corroborates the hierarchical and modular

structure of the human motor control system. Focus was especially given to inter-subject variability and individual nuances of the mechanisms of motor control, in terms of recruitment patterns and biomechanics. Even when subjects conduct the exact same task, under set biomechanical guidelines and control, significant variability is encountered in their MAPs. As per individual, the identified MAPs demonstrate a robust approach to the task at hand, showing little to no variation in the pattern across the trials of the subject. Several factors may contribute to the witnessed force profiles and consistency of MAPs within the subjects, including:

- Neuromuscular: for a given biomechanical configuration, a set pattern, number and distribution of motor units in the core actuator muscles of the task may influence both MAPs and individual muscle forces (De Luca 2006; Fitts et al. 1991; York et al. 2022; Saul Holzbaur et al. 2005);
- Cognitive/Behavioural: this relates to the subject's approach to the motor task at hand. The assessment of the task's requirements, task completion plan and understanding of the involved movements may all contribute towards the approach taken. In other words, how familiar the subject is with the task or similar tasks may bias their approach (Silva Costa et al. 2023).
- Training and condition: the extracted MAPs of the individual may be influenced by their physical condition and skill set. Especially relevant in active individuals, their training and sports expertise may bias the recruitment of specific muscle groups to execute a task. An active swimmer may have more developed shoulder muscles and aptitude to generate higher torques at the shoulder joint, while a weightlifter may focus the higher torques on their elbow joint and respective muscles (Kargo and Nitz 2003; Shadmehr and Mussa-Ivaldi 1994; Bastian 2008).
- Neural pathways: the activity of different neural pathways, as CST, RST and SPN, may have a direct impact on the resulting outputs of the motor task. While MAPs remain similar, if recruited by different neural structures or with different parameters, a different net force outcome may be witnessed (Richards 2018; Liu et al. 2019; Oya et al. 2020).
- Fatigue: the individual's fatigue levels will have a direct and strong impact over the selection of muscles and force generation capabilities over the execution of a motor task (Viitasalo and Komi 1981; Stevens and Cain 1970; Wærsted 2000; Lee et al. 2022; Garcia-

Aguilar et al. 2022).

Current neurophysiology practice uses the relationship between maximal force and muscle activity in one or more muscles as the basis of assessing strength, particularly when there is suspected or confirmed neuromuscular impairment. During these experiments we were not able to observe distinguishable features that allowed us to match force profiles to their corresponding muscle activation patterns, either between or within subjects. We validate here the that the magnitude of muscle activation alone is neither sufficient or useful as direct measure or predictor of force output. The identification of individual MAPs and correlations between agonistic and antagonistic pairs of muscles are here demonstrated to be more valuable methods to characterise and analyse the performance of an individual, conducting a motor task.

As previously mentioned, MAPs varied considerably across subjects. Although, particular correlations found between agonistic and anagonistic muscle pairs were discovered to be shared between select subjects. The possible anatomical explanation for these witnessed relationships is presented in the analysis of the following muscle pairs:

AD/PD: Function: Antagonistic pair of the shoulder (flexion/extension). It is expected that there will be a negative correlation between these two muscles to allow shoulder flexion, specifically in shoulder dominant subjects. However, it was found that these subjects (n=6) were more likely to have a positive correlation between their anterior and posterior deltoids. It is possible that those who are more AD dominant required the activation of PD to stabilise the shoulder in position, indicating that PD acted as a stabiliser rather than an actuator.

LT/MT: Function: Agonist pair of elbow extension. The majority (n=9) of subjects had a negative correlation between these two muscles, with no skew in distribution towards elbow or shoulder dominance. An element of cross talk between electrodes may be considered, especially in the case of strong correlations higher than 0.70 (AL and AN). Nevertheless, the fact that this relationship occurs reinforces the argument that the activation of muscles as recorded by sEMG is not an accurate measure of muscle strength, at least in the context of concentric movement.

BB/LT: Function: Antagonistic pair of the elbow (flexion/extension) Similarly to AD/PD, it was expected that the of subjects who were classified as elbow dominant (n=3) would have a negative correlation between these antagonistic muscle pairs. Two of the three shoulder dominant subjects demonstrated this. The relationship between correlation of these muscles

and elbow dominant actuation of force is inconclusive due to the small sample size.

Our results show that the two core muscles with highest activity across subjects are AD and BB, prime actuators for shoulder and elbow flexion respectively. As witnessed in our results, either one or both dominate the MAPs during this task. Based on the dominance of either muscle, previously discussed in the Results section, we can classify the execution of the task to be either shoulder dominant in the case of higher AD activation, elbow dominant in the case of higher BB activation, or co-dominant with similar muscle activities. For the population recorded in our experiment, shoulder dominance (n=6) and co-dominance (n=6) were more common across all subjects. With these relationships considered, one of the explanations for the incongruities between MAPs and force output is that, in different subjects, different muscles may be activated to produce the same net force, characteristic of an over-actuated system with high redundancy. The selection of these muscles may be dependent on the previously highlighted factors, but are not fully understood at current.

As presented in the Results, the force profiles of the subjects demonstrate a clear engineering controller (PID) behaviour, in which the controller fine tunes an outcome measure based on a series of signal inputs and a closed feedback loop. Three distinct profiles were previously identified, stemming from the response time to reach the desired outcome of the motor task, in this case maximum force level, and the witnessed rippling effect of the force outcome throughout the task duration. This force stability or plateauing effect may be indicative of the previously discussed motor control factors, suggesting a higher aptitude or familiarity of the subject towards the task. Further research into this behaviour may be used quantify a subject's initial response towards a defined motor task, comparing the results to pre-defined healthy benchmark profiles.

Through the use of spectral analysis, we discuss as well the possibility of using non-invasive physiological recordings to infer on neural pathway activity. Previous studies (Richards 2018; Liu et al. 2019; Oya et al. 2020) have shown that certain frequency bands may correspond to specific neural pathways. Through brain and brainstem stimulation, links have been found between descending pathways and the frequency bands of sEMG signals, suggesting that the CST operates within a beta frequency band, RST operates in the low-gamma band and local spinal interactions may operate in the high-gamma band. In line with these studies we have investigated the changes in activity levels of each pathway. Although preliminary results show promising evidence of a frequency oscillating behaviour per pathway, further evidence is needed

to support the characterisation of frequency bands to different pathways. However, these preliminary findings suggest a possible link between force levels in static tasks and specific neural pathways, indicating a constantly updating, adaptive recruitment loop. Further studies are needed to clarify the mechanisms at play and the interactions between different active pathways and motor task variables. The integration of these findings with neuronal population models may help to assess possible implications if the pathways are disturbed, such as in stroke or spinal cord injury scenarios.

3.2.7 Conclusion

The clinical relevance of the findings of this experiment, although preliminary, can be used to guide further experiments and clinical practice. As it has been shown that the relationship between muscle activation and force is not linear, it is recommended that either is not a reliable assessment of the other. Further experiments may clarify how we may interpret EMG data in relation to predicting kinematics.

In addition, we here demonstrate the impact of different factors in a subject's MAPs and performance when conducting unconstrained motor tasks. If unfamiliar with subject's performance, we are simply unable to predict how they will perform the task. Although, if the subject is observed and recorded while conducting the task even if just once, we may be able to estimate potential individual MAPs the subject may employ. With the consistency in employing the same individual MAPs, even if force produced may vary, a pattern of force production may be estimated.

With further research into the presented method to investigate neural pathways activity, the involvement and dynamic activity of neural pathways may be an extremely useful tool in assessing neural pathway damage. If MAPs are preserved but pathway variability and force are reduced, it may indicate that the neural drive is impaired or altered at a certain pathway. If enough data is collected from both healthy and pathological cases, and integrated into neuronal population models, these dynamic pathway changes may become a useful biomarker for neural pathway damage and diagnosis.

3.2.8 References

Bastian, A. J. (2008). "Understanding sensorimotor adaptation and learning for rehabilitation". In: *Current opinion in neurology* 21.6, p. 628.

De Luca, C. (2006). "Electromyography". In: *Encyclopedia of Medical Devices and Instrumentation*. John Wiley & Sons, Ltd. ISBN: 9780471732877. DOI: https://doi.org/10.1002/0471732877.emd097.

Fitts, R. H., McDonald, K. S., and Schluter, J. M. (1991). "The determinants of skeletal muscle force and power: their adaptability with changes in activity pattern". In: *Journal of biomechanics* 24, pp. 111–122.

Garcia-Aguilar, F., Caballero, C., Sabido, R., and Moreno, F. J. (2022). "The use of non-linear tools to analyze the variability of force production as an index of fatigue: A systematic review". In: *Frontiers in Physiology* 13, p. 1074652.

Green, L. A., Parro, J. J., and Gabriel, D. A. (2014). "Beneficial effects of serial contractions on muscle performance after a brief period of rest". In: *European Journal of Applied Physiology* 114.8, pp. 1657–1665. DOI: 10.1007/s00421-014-2896-8.

Kargo, W. J. and Nitz, D. A. (2003). "Early skill learning is expressed through selection and tuning of cortically represented muscle synergies". In: *Journal of Neuroscience* 23.35, pp. 11255–11269.

Lee, C.-L., Lu, S.-Y., and Wu, C.-Y. (2022). "Rest period and object load effects on upper limb muscle strength recovery for manual load transfer". In: *International Journal of Industrial Ergonomics* 89, p. 103274.

Liu, J., Sheng, Y., and Liu, H. (2019). "Corticomuscular coherence and its applications: A review". In: *Frontiers in human neuroscience* 13, p. 100.

Oya, T., Takei, T., and Seki, K. (2020). "Distinct sensorimotor feedback loops for dynamic and static control of primate precision grip". In: *Communications Biology* 3.1, p. 156.

Richards, T. C. (2018). "Identifying Shared Pathways Across Multiple Muscle Groups of the Human Upper Limb". URL: https://etheses.whiterose.ac.uk/24138/.

Saul Holzbaur, K. R., Murray, W. M., and Delp, S. L. (2005). "A Musculoskeletal Model Of The Upper Extremity For Surgical Simulation And Neurocontrol Applications". In: *Annals of BIomedical Engineering* 6.33, pp. 829–840.

Shadmehr, R. and Mussa-Ivaldi, F. A. (1994). "Adaptive representation of dynamics during learning of a motor task". In: *Journal of neuroscience* 14.5, pp. 3208–3224.

Silva Costa, A. A. da, Hortobágyi, T., Otter, R. den, Sawers, A., and Moraes, R. (2023). "Age, cognitive task, and arm position differently affect muscle synergy recruitment but have similar effects on walking balance". In: *Neuroscience*.

Stevens, J. C. and Cain, W. S. (1970). "Effort in isometric muscular contractions related to force level and duration". In: *Perception & Psychophysics* 8.4, pp. 240–244.

Trossman, P. B. and Li, P.-W. (1989). "The effect of the duration of intertrial rest periods on isometric grip strength performance in Young Adults". In: *The Occupational Therapy Journal of Research* 9.6, pp. 362–378. DOI: 10.1177/153944928900900604.

Viitasalo, J. T. and Komi, P. V. (1981). "Effects of fatigue on isometric force-and relaxation-time characteristics in human muscle". In: *Acta Physiologica Scandinavica* 111.1, pp. 87–95.

Wærsted, M. (2000). "Human muscle activity related to non-biomechanical factors in the workplace". In: *European Journal of Applied Physiology* 83.2–3, pp. 151–158. DOI: 10.1007/s004210000273.

Walters, S. J., Campbell, M. J., and Machin, D. (2021). *Medical statistics: a textbook for the health sciences*. John Wiley & Sons.

York, G., Osborne, H., Sriya, P., Astill, S., Kamps, M. de, and Chakrabarty, S. (2022). "The effect of limb position on a static knee extension task can be explained with a simple spinal cord circuit model". In: *Journal of Neurophysiology* 127.1, pp. 173–187.

3.3 Short Summary

To identify MAPs in an unconstrained scenario, we collected sEMG signals of 9 different upper-limb muscles, while subjects performed a static task. Results reveal significant variability in the

MAPs among subjects, even when following the same task protocol. On the other hand, some similarities were found on muscle groupings and force profiles amongst subjects, suggesting a possible clustering based on the most active muscles during the task. This clustering may be indicative of similar motor control mechanisms shared among some of the subjects, and can potentially be used as a first stage distinction factor for motor task behaviour based on muscle group dominance.

MAPs show little variation across the duration of the task, even when force profiles fluctuate. Spectral analysis was used to identify possible active neural pathways, based on previous findings on active frequency bands, and suggests an adaptive, oscillatory input that constantly corrects possible errors and adapts MAPs during the task duration. The ability to identify active neural pathways during different stages of a motor task may aid in the design of targeted interventions, when looking for possible affected pathways.

Understanding the personal recruitment scheme of a subject, through MAPs and the activity of the neural pathways, can lead to improved diagnoses and may be used further in performance assessments. Nevertheless, alone MAPs and static tasks are not sufficient to characterise the motor control strategies on an individual. Kinematics of a task, as mention in Chapters 1 and 2 will influence the identified MAPs. With this in mind, the study presented in Chapter 4 establishes a tool to relate kinematics of a dynamic task with synchronously recorded MAPs.

Chapter 4

Markerless sEMG segmentation in ADL locomotion

4.1 Short Introduction

Dynamic tasks involve displacements of one or more kinematic degrees of freedom (DoF), associated with changing joint angles and muscle lengths. A dynamic scenario is, due to this DoF displacement, several orders of magnitude more complex than a static task. Nevertheless, relationships can be estimated between the varying, select kinematic variables (such as limb acceleration) and the MAPs recorded during the dynamic task.

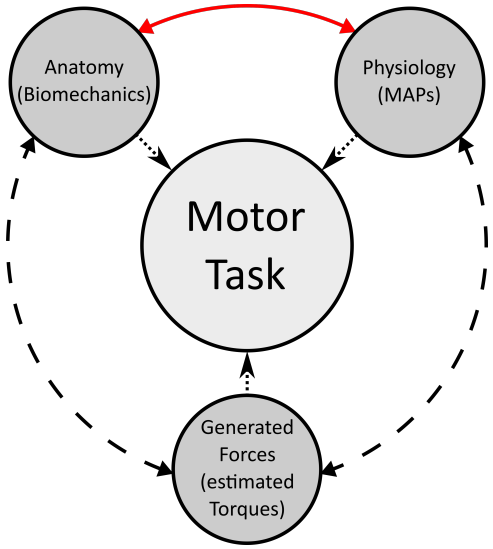


Figure 4.1: **Summary diagram for "Simplified markerless stride detection pipeline (sMaSDP) for surface EMG segmentation" article**. Focus is on the relationship between the physiology and the gait biomechanics of natural unconstrained walking.

In this study, we design an algorithm to identify key-event moments in gait, the heel-strike (HS), through the analysis of the acceleration profile of the participant's right foot. Through synchronous recordings, the HS time-points are identified and matched in the sEMG recordings. This isolates the sEMG activity per gait cycle, in different walking modalities, in order to identify the MAPs for each participant.

4.2 Article

4.2.1 Metadata

Title: Simplified markerless stride detection pipeline (sMaSDP) for surface EMG segmentation.

Authors: Rafael Castro Aguiar[1], Edward Jero[2] and Samit Chakrabarty[1].

Details:

- [1] R. Castro Aguiar and S. Chakrabarty are with the School of Biomedical Sciences, Faculty of Biological Sciences, University of Leeds, Leeds LS2 9JT, UK.
- [2] Edward Jero is with the Indian Institute of Technology Madras. Chennai 600036, India.
- Correspondence: bsrdca@leeds.ac.uk.
- Current address: Faculty of Biological Sciences, University of Leeds, Leeds LS2 9JT, UK.

4.2.2 Abstract

To diagnose mobility impairments and select appropriate physiotherapy, gait assessment studies are often recommended. These studies are usually conducted in confined clinical settings, which may feel foreign to a subject and affect their motivation, coordination, and overall mobility. Conducting gait studies in unconstrained natural settings instead, such as the subject's Activities of Daily Life (ADL), could provide a more accurate assessment. To appropriately diagnose gait deficiencies, muscle activity should be recorded in parallel with typical kinematic studies. To achieve this, Electromyography (EMG) and kinematic are collected synchronously.

Our protocol sMaSDP introduces a simplified markerless gait event detection pipeline for the segmentation of EMG signals via Inertial Measurement Unit (IMU) data, based on a publicly available dataset. This methodology intends to provide a simple, detailed sequence of processing steps for gait event detection via IMU and EMG, and serves as tutorial for beginners in un-

constrained gait assessment studies. In an unconstrained gait experiment, 10 healthy subjects walk through a course designed to mimic everyday walking, with their kinematic and EMG data recorded, for a total of 20 trials. Five different walking modalities, such as level walking, ramp up/down, and staircase up/down are included. By segmenting and filtering the data, we generate an algorithm that detects heel-strike events, using a single IMU, and isolates EMG activity of gait cycles.

Applicable to different datasets, sMaSDP was tested in healthy gait and gait data of Parkinson's Disease (PD) patients. Using sMaSDP, we extracted muscle activity in healthy walking and identified heel-strike events in PD patient data. The algorithm parameters, such as expected velocity and cadence, are adjustable and can further improve the detection accuracy, and our emphasis on the wearable technologies makes this solution ideal for ADL gait studies.

Keywords: gait detection algorithms; EMG; IMU; segmentation; muscle activity.

4.2.3 Introduction

Investigation of gait patterns is a valuable diagnostic tool that provides clinicians with the ability to diagnose a range of impairments affecting a patient's mobility, such as trauma, stroke, or neurological conditions. Features extracted from these gait patterns, such as key-event times, duration, and joint behaviour properties, are all quantifiable measures that allow a clinician to benchmark and make informed decisions regarding the selection of appropriate therapies.

The core element of gait assessment studies is the identification and analysis of gait cycles. A gait cycle is comprised of two core phases for each limb: stance and swing. This phase differentiation is associated with foot contact with the floor (stance) and swinging motion of the limb through the air, preceding the following step (swing). Taking the example of a right leg dominant subject, Figure 4.2 describes the gait cycle for a naturalistic walking pattern. For more detailed explanations of the gait cycle, please refer to Whittle 2007; Tao et al. 2012; Gujarathi and Bhole 2019.

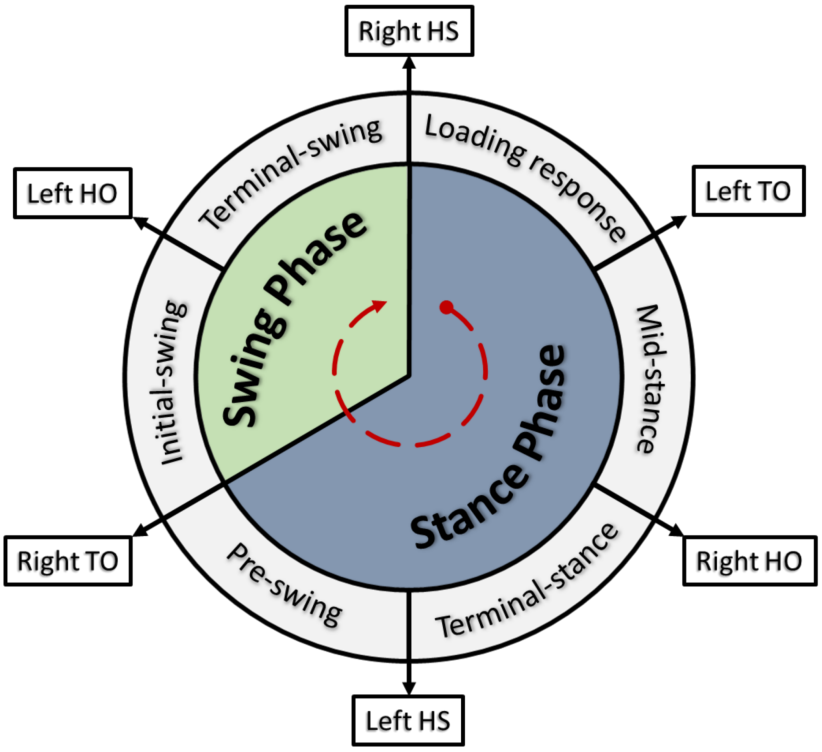


Figure 4.2: **Simplified stages of a typical gait cycle** for a right leg dominant subject. A new cycle begins with the right heel strike (HS) and both feet in contact with the floor. After a loading response, the left foot is lifted off the floor following the left Toe-off (TO), and weight starts shifting on the right foot from heel to mid-foot as the body moves forward. Once the body reaches mid-stance, the right heel loses contact with the floor during the right Heel-off (HO) stage, and weight shifts towards the right forefoot. To prepare for the right limb swing phase, the left foot contacts the floor again with a left heel strike (HS), and both feet are in contact with the floor, which is called double support. The right foot then enters the swing phase following the right Toe-off (TO), and the same stance process happens on the left foot, with weight shifting from heel to toe, and the respective left Heel-off (HO). The current gait cycle ends with the right HS, and a new cycle starts.

To record and study gait cycles, typical studies rely primarily and solely on the investigation of biomechanics of a subject's walking behaviours. Kinematic and kinetic analysis of gait allows for the investigation of joint displacements, torques, motor behaviours, and gait patterns, among others. However, alone, it is insufficient to fully characterise a subject's gait parameters. A purely anatomical/biomechanical exploration of gait disregards important physiological aspects that may be affecting the pathological gait. To mitigate this issue, any biomechanical studies of gait should be accompanied by synchronised muscle activity recordings. Through the association of kinematic analysis with electromyography, a more complete anatomical and physiological investigation of gait is made possible.

Clinical gait assessment relies on a trained clinician's visual and qualitative assessment of a sub-

ject's biomechanics. Several technologies have been developed over the past decades to assist the clinicians visual inspection and validation of the subject's mobility patterns, joint angles and general gait analysis. Employed solutions for gait analysis range nowadays from optical recording systems, to mechanical sensors and more advanced artificial intelligence characterisation tools via physiological signals.

The common practice for conducting gait analysis is to capture a subject's walking behaviour through optical motion capture systems. These systems are highly precise and can capture motion data with millimetre-level accuracy. However, they are restricted to laboratory settings due to the requirement for a controlled environment and equipment setup, limiting the ability to analyse natural walking patterns in real-life situations. Furthermore, the use of these systems is expensive, time-consuming, and requires expert technical staff to set up and operate the equipment. To address these challenges, wearable sensor technology has emerged as a cost-effective and accessible alternative for conducting gait analysis. These sensors can be attached to the subject's body or clothing and capture kinematic and physiological data during natural walking in unconstrained settings. The use of wearable technology also provides opportunities to conduct long-term monitoring of gait patterns, which can be used to assess changes in a patient's gait over time and evaluate the efficacy of treatment plans. To identify the most appropriate sensors for gait event detection during Activities of Daily Living (ADLs) and to pair with EMG analysis, a short review of available sensor technologies was conducted. One of the earliest reported wearable technologies for gait event detection uses foot-switches Winter et al. 1972. These sensors are usually embedded into the shoe or insole, located underneath the heel and hallux of the individual, allowing for the recording of two key gait events: Initial-Contact (IC), reported in healthy scenarios as the heel strike (HS), and End-of-Contact (EC) or Terminal Contact (TC), reported in healthy scenarios as the toe-off (TO). With current iterations such as insole pressure sensors (IPS) and force-sensitive resistors (FSR) fitted into footwear (e.g., Hanlon and Anderson 2009; Han et al. 2019; Nazmi et al. 2019), this technology is widely employed today and used as a benchmark for other motion capture systems (see Prasanth et al. 2021 for an up-to-date review). A common issue with these IPS and FSR systems is the constant wear-and-tear of the sensors due to associated shear forces in the sole or against the walking surface. This leads to short sensor lifespans and sensing accuracy loss after sustained periods of usage.

Nowadays, the most commonly employed wearable technology for gait event detection is accelerometry (Prasanth et al. 2021). First described in Morris 1973, this method makes use of acceleration sensors, strategically placed near a subject's joints on predetermined sites. The choice of placement will greatly influence the gait parameters extracted and takes into consideration possible noise motion artefacts that contaminate the recordings (e.g., poor sensor adhesion or loose clothing). With advances in wearable technology, typical accelerometer sensors were adapted into IMUs (Inertial Measurement Units), sensors that are able to detect both acceleration and angular velocity (through an integrated gyroscope) in all three dimensions. Depending on the desired gait parameters, the IMU sensors are most often placed at the foot (Jasiewicz et al. 2006; Hanlon and Anderson 2009; Tadano et al. 2013; Nwanna 2014; Ju et al. 2016; Park et al. 2016; Zhao et al. 2017; Mei et al. 2019; Zhen et al. 2019; Perez-Ibarra et al. 2020; Liu et al. 2021; Wouda et al. 2021) or shank/calf (Jasiewicz et al. 2006; Tadano et al. 2013; Grimmer et al. 2019; Gujarathi and Bhole 2019; Han et al. 2019; Zhen et al. 2019; Romijnders et al. 2021), but other studies present interesting alternatives as knee/thigh (Torrealba et al. 2007; Hanlon and Anderson 2009; Wentink et al. 2013; Ryu et al. 2019; Grimmer et al. 2019, waist (Yang et al. 2011) or even head (Hwang, Reh, A. Effenberg, et al. 2016; Hwang, Reh, A. O. Effenberg, et al. 2021) placements.

During the aforementioned gait events (i.e., HS and TO), there are distinguishable peaks in the vertical acceleration profiles that can be used to identify the timing of HS and TO. Upon contacting the surface, the heel experiences a vertical force (ground-reaction force) and its respective upward acceleration, which is identifiable when inspecting the recorded signal. In addition to gait event detection, IMUs also present benefits in the detection of angular displacements and velocities of different joints (Wouda et al. 2021; Han et al. 2019; Zhao et al. 2017) as well as pedestrian tracking solutions (Ju et al. 2016). With state-of-the-art sensor synchronisation, current IMU solutions also provide accurate position estimation for the subjects wearing the sensors, as described in Schepers et al. 2018. Due to all these features, comparison studies (Tadano et al. 2013; Prasanth et al. 2021; Han et al. 2019; Nazmi et al. 2019; Wouda et al. 2021; Hanlon and Anderson 2009) often place the IMU as a preferable wearable solution over the previously discussed alternatives (i.e., FSR and Optical systems). Even if the IMU is not as accurate as the FSR or as thorough in limb position detection through optical systems, the IMU sensor's durability, robustness, cost, and applicability outweigh the benefits of these other technologies in ADL gait detection applications.

So far, the wearable technologies presented here rely on external interactions of the individual with the sensors (e.g., pressure applied on the IPS) or measurements of external inferred parameters (e.g., the body part acceleration or angular velocity as measured by the IMU) to identify key gait events. An alternative is to make use of the aforementioned patient's physiological signals, as muscle activity recordings through surface Electromyography (sEMG), to estimate the timing of the events. sEMG provides a reliable non-invasive solution to analyse muscle activity levels during varied motor tasks, and in a non-invasive manner. sEMG can be used to diagnose motor activity, where the recorded muscle activity is analysed to identify muscle deficiencies, and/or establish individual muscle function levels during pre-defined tasks. This has been specifically used for the analysis of gait, using analysis of the sEMG recorded from hip, knee and ankle flexor and extensor muscles, reported in Tao et al. 2012; Wentink et al. 2013; Suwansawang 2018; Morbidoni et al. 2019; Nazmi et al. 2019; Ryu et al. 2019 with positive evidence for differentiating activity in different segments of the gait cycle. However, as it is a biological signal, sEMG is prone to high noise and variability, depending on sensor location and other biological factors.

To interpret muscle activity features and classify these into gait events, studies often return to the use of machine learning algorithms (Wentink et al. 2013; Morbidoni et al. 2019; Nazmi et al. 2019; Ryu et al. 2019). Unfortunately, as mentioned, there are several factors that may interfere with the sEMG quality and the accuracy of these classification algorithms, especially when recognising how volatile and different the recorded signals can be across different individuals, and even in different muscles of the same individual.

All these wearable solutions present promising results for gait event detection, through varied technologies and algorithms. The complexity of such tools decides how viable it is for applications of gait assessment during ADLs. A summary of the advantages and disadvantages of the discussed technologies is presented in Table 4.1. Unfortunately, these solutions seldom come with a clear methodology of how to apply these tools to detect the most simple of gait events, rarely offering the algorithms to do so. In this method paper, we propose a simplified method of heel strike detection for synchronised sEMG segmentation through IMU data paired with sEMG recordings, applied to the diverse and unconstrained dataset of Brantley et al. 2018. This method allows for a joint biomechanical and physiological investigation of gait. We further test sMaSDP with kinematic IMU samples of data from Bächlin et al. 2010, looking at

Parkinson's Disease (PD) gait.

Table 4.1: Summary of advantages and disadvantages of presented gait event detection solutions, in terms of applicability, interface, robustness and cost.

Sensor Type	Advantages	Disadvantages
Optical Systems	Full-body kinematics. High marker detection precision and accuracy. Accurate estimation of joint position, angle, velocity and acceleration. Synchronisation solutions with other gait assessment hardware (EMG kits).	High cost and maintenance. High performance requirements. Restricted experimental environments. Multiple camera synchronisation and calibration. Setup and collection learning curve. Imposes long donning and doffing times of retroreflective markers, as well as initial setup per subject.
FSRs and IPSs	Ideal for detection of key gait events as heel-strike and toe-off. Low-cost solution, with lower number of sensors required for event detection. Typical benchmark for other gait assessment technologies	Low durability, sensor wearing out. Depending on sensor application site, may impact the subject's walking style. Uneven terrain and uncharacteristic gait behaviours may lead to accidental noise event recordings.
IMUs	Simple configuration and multitude of solutions to interface with other hardware (EMG kits). Low-cost and high availability. Applicability to diverse gait environments, especially when using wearable solutions. Easy and quick donning and doffing of the sensors to and across subjects.	Lower accuracy. Wearable solutions are battery dependent. High susceptibility to motion artefact noises, depending on application site and surface (directly on the skin or over clothing). Position estimation requires multiple synchronised sensors.
Surface EMG	Valuable physiological information of muscle activity patterns involved in gait. May be used to identify personal muscle recruitment schemes used per individual.	Extremely high inter-subject variability. Hard to characterise gait by itself and requires significant subject by subject adjustments.

4.2.4 Methodology

The following section details the steps, and associated scripts, to isolate sEMG activity patterns in different unconstrained gait modalities, based on the kinematic dataset of Brantley et al. 2018. This guide contains step-by-step information about using recordings from an IMU system (XSens 2021), with focus on an IMU sensor on the subject's dominant leg foot, to identify heel strike events and timestamps during different gait modalities. The presented preprocessing and processing steps described for the gait event detection and sEMG segmentation are demonstrated and discussed in the following separate subsections. The designed presented algorithms were coded in *MATLAB*(MATLAB 2020).

The dataset provided in Brantley et al. 2018 contains unconstrained walking data from 10 healthy subjects (five males, five females, ages between 18–31 years old), with no known neurological disorders. Kinematic (through IMU system XSens 2021) and sEMG recordings were collected from each subject participating in the experiment. For the design of the sMaSDP algorithm herein presented, special focus was given only to the sensors presented in Figure 4.3.

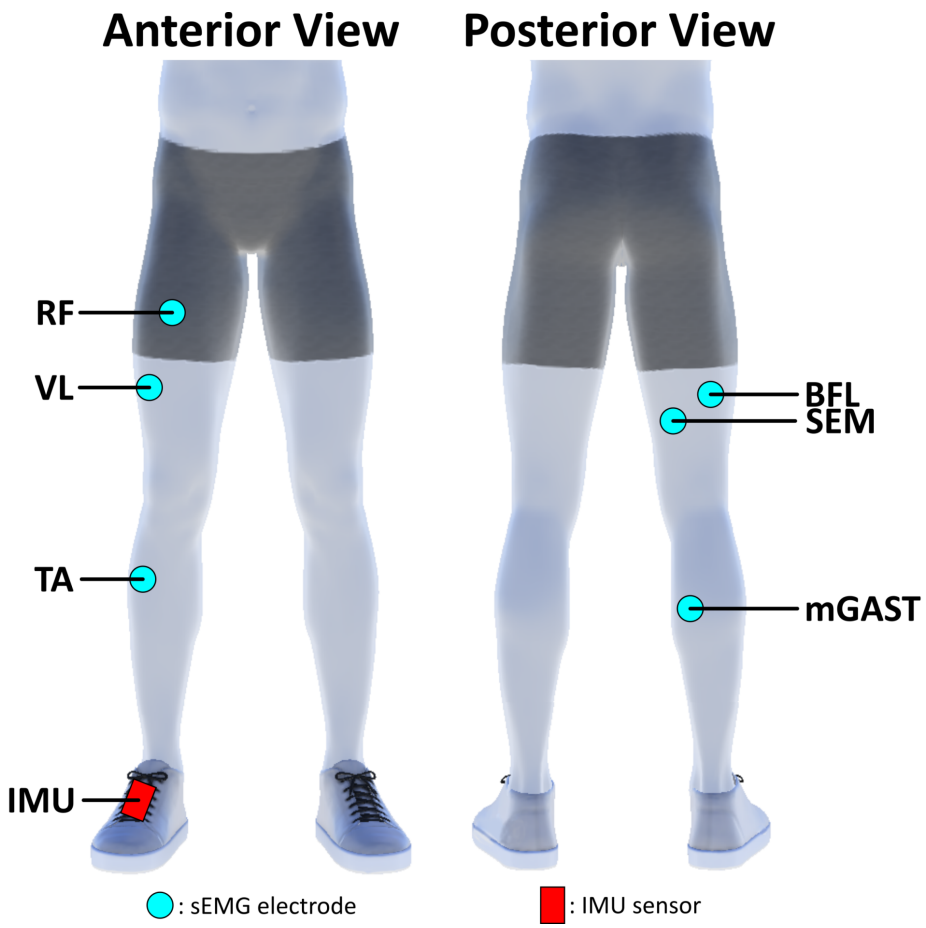


Figure 4.3: **Schematic of the sEMG and IMU sensor placement locations**. sEMG recordings were taken from Tibialis Anterior (TA), Medial Gastrocnemius (mGAST), Vastus Lateralis (VL), Rectus Femoris (RF), Semitendinosus (SEM) and Biceps Femoris Longus (BFL). The IMU sensor was attached on top of the subject's shoe, at the centre of the right foot.

In this experiment, subjects walk through a designed walking course, encompassing a ramp, level ground and staircase sections, for a total of 20 trials per subject. In each trial, the subject walks up and down the ramp and staircase, as well as a section of level ground walking, providing recordings for five different walking modalities. For ease of referencing, please consider the following acronyms:

- RA: ramp ascent.
- RD: ramp descent.
- SA: staircase ascent.
- SD: staircase descent.
- LGW: level ground walking.

To accompany and summarise the following methodology, Figure 4.4 details the required steps and processes for the kinematic and sEMG data.

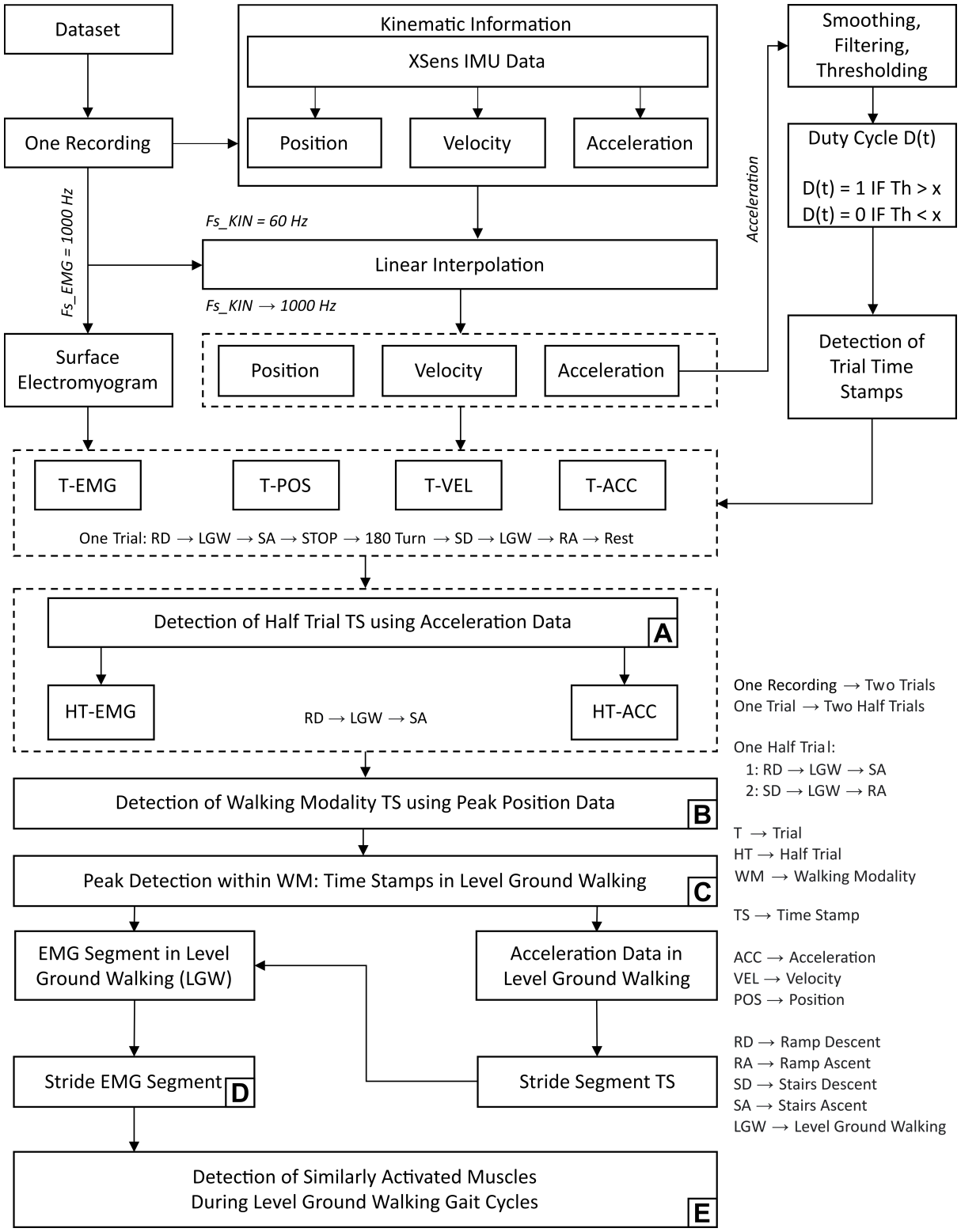


Figure 4.4: **Summary of method architecture**: the diverse multi-step process, from the recorded IMU signals, filtering of movement periods, segmentation into different walking modalities and identification of HS moments. Steps labelled **A** to **E** establish a logical link between this architecture and the results.

4.2.4.1 Interpolation and Kinematic Activity Segmentation

Kinematic data (KIN) and sEMG data were recorded at the synchronously, but they have different sampling rates. Temporal synchronisation ensures that both recordings have the same duration, but the number of samples captured for each signal during this time varies due to the different sampling rates. The difference in sampling frequencies between KIN and sEMG is primarily due to the sample capture and processing capabilities of the recording equipment, as well as the amount of data generated per sample. Optical kinematic systems typically use a sampling frequency of around 120 Hz (Marmelat et al. 2019), which is much lower than the typical frequencies of 1000 Hz or higher for sEMG systems. For IMUs, research has shown that a capture frequency of 60 Hz is sufficient to record kinematic events while maintaining acceptable processing requirements (Zhou et al. 2020). However, for sEMG, the higher end of the sEMG signal frequency band can reach 500 Hz (see Clancy et al. 2002). Therefore, to capture all the nuances of the sEMG signal effectively, a sampling frequency of 1000 Hz or higher is required according to the Nyquist frequency principle. In the dataset of Brantley et al. 2018, sEMG was recorded at a sampling frequency of 1000 Hz, while the IMU was recorded at a sampling frequency of 60 Hz. Consequently, sEMG data had approximately 17 times more samples than IMU data.

To use kinematics as an indicator for segmentation timestamps in the sEMG counterpart, the kinematic signal requires upsampling to match the number of sEMG datapoints. This process ensures that both KIN and sEMG recordings are synchronised in time and samples, in order to use the kinematic datapoints to achieve pinpoint accuracy. A moving average smoothing filter is then applied to KIN to remove unwanted oscillations and initial motion noise from the signal. After the smoothing filter is applied, the kinematic signals are upsampled via linear interpolation (Equation (4.1)):

$$y = y_1 + (x - x_1)\frac{(y_2 - y_1)}{(x_2 - x_1)} \tag{4.1}$$

where y is the interpolated value, x is the sample datapoint to perform interpolation, y_1 and y_2 are the first and second signal samples, and x_1 and x_2 are the first and second datapoints.

This pre-processed sEMG and the upsampled KIN data consist of two complete walk trials, each including all five walking modalities previously discussed (RA, RD, SA, SD, and LWG)

for each subject. A minimal energy threshold and window is created to isolate and timestamp meaningful movement identified using the IMU acceleration. Any signal fragment discovered inside a passing window that is less than a certain energy level is categorised as '0'. Similarly, if significant acceleration is generated beyond the threshold regarded as evidence of the subject walking, it is recorded as '1'. As a result, a binary signal is generated identifying data points of relevant walking activity.

4.2.4.2 Filtering Small Movement Artefacts and Separating Trials from a Single Recording

The core objectives of this section are to filter out movement and/or transition artifacts from the IMU signal, considered as noise, and to identify the direction of movement, as the walking modalities presented are dependent on the direction of the walking course. The output of the previous section is a duty-cycle type wave, depicted as the grey square wave in Figure 4.5A, which presents binary values of 1 when the subject is active and 0 when the subject is standing still. The start and end of active periods define the timepoints at which walking starts and ends. As the subjects complete the trials continuously without taking unnecessary breaks between walking modalities, any detected activity below a threshold of 6000 data points (or 6 s) is classified as a motion artifact or noise.

In the experiment, each recording consists of two trials. In a single trial, a subject walks the course in a forward direction, rests at a designated location (B), and then returns to the starting point (A) by walking in the reverse direction of the course. Each walking direction (A-B and B-A) is defined as a "half-trial". Therefore, a single recording has four half-trials, with two being the subject walking from the starting point (A) to point (B), and two where the subject walks in the reverse direction from point (B) to point (A). From the complete recordings, four moments of activity are extracted and stored as an independent variable to define the direction in which the subject walked the course.

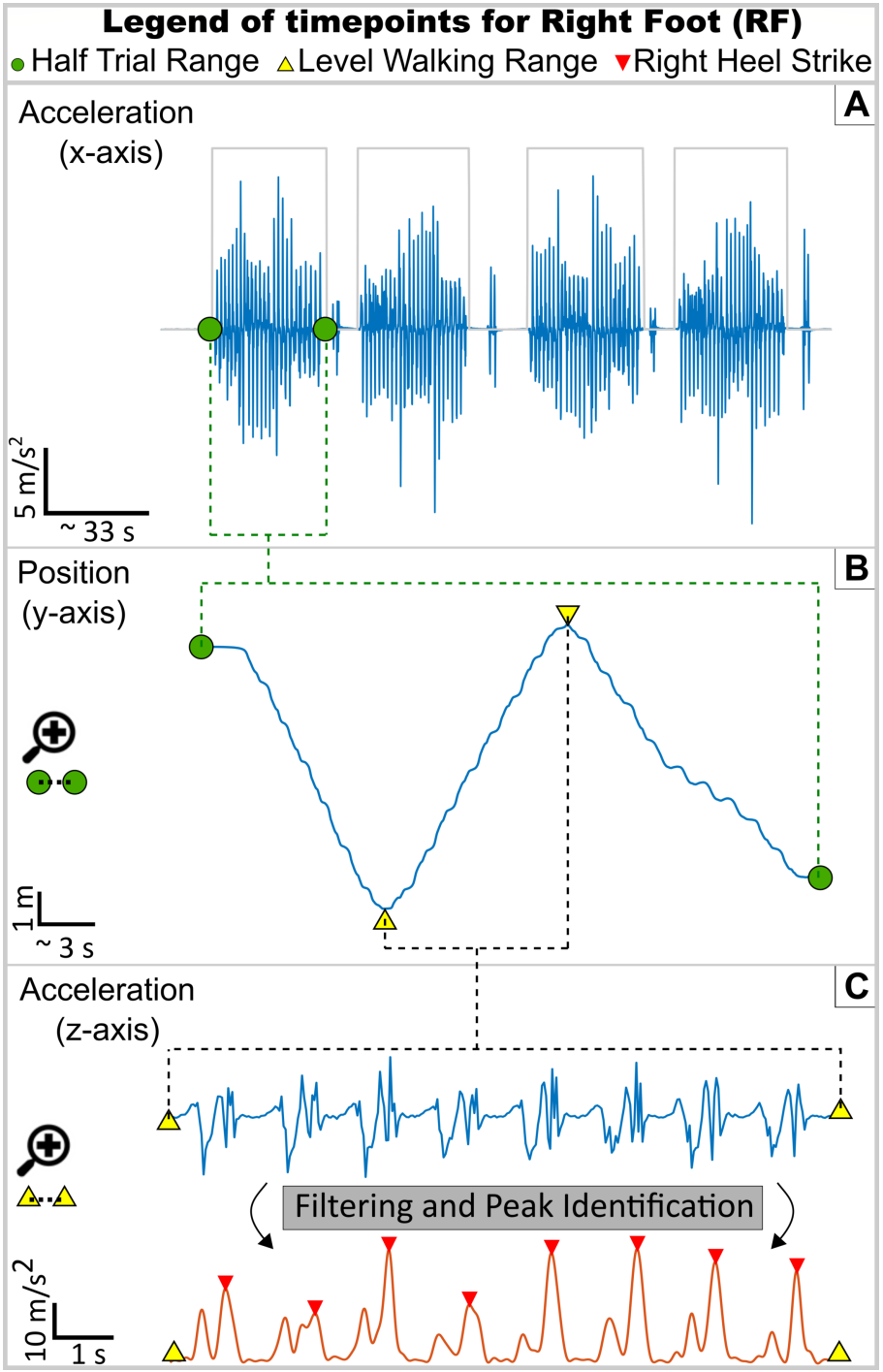


Figure 4.5: **Summary diagram illustrating the different stages of the method**, presented and linked in Figure 4.4, for the duration of an HT (RD,LGW,SA): in Section (**A**), the x-axis acceleration of the right-foot IMU is used to identify the initial HT start and end timepoints, marked with the green circles; within the time range defined by the HT green circles, Section (**B**) now takes the y-axis position data from the IMU to identify the sharp direction turns related to switches in walking modality, represented here by the yellow triangles; lastly, within the isolated LGW modality between the yellow triangles, Section (**C**) uses the z-axis acceleration from the IMU, and through our filtering and peak identification algorithm, identifies the HS events, marked by the red triangles.

4.2.4.3 Initial sEMG Segmentation and Direction, Using the Timepoints Defined by the Four Moments of Activity per Complete Trial

The extracted timestamps for the start and end of each half-trial are used to segment the sEMG and KIN signals. The sEMG recordings provided in this dataset are in raw format. The objective of this stage is to remove noise from movement artefacts, possible recording interference, and isolate relevant frequency content from the data. To achieve this purpose, a fourth-order Butterworth bandpass filter is designed to filter out any sEMG signals outside the 10 to 150 Hz band. Additionally, a notch filter is used to remove powerline interference at 60 Hz.

The next objective is to cut both sEMG and KIN signals using the previously defined half-trial timestamps. For this purpose, a timestamp with a safety margin of 2000 data points (2 s) is used to ensure the inclusion of all relevant activity. sEMG and KIN are then segmented into activity bins based on half-trials for all trials and all subjects.

As mentioned, per complete trial, four moments of walking activity are detected (example in Figure 4.5A), related to walking the course twice in the forward and twice in the reverse directions, as described previously between (A) to (B). Based on the extracted timestamps and the experiment methodology, the sequence of modalities in the forward direction is separated into RD, LGW and SA, and for the reverse course direction, separated into SD, LGW and RA.

4.2.4.4 Walking Modality Identification within Each Direction of the Course and Trials

At this stage, sEMG and KIN signals for all trials are segmented and separated according to the direction of the course the subject is walking along. The next step is to identify the timestamps for each walking modality within the forward and reverse courses, and isolate these in both the sEMG and KIN signals. Due to the design of the course, subjects take a sharp turn at the transition between each modality (example on Figure 4.5B). This is identified via the estimated position changes as recorded by the IMU. Focusing on the y-axis, any time there is a peak transition, a new modality begins, according to the course guide mentioned earlier. This, paired with safety margins, is then used to further segment both sEMG and KIN into the individual walking modalities.

4.2.4.5 Using Acceleration Data to Identify the Moment of Heel Strike

Having the data segmented into different walking modalities, the next step is to identify gait cycles within each walking modality. Through acceleration data in the vertical direction (z-axis), the moment of HS can be identified. To do so, new filters are designed to isolate the vertical peaks of acceleration witnessed when the heel strikes the ground, and experiences the ground-reaction force. Two separate seventh-order Butterworth filters are created: a high-pass at 9 Hz and a low-pass at 6 Hz. These remove a band where specific motion artefacts lie, and isolate the striking moments. Being post-hoc, these filters are ideal and do not impose any delays on the data.

The filtering process is as follows:

- the high-pass filter is applied to the raw KIN data, removing frequencies below the 20 Hz band, and potential movement artefacts.
- a half-wave rectifier is applied to the resulting filtered data, removing unnecessary negative electrical oscillations imposed by the sensor readings.
- a low-pass filter is applied to the rectified data, serving as an anti-aliasing filter at 5 Hz, to remove oscillations from the signal.

The HS moment is identified as the highlighted peaks in the Filtering and Peak section of Figure 4.5C. Extracting the timestamps of each of these peaks allows then for the isolation of a complete stride, or gait cycle, from one heel strike moment to the immediate next of the same limb. These timestamps are then finally used to segment the sEMG activity into separate gait cycles.

4.2.5 Results

Figure 4.5C presents the identified the moments of HS, for a segment of level ground walking, from a randomly selected subject. In the other walking modalities, there was a noticeable shift in the amplitude of the ground-reaction force acceleration and an adjusted cadence. Through simple adjustment of the expected acceleration peaks allowed for HS to equally as recognisable and identified in these different walking modalities using sMaSDP.

Through the identified gait event timestamps, computed from the IMU data, individual gait cycles are then extracted. Using the timestamps of each gait cycle, sEMG and kinematic data is

segmented per cycle. In Figure 4.6, an example of sEMG activity is presented for the same level ground walking segment of Figure 4.5. Within the isolated gait cycles, we can identify the muscle activity patterns from the segmented sEMG data, as seen in Figure 4.7. Both biomechanical data and physiological data can be correlated at this point, to best characterise this subject's gait. The noticeable variability seen in the muscle activity levels of Figure 4.7 highlights once more the necessity of a paired kinematic measure associated with the this physiological data to best discriminate the witnessed motions. This muscle activity variability also demonstrates the adaptability of our physiological neural control signal, even in seemingly simple and rhythmic motions, as level ground gait.

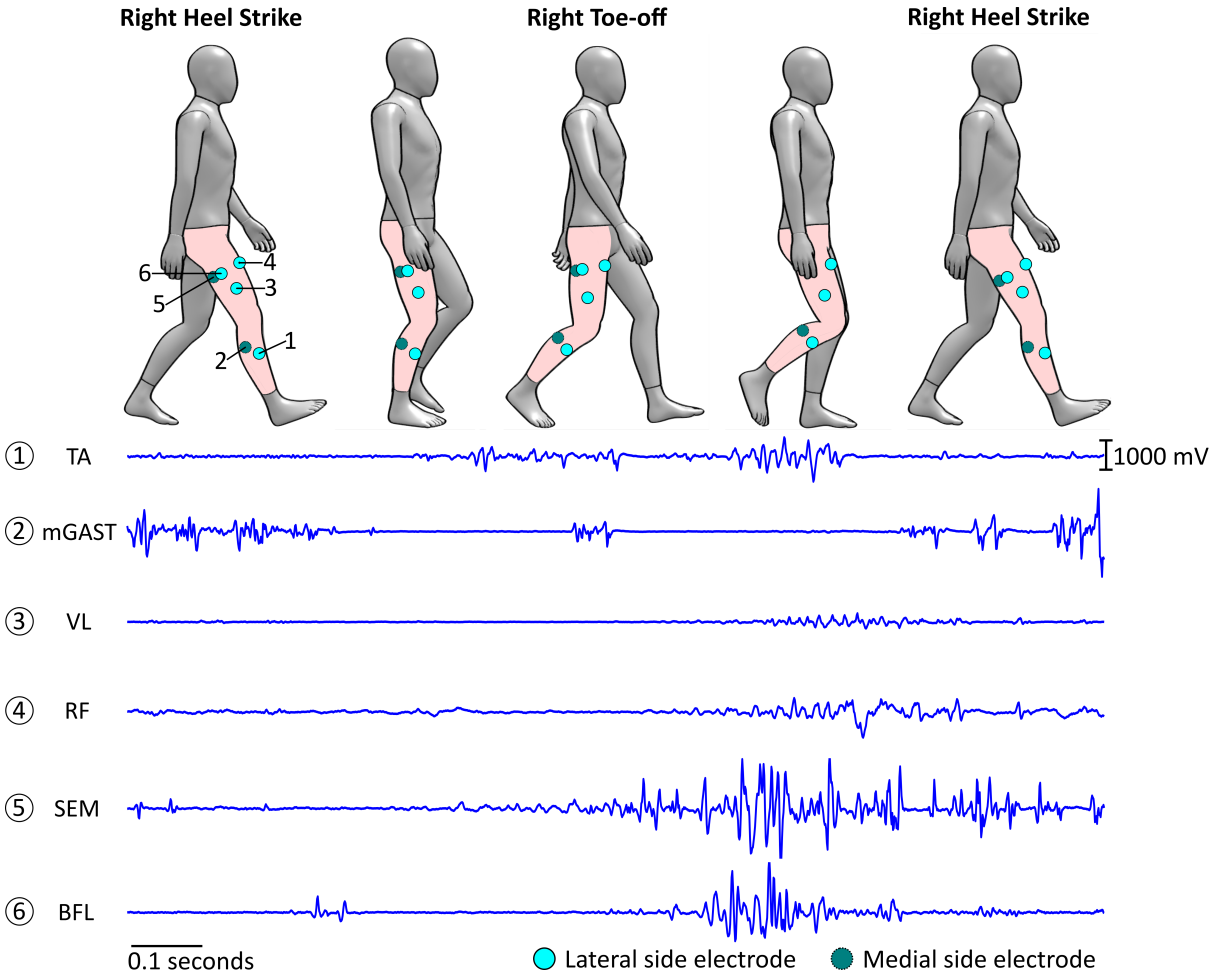


Figure 4.6: **Segmented sEMG from a single extracted gait cycle**: top section diagram represents a full gait cycle, as initially described (Figure 4.2), with the respective locations of the sEMG sensors; the bottom traces are the segmented sEMG recordings for the respective gait cycle. Linked, as labelled, to step **D** of the method architecture (Figure 4.4).

As a proof of concept, this algorithm was applied to another unconstrained walking dataset Bächlin et al. 2010, to PD patient data, where subjects performed a series of walking tasks in

a therapy scenario. PD patients have known abnormal gait patterns, as irregular stepping and shuffle gait. In the dataset of Bächlin et al. 2010, patients were fitted with an IMU placed on their dominant foot, following a similar placement as seen in Brantley et al. 2018 and Figure 4.3. Unlike the dataset (Brantley et al. 2018) used to design our algorithm, the experiment with the PD patients did not collect sEMG recordings, and the focus in this scenario is only on the kinematic gait data. With fine tuning of cadence and velocity parameters, through adjustments of the peak detection section, all the moments of HS are detected over an entire trial (over 1 min). Results for the sMaDSP detection of the HS events, from a randomly selected trial and subject of this dataset, are presented in Figure 4.8.

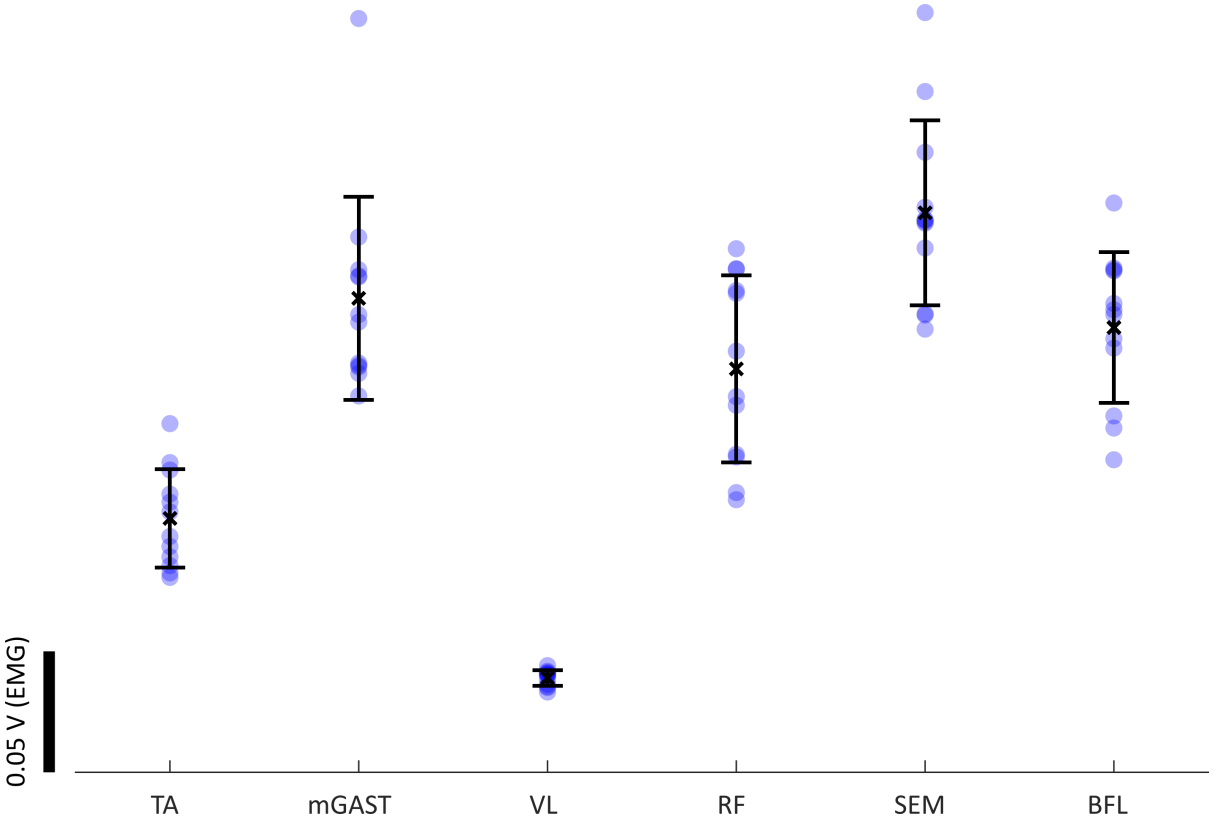


Figure 4.7: **Observations with mean and standard deviation of muscle activity extracted** from 12 LGW gait cycles from a randomly selected trial and subject. Analysing this activity in different walking modalities allows for quantification of the variability in each muscle and the impact on the person's mobility. Linked, as labelled, to step **E** of the method architecture (4.4).

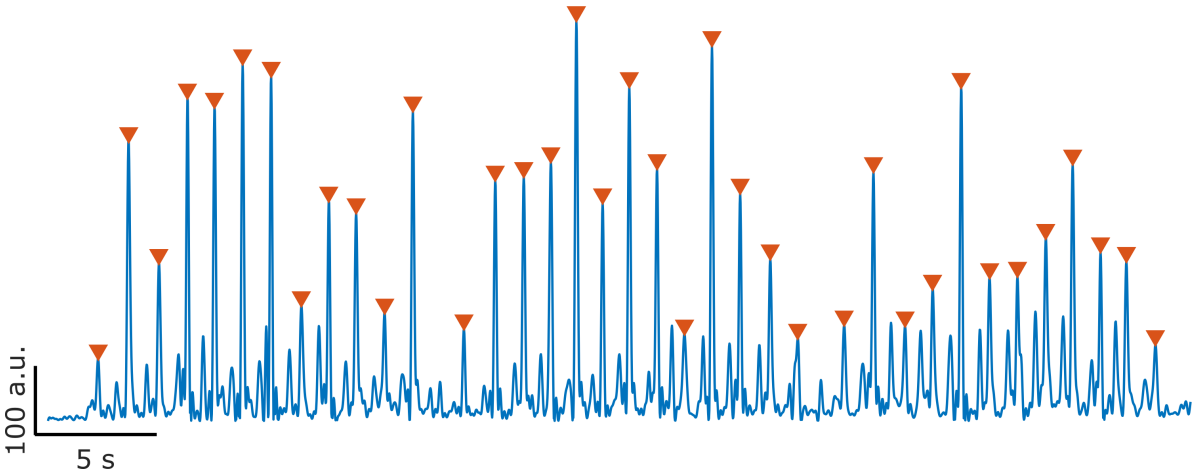


Figure 4.8: **HS detection on unconstrained Parkinson gait**, computed from IMU data from the publicly available dataset of Bächlin et al. 2010; Dua and Graff 2017. The presented data were recorded from a PD patient, supervised by a therapist. Within this recording the PD patient walks freely in three separate modalities: straight walking, "random walking" and ADL walking. HS events are here detected for all modalities.

4.2.6 Discussion and Conclusions

Tracking patients' performance levels at their own homes and through their daily lives is of massive benefit for the design of smarter continued therapies. With the ambition of continued, supervised at-home therapies and improved rehabilitation, it is essential that researchers are provided with simple guides on using the technology and appropriate methodology to provide them the foundation for exploring therapeutic mobility. With advancements in sensor design, it is now possible to bring these tools to our everyday lives, and gait assessment to activities of daily living.

Even in the ADL scenario, as demonstrated, kinematics alone may not provide sufficient information to therapists to fully assess patients' mobility. Integration of muscle activity levels, associated with recorded movements and gait events will benefit not only diagnosis but performance assessment. With simplification of the acquisition and processing algorithms, as well as selection of appropriate wearable sensors, a platform that integrates both kinematics and sEMG for home use becomes feasible. With this report, a simplified guide for kinematic and sEMG recording segmentation, and gait event detection was presented and fully documented. Codes and algorithms, that work with the dataset of Brantley et al. 2018 are made available alongside this method. To adapt to other datasets, users can easily adjust expected cadence or filter level

variables, improving detection and allowing the study of different walking modalities, providing an initial framework for researchers to explore and adjust to their needs and data.

Synchronising both sEMG and kinematic information is the step forward to better characterise movement, and it is crucial that both signals are analysed concurrently. Analysis of non-invasive sEMG recordings in ADLs should be prioritised to define the patterns of muscle activity that generate movement. The same level of "wearable" exploration that kinematics and gait cycle has received over the past decades, needs to be pursued for the sEMG case.

With adjustable parameters, our sMaSDP algorithm can be adapted to further ADLs scenarios, and potentially applied to patient's smartphones, for a continuous kinematic recording. Due to its simplicity and focus to aid newcomers to the gait studies area, this algorithm can also be combined with machine learning in future iterations, to allow ad-hoc heel strike identification.

4.2.7 Abbreviations

The following abbreviations are used in this manuscript:

ACC Acceleration

ADLs Activities of Daily Living

EMG Electromyography

EC End-of-Contact

FSR Force Sensitive Resistors

HS Heel-strike

HO Heel-off

HT Half Trial

IC Initial Contact

IPS Insole Pressure Sensors

IMU Inertial Measurement Unit

KIN Kinematics

LGW Level Ground Walking

PD Parkinson's Disease

POS Position

RA Ramp Ascent

RD Ramp Descent

SA Stairs Ascent

SD Stairs Descent

T Trial

TC Terminal Contact

TO Toe-off

TS Time Stamps

VEL Velocity

4.2.8 References

Bächlin, M., Plotnik, M., Roggen, D., Maidan, I., Hausdorff, J. M., Giladi, N., and Tröster, G. (2010). "Wearable Assistant for Parkinson's Disease Patients with the Freezing of Gait Symptom". In: *Trans. Info. Tech. Biomed.* 14.2, pp. 436–446. ISSN: 1089-7771. DOI: 10.1109/TITB.2009.2036165. URL: https://doi.org/10.1109/TITB.2009.2036165.

Brantley, J. A., Luu, T. P., Nakagome, S., Zhu, F., and Contreras-Vidal, J. L. (2018). "Full body mobile brain-body imaging data during unconstrained locomotion on stairs, ramps, and level ground". en. In: *Scientific Data* 5.1, p. 180133. ISSN: 2052-4463. DOI: 10.1038/sdata.2018.133. URL: http://www.nature.com/articles/sdata2018133 (visited on 04/04/2022).

Clancy, E., Morin, E., and Merletti, R. (2002). "Sampling, noise-reduction and amplitude estimation issues in surface electromyography". In: *Journal of Electromyography and Kinesiology* 12.1, pp. 1–16. DOI: 10.1016/s1050-6411(01)00033-5.

Dua, D. and Graff, C. (2017). *UCI Machine Learning Repository*. URL: http://archive.ics.uci.edu/ml.

Grimmer, M., Schmidt, K., Duarte, J. E., Neuner, L., Koginov, G., and Riener, R. (2019). "Stance and Swing Detection Based on the Angular Velocity of Lower Limb Segments During Walking". en. In: *Frontiers in Neurorobotics* 13, p. 57. ISSN: 1662-5218. DOI: 10.3389/fnbot.2019.00057. URL: https://www.frontiersin.org/article/10.3389/fnbot.2019.00057/full (visited on 04/04/2022).

Gujarathi, T. and Bhole, K. (2019). "Gait Analysis using IMU sensor". en. In: *2019 10th International Conference on Computing, Communication and Networking Technologies (ICCCNT)*. Kanpur, India: IEEE, pp. 1–5. ISBN: 978-1-5386-5906-9. DOI: 10.1109/ICCCNT45670.2019.8944545. URL: https://ieeexplore.ieee.org/document/8944545/ (visited on 04/04/2022).

Han, Y. C., Wong, K. I., and Murray, I. (2019). "Gait Phase Detection for Normal and Abnormal Gaits Using IMU". en. In: *IEEE Sensors Journal* 19.9, pp. 3439–3448. ISSN: 1530-437X, 1558-1748, 2379-9153. DOI: 10.1109/JSEN.2019.2894143. URL: https://ieeexplore.ieee.org/document/8620997/ (visited on 04/04/2022).

Hanlon, M. and Anderson, R. (2009). "Real-time gait event detection using wearable sensors". en. In: *Gait & Posture* 30.4, pp. 523–527. ISSN: 09666362. DOI: 10.1016/j.gaitpost.2009.07.128. URL: https://linkinghub.elsevier.com/retrieve/pii/S0966636209003373 (visited on 04/04/2022).

Hwang, T.-H., Reh, J., Effenberg, A., and Blume, H. (2016). "Real-time gait event detection using a single head-worn inertial measurement unit". en. In: *2016 IEEE 6th International Conference on Consumer Electronics - Berlin (ICCE-Berlin)*. Berlin, Germany: IEEE, pp. 28–32. ISBN: 978-1-5090-2096-6. DOI: 10.1109/ICCE-Berlin.2016.7684709. URL: http://ieeexplore.ieee.org/document/7684709/ (visited on 04/04/2022).

Hwang, T.-H., Reh, J., Effenberg, A. O., and Blume, H. (2021). "Validation of Real Time Gait Analysis Using a Single Head-Worn IMU". en. In: *EKC 2019 Conference Proceedings*. Ed. by J. M. Park and D. R. Whang. Singapore: Springer Singapore, pp. 87–97. DOI: 10.1007/978-981-15-8350-6_8. URL: http://link.springer.com/10.1007/978-981-15-8350-6_8 (visited on 04/04/2022).

Jasiewicz, J. M., Allum, J. H., Middleton, J. W., Barriskill, A., Condie, P., Purcell, B., and Li, R. C. T. (2006). "Gait event detection using linear accelerometers or angular velocity transducers in able-bodied and spinal-cord injured individuals". en. In: *Gait & Posture* 24.4, pp. 502–509. ISSN: 09666362. DOI: 10.1016/j.gaitpost.2005.12.017. URL: https://linkinghub.elsevier.com/retrieve/pii/S0966636206000129 (visited on 04/04/2022).

Ju, H., Lee, M. S., Park, S. Y., Song, J. W., and Park, C. G. (2016). "A pedestrian dead-reckoning system that considers the heel-strike and toe-off phases when using a foot-mounted IMU". en. In: *Measurement Science and Technology* 27.1, p. 015702. ISSN: 0957-0233, 1361-6501. DOI: 10.1088/0957-0233/27/1/015702. URL: https://iopscience.iop.org/article/10.1088/0957-0233/27/1/015702 (visited on 04/04/2022).

Liu, X., Li, N., Xu, G., and Zhang, Y. (2021). "A Novel Robust Step Detection Algorithm for Foot-Mounted IMU". en. In: *IEEE Sensors Journal* 21.4, pp. 5331–5339. ISSN: 1530-437X, 1558-1748, 2379-9153. DOI: 10.1109/JSEN.2020.3030771. URL: https://ieeexplore.ieee.org/document/9222113/ (visited on 04/04/2022).

Marmelat, V., Duncan, A., and Meltz, S. (2019). "Effect of sampling frequency on fractal fluctuations during treadmill walking". In: *PLOS ONE* 14.11. DOI: 10.1371/journal.pone.0218908.

MATLAB (2020). *version 9.8.0 (R2020a)*. Natick, Massachusetts, USA: The MathWorks Inc.

Mei, C., Gao, F., and Li, Y. (2019). "A Determination Method for Gait Event Based on Acceleration Sensors". en. In: *Sensors* 19.24, p. 5499. ISSN: 1424-8220. DOI: 10.3390/s19245499. URL: https://www.mdpi.com/1424-8220/19/24/5499 (visited on 04/04/2022).

Morbidoni, C., Cucchiarelli, A., Fioretti, S., and Di Nardo, F. (2019). "A Deep Learning Approach to EMG-Based Classification of Gait Phases during Level Ground Walking". en. In: *Electronics* 8.8, p. 894. ISSN: 2079-9292. DOI: 10.3390/electronics8080894. URL: https://www.mdpi.com/2079-9292/8/8/894 (visited on 04/04/2022).

Morris, J. (1973). "Accelerometry—A technique for the measurement of human body movements". In: *Journal of Biomechanics* 6.6, pp. 729–736. ISSN: 0021-9290. DOI: https://doi.org/10.1016/0021-9290(73)90029-8. URL: https://www.sciencedirect.com/science/article/pii/0021929073900298.

Nazmi, N., Abdul Rahman, M. A., Yamamoto, S.-I., and Ahmad, S. A. (2019). "Walking gait event detection based on electromyography signals using artificial neural network". en. In: *Biomedical Signal Processing and Control* 47, pp. 334–343. ISSN: 17468094. DOI: 10.1016/j.bspc.2018.08.030. URL: https://linkinghub.elsevier.com/retrieve/pii/S1746809418302283 (visited on 04/04/2022).

Nwanna, O. (2014). "Validation of an Accelerometry Based Method of Human Gait Analysis". en. PhD thesis. Cleveland State University,USA, p. 87.

Park, S. Y., Ju, H., and Park, C. G. (2016). "Stance Phase Detection of Multiple Actions for Military Drill Using Foot-mounted IMU". en. In: *International Conference on Indoor Positioning and Indoor Navigation*, p. 4.

Perez-Ibarra, J. C., Siqueira, A. A. G., and Krebs, H. I. (2020). "Real-Time Identification of Gait Events in Impaired Subjects Using a Single-IMU Foot-Mounted Device". en. In: *IEEE Sensors Journal* 20.5, pp. 2616–2624. ISSN: 1530-437X, 1558-1748, 2379-9153. DOI:

10.1109/JSEN.2019.2951923. URL: https://ieeexplore.ieee.org/document/8892503/ (visited on 04/04/2022).

Prasanth, H., Caban, M., Keller, U., Courtine, G., Ijspeert, A., Vallery, H., and Zitzewitz, J. von (2021). "Wearable Sensor-Based Real-Time Gait Detection: A Systematic Review". en. In: *Sensors* 21.8, p. 2727. ISSN: 1424-8220. DOI: 10.3390/s21082727. URL: https://www.mdpi.com/1424-8220/21/8/2727 (visited on 04/04/2022).

Romijnders, R., Warmerdam, E., Hansen, C., Welzel, J., Schmidt, G., and Maetzler, W. (2021). "Validation of IMU-based gait event detection during curved walking and turning in older adults and Parkinson's Disease patients". en. In: *Journal of NeuroEngineering and Rehabilitation* 18.1, p. 28. ISSN: 1743-0003. DOI: 10.1186/s12984-021-00828-0. URL: https://jneuroengrehab.biomedcentral.com/articles/10.1186/s12984-021-00828-0 (visited on 04/04/2022).

Ryu, J., Lee, B.-H., Maeng, J., and Kim, D.-H. (2019). "sEMG-signal and IMU sensor-based gait sub-phase detection and prediction using a user-adaptive classifier". en. In: *Medical Engineering & Physics* 69, pp. 50–57. ISSN: 13504533. DOI: 10.1016/j.medengphy.2019.05.006. URL: https://linkinghub.elsevier.com/retrieve/pii/S1350453319300931 (visited on 04/04/2022).

Schepers, M., Giuberti, M., and Bellusci, G. (2018). *Xsens MVN: Consistent Tracking of Human Motion Using Inertial Sensing*. en. Unpublished. DOI: 10.13140/RG.2.2.22099.07205. URL: http://rgdoi.net/10.13140/RG.2.2.22099.07205 (visited on 04/04/2022).

Suwansawang, S. (2018). "Analysis of human locomotion using analytic wavelets applied to electromyographic data from healthy controls and Parkinson's patients". en. PhD thesis. University of York, UK, p. 178.

Tadano, S., Takeda, R., and Miyagawa, H. (2013). "Three Dimensional Gait Analysis Using Wearable Acceleration and Gyro Sensors Based on Quaternion Calculations". en. In: *Sensors* 13.7, pp. 9321–9343. ISSN: 1424-8220. DOI: 10.3390/s130709321. URL: http://www.mdpi.com/1424-8220/13/7/9321 (visited on 04/04/2022).

Tao, W., Liu, T., Zheng, R., and Feng, H. (2012). "Gait Analysis Using Wearable Sensors". en. In: *Sensors* 12.2, pp. 2255–2283. ISSN: 1424-8220. DOI: 10.3390/s120202255. URL: http://www.mdpi.com/1424-8220/12/2/2255 (visited on 04/04/2022).

Torrealba, R., Castellano, J., Fernández-López, G., and Grieco, J. (2007). "Characterisation of gait cycle from accelerometer data". en. In: *Electronics Letters* 43.20, p. 1066. ISSN: 00135194. DOI: 10.1049/el:20071667. URL: https://digital-library.theiet.org/content/journals/10.1049/el_20071667 (visited on 04/04/2022).

Wentink, E., Beijen, S., Hermens, H., Rietman, J., and Veltink, P. (2013). "Intention detection of gait initiation using EMG and kinematic data". en. In: *Gait & Posture* 37.2, pp. 223–228. ISSN: 09666362. DOI: 10.1016/j.gaitpost.2012.07.013. URL: https://linkinghub.elsevier.com/retrieve/pii/S0966636212002834 (visited on 04/04/2022).

Whittle, M. (2007). *Gait Analysis: An Introduction*. Butterworth-Heinemann. ISBN: 9780750688833. URL: https://books.google.co.uk/books?id=HtNqAAAAMAAJ.

Winter, D. A., Greenlaw, R. K., and Hobson, D. A. (1972). "A microswitch shoe for use in locomotion studies". In: *Journal of Biomechanics* 5.5, 553–IN15. ISSN: 0021-9290. DOI: https://doi.org/10.1016/0021-9290(72)90011-5. URL: https://www.sciencedirect.com/science/article/pii/0021929072900115.

Wouda, F. J., Jaspar, S. L. J. O., Harlaar, J., Beijnum, B.-J. F. van, and Veltink, P. H. (2021). "Foot progression angle estimation using a single foot-worn inertial sensor". en. In: *Journal of NeuroEngineering and Rehabilitation* 18.1, p. 37. ISSN: 1743-0003. DOI: 10.1186/s12984-021-00816-4. URL: https://jneuroengrehab.biomedcentral.com/articles/10.1186/s12984-021-00816-4 (visited on 04/04/2022).

XSens (2021). *MVN User Manual*.

Yang, C.-C., Hsu, Y.-L., Shih, K.-S., and Lu, J.-M. (2011). "Real-Time Gait Cycle Parameter Recognition Using a Wearable Accelerometry System". en. In: *Sensors* 11.8, pp. 7314–7326. ISSN: 1424-8220. DOI: 10.3390/s110807314. URL: http://www.mdpi.com/1424-8220/11/8/7314 (visited on 04/04/2022).

Zhao, H., Wang, Z., Qiu, S., Shen, Y., and Wang, J. (2017). "IMU-based gait analysis for rehabilitation assessment of patients with gait disorders". en. In: *2017 4th International Conference on Systems and Informatics (ICSAI)*. Hangzhou: IEEE, pp. 622–626. ISBN: 978-1-5386-1107-4. DOI: 10.1109/ICSAI.2017.8248364. URL: http://ieeexplore.ieee.org/document/8248364/ (visited on 04/04/2022).

Zhen, T., Yan, L., and Yuan, P. (2019). "Walking Gait Phase Detection Based on Acceleration Signals Using LSTM-DNN Algorithm". en. In: *Algorithms* 12.12, p. 253. ISSN: 1999-4893. DOI: 10.3390/a12120253. URL: https://www.mdpi.com/1999-4893/12/12/253 (visited on 04/04/2022).

Zhou, L., Fischer, E., Tunca, C., Brahms, C. M., Ersoy, C., Granacher, U., and Arnrich, B. (2020). "How we found our imu: Guidelines to IMU selection and a comparison of seven Imus for Pervasive Healthcare Applications". In: *Sensors* 20.15, p. 4090. DOI: 10.3390/s20154090.

4.3 Short Summary

The designed algorithm presents a simple tool to relate sEMG activity with kinematics. Looking at key events in the biomechanics data, more easily identified than the physiological counterpart, allows for the segmentation of sEMG data into relevant muscle activity windows to best identify MAPs. This forms a basis for a framework to analyse synchronously MAPs and biomechanics, in both static and dynamic tasks. The following study, in Chapter 5, explores in full the relationships between MAPs, generated forces and kinematics, previously presented in Figure 1.3.

Chapter 5

MAPs and biomechanics in dynamic ADLs

5.1 Short Introduction

Human-robot-interaction is an exciting new area that envisions the execution of collaborative tasks between humans and robots to simplify the work load for the human. Based on ergonomics and biomechanics, a series of studies has been conducted to analyse how can robots assist human workers in strenuous, repetitive tasks, especially in industrial workplaces.

In our study we present an efficacy optimisation algorithm, based on an HRI experiment. Combining information on subjects biomechanics, predicted muscle activity and generated forces, the algorithm optimises an ideal joint configuration and defines a workspace for the human to act upon, and complete a drilling/cutting task.

Subjects executed a series of trials in 3 different conditions: User-defined, Comfort (i.e., efficacious) and Random. The User-defined condition allowed the subjects to manipulate the workspace to their liking, positioning it in the most natural place for them to conduct the task. In the Comfort condition, the robot would estimate, based on the subject's biomechanics and predicted muscle activity levels, which position would minimise the subject's effort to conclude the task. Lastly, for the Random condition, the robot would position the workspace in a configuration where the robot's arms could withstand the largest amount of force possible, regardless of the human's ability to perform the task or not. For each of the trials, the robot adjusted

then the position of the workspace for the human to act upon depending on which condition was tested.

To validate the efficacy of the optimisation algorithms in each condition, sEMG and force data was also collected. A metric for efficacy was established by relating sEMG and the force necessary to complete the tasks.

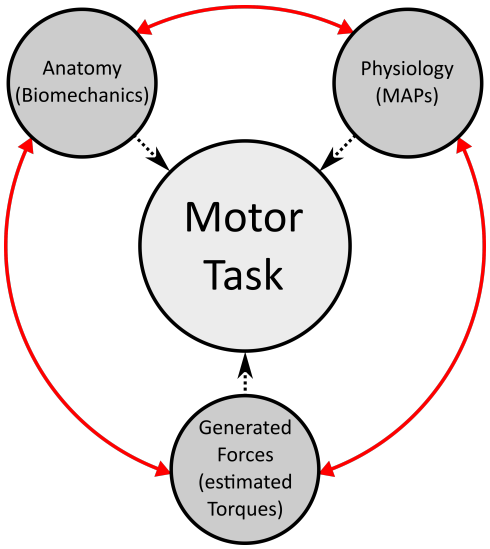


Figure 5.1: **Summary diagram for "Planning to Minimize the Human Muscular Effort during Forceful Human-Robot Collaboration" article**. With physiological, anatomical and force recordings, relationships between all variables are considered and used to inform an effort minimisation predictor for human-robot collaborative tasks.

5.2 Article

5.2.1 Metadata

Title: Planning to Minimize the Human Muscular Effort during Forceful Human-Robot Collaboration.[1]

Authors: Luis F.C. Figueredo[2], Rafael de Castro Aguiar [1], Lipeng Chen[2], Thomas C. Richards[1], Samit Chakrabarty[1], Mehmet Dogar[2]

Details:

- [1] R. Castro Aguiar, Thomas C. Richards and S. Chakrabarty were with the School of Biomedical Sciences, Faculty of Biological Sciences, University of Leeds, Leeds LS2 9JT, UK.

[1]Written in US English, for submission in ACM Journal.

- [2] Luis F.C. Figueredo, Lipeng Chen and Mehmet Dogar were with the School of Computing, University of Leeds, Leeds LS2 9JT, UK.
- Both Luis F.C. Figueredo and Rafael de Castro Aguiar contributed equally to the paper.

5.2.2 Abstract

This work addresses the problem of planning a robot configuration and grasp to position a shared object during forceful human-robot collaboration, for example, a puncturing or a cutting task. Particularly, our goal is to find a robot configuration that positions the jointly manipulated object such that the muscular effort of the human, operating on the same object, is minimized, while also ensuring the stability of the interaction for the robot. This raises three challenges. First, we predict the human muscular effort given a human-robot combined kinematic configuration and the interaction forces of a task. To do this, we perform task-space to muscle-space mapping for two different musculoskeletal models of the human arm. Second, we predict the human body kinematic configuration given a robot configuration and the resulting object pose in the workspace. To do this, we assume that the human prefers the body configuration that minimizes the muscular effort. And third, we ensure that, under the forces applied by the human, the robot grasp on the object is stable and the robot joint torques are within limits. Addressing these three challenges, we build a planner that, given a forceful task description, can output the robot grasp on an object and the robot configuration to position the shared object in space. We quantitatively analyze the performance of the planner and the validity of our assumptions. We conduct experiments with human subjects to measure their kinematic configurations, muscular activity, and force output, during collaborative puncturing and cutting tasks. The results illustrate the effectiveness of our planner in reducing the human muscular load. For instance, for the puncturing task, our planner is able to reduce muscular load by 69.5% compared to a user-based selection of object poses.

Keywords: Computer systems organization → Robotic autonomy; Human-centered computing → User centered design. Physical human-robot collaboration, forceful human-robot collaboration, muscle estimation, biomechanical modeling and limits.

5.2.3 Introduction

When a human and a robot jointly manipulate an object, the robot must take into account the human kinematic and biomechanical response to different possible robot actions. If the robot can predict such response, then it can plan actions that reduce the biomechanical load on the human, leading to more efficient and comfortable human-robot collaboration.

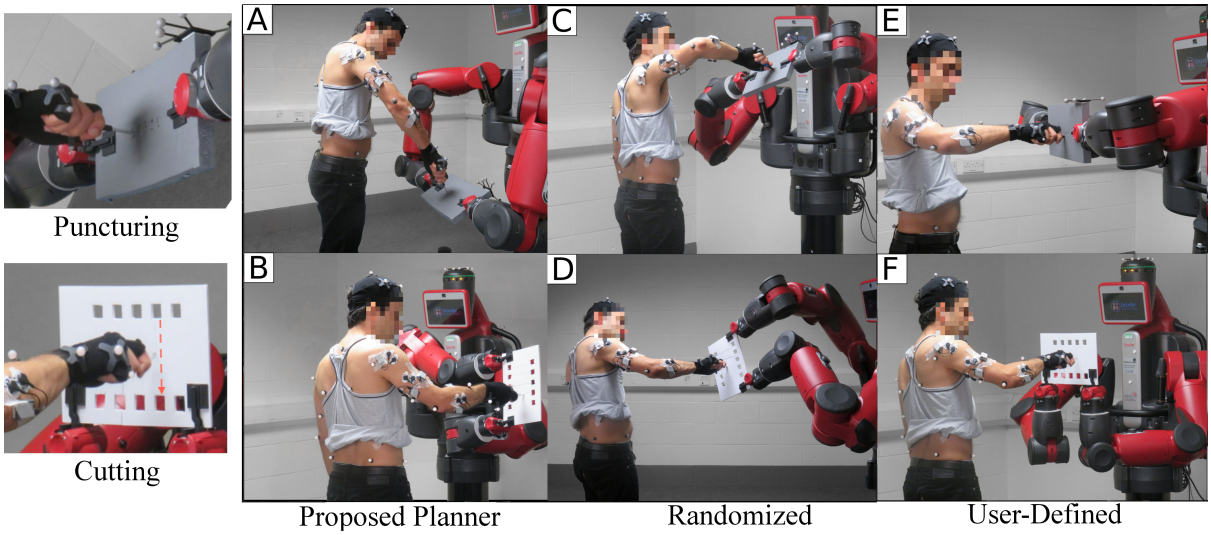


Figure 5.2: **Example forceful human-robot collaborative tasks and configurations**. *Top row:* Puncturing task, where the human forcefully inserts a pointed tool into a hard foam board at a designated point on the board. Different configurations to perform the same task are shown in A, C, and E. *Bottom row:* Cutting task, where the human uses a cutter to cut a foam board along a straight line (shown as dashed red arrow), starting at an existing square hole on the board and finishing the cut at another hole. Different configurations are shown in B, D, and F. *A and B:* Outputs of our planner that minimizes predicted muscle-effort. *C and D:* Randomized configurations. *E and F:* User-defined configurations.

In this work, we present a method that simultaneously predicts the kinematic and biomechanical response of the human during forceful human-robot collaboration (fHRC). We then use these predictions to plan robot grasps and configurations that reduce the load on the human biomechanical system, particularly by minimizing the predicted human muscular effort.

Take for example the collaborative tasks in Figure 5.2. We show a 'puncturing' task (top-left) where the human forcefully inserts a pointed tool into a hard foam board at a designated point on the board. In the top row, i.e., Figures 5.2-A, C, and E, we show three different human-robot configurations to perform the same puncturing task. Notice that, given the same task, e.g. puncturing, the human body takes a different kinematic configuration, and exerts different amounts of muscular effort, depending on where the robot holds the object (the board). In this work, we explore this interaction. We present a planner that, given a forceful task like

puncturing or cutting, intelligently decides on the robot configuration, grasp, and position of the object in order to proactively instruct humans to configurations which demand less physical muscular effort. For example, in Figure 5.2, our planner produces the robot configuration in A for puncturing, and B for cutting. After the robot attains the planned configuration, the human performs the task. (C and D are randomized configurations; E and F are human-designed configurations.)

To produce such configurations, our planner solves three problems: (i) predicting the human muscular effort, (ii) predicting the human kinematic configuration, (iii) ensuring the stability of the robot grasp and joints.

Predicting the human muscular effort. Given a particular human biomechanical model, kinematic configuration (i.e. the joint angles of a kinematic model of the human body), the object pose, and an estimate of the tooltip forces required to complete a task (e.g. puncturing), our planner predicts the human muscular effort required.

To do this, we transform cooperative task-space forces, to human muscle-space—where human motor-control signals are applied and muscle-tendon forces generate the output joint-torques. The muscle space actuation is nonetheless highly redundant (take for instance, the 7-joint kinematic model in Saul et al. 2015 which is actuated by a set of 50 muscles). Consequently, a given forceful human-robot collaborative operation often has infinite solutions in the muscle-space. To solve this indeterminacy, we use two well-known approaches for dimensionality reduction in muscle-space. These produce two fundamentally different muscle activity prediction paradigms—and therefore two different planners. Our main objective in using both methods is to understand the influence of redundancy resolution techniques over the actual minimization of muscle effort. We present the details of how we predict the muscular effort in Section 5.2.5.

Predicting the human kinematic configuration. Above, to predict the muscular effort, we assumed that we know the kinematic configuration of the human body. However, there is also kinematic redundancy in the human body. Given an object pose, the human can choose among many different body configurations to perform the task. Therefore, when the robot is choosing an object pose, before it can predict the muscular effort, it first needs to predict the likely kinematic configuration the human will choose. In this work, we focus on a 7-joint model of the human shoulder, elbow and wrist. In most literature Kang et al. 2005; Khatib et al. 2009; Anderson and Pandy 2001; Thelen et al. 2003, it is assumed that humans resolve

this redundancy in a consistent manner: choosing a limb configuration that minimizes energy expenditure in terms of muscle activity. Therefore, in this work, we assume that the human chooses the kinematic configuration that results in the minimum muscle effort. We name this the *kinematic minimum effort assumption (KMEA)*. We present the details of how we predict the human kinematic configuration through this assumption in Section 5.2.6.

Ensuring the stability of the robot grasp and joints. Finally, it is also important for the planner to choose: (a) grasp points on the object such that the external human applied force can be resisted in a stable manner (e.g. the object does not slip through the fingers), and (b) robot arm configurations such that the predicted torque load on the robot joints are within limits. These constraints must be satisfied while the predicted human muscle effort, as explained above, is minimized, therefore tightly coupling these different constraints and requiring a simultaneous solution to the human and robot related constraints. We explain the details of how we model the stability of the robot grasp and robot joints in Section 5.2.7. To do this we mostly rely on an existing formulation of ours from previous work Chen, L. F. Figueredo, et al. 2020 but integrate it here with human-related constraints.

To evaluate the performance of the proposed planner, we conducted fHRC experiments in puncturing and cutting tasks, examples of which are shown in Figure 5.2. These were performed with different participants and conditions—measuring task-space forces, joint-space kinematics (using a motion-capture system), muscle-space biofeedback (using 9 electromyography sensors, EMGs), and participant perception. We particularly analyze (i) whether the human muscular effort, as indicated by EMG readings, is indeed reduced when we use the proposed planners, and (ii) how well the predictions of the KMEA assumption agrees with the actual human kinematic configurations, as indicated by the motion capture readings. The results show a reduction in the muscle effort when our planner is used, and show KMEA to be effective, though open to improvement.[2]

We call our proposed planner the 'comfort-based planner', since achieving comfortable human-robot collaboration is our overall goal and since muscular effort plays an important part in a human's comfort perception. Though we also acknowledge that muscular effort is probably not the only factor, and other psychological, spatial, and postural factors may also be contributing to a subject's comfort perception. To evaluate how well a decrease in muscle effort translates

[2]The compiled experimental data will be available at data.leeds.ac.uk.

into an increase in comfort perception, we conduct a psychometric questionnaire.

Building human-robot collaboration systems that are more *comfortable* for humans is important. Particularly, a comfortable configuration can improve performance, alleviate and reduce stress and lower incidence of musculoskeletal disorders—musculoskeletal strains are the largest cause of work related injuries in many industrial countries Lasota et al. 2014; Australian Bureau of Statistics 2010; Kim, Lorenzini, et al. 2019. The proposed formulation of muscle effort minimization and planning contributes to the understanding of human muscular response to daily activities and it is a building block to developing comfortable human-robot collaboration systems.

We have previously presented part of the formulation here in a conference paper Chen, L. F. Figueredo, et al. 2018. The current work, however, extends it significantly. Most importantly, here (i) we use an additional and more realistic higher-dimensional muscular model; (ii) we discuss the redundancy-resolution techniques that the higher-dimensional model requires; (iii) we use EMG, kinematic, and force data to analyze the performance of our planners during human-robot experiments (while our previous set of experiments only used questionnaires to evaluate the planners); and (iv) we conduct experiments to analyze the KMEA assumption, a key aspect of our formulation.

The rest of this paper is structured as follows. Section 2 presents the related work. Section 3 formalizes the overall planning problem we aim to solve. Sections 4, 5, and 6 detail the key building blocks of the system as explained above, i.e. the muscle effort prediction, human configuration prediction, and robot stability, respectively. Section 7 present our simulation experiments, and Section 8 our human subject experiments. Section 9 further analyzes the human experiment results in terms of muscle selection and discusses the contribution of individual muscles to the task. Section 10 concludes the paper and discusses future work.

Designing physical human-robot collaborative (pHRC) actions is a complex procedure that involves planning and control over the tightly coupled constrained dynamical system Chen, L. F. C. Figueredo, et al. 2018; Albu-Schäffer et al. 2007; Dimeas and Aspragathos 2016; Wan et al. 2018. Among the many challenges pHRC poses, this work mainly focuses in two areas which have often been studied separately: *human motion synthesis and prediction*; and *bio-informed physical human-robot collaboration* Ajoudani et al. 2018; Kragic et al. 2018; Haddadin and Croft 2016; Santis et al. 2008.

Human motion synthesis: has long been a topic of investigation in physiology, anatomy, biomechanics, and neuroscience. In recent years, it also became a topic of robotics research which produced novel insights into human motion mechanisms Kulić et al. 2016; Demircan et al. 2015. Particularly, with improved simulation tools Delp et al. 2007; Damsgaard et al. 2006 and musculoskeletal models Tanaka et al. 2015; Saul Holzbaur et al. 2005; Saul et al. 2015, task-space-oriented approaches extended to muscle-space have successfully leveraged robotics techniques to movement sequence reconstruction Khatib et al. 2009, tracking and/or performance assessment/filtering Baptista et al. 2017; Khatib et al. 2009, and instantaneous task- to muscle-nullspace assessment Stanev and Moustakas 2019; Stanev and Moustakas 2018. These methods nonetheless fail to cover sensory-motor planning and long-term prediction (e.g., how to predict reaching and forceful interaction prior to the start of the motion). This work fills this gap and assesses the performance of the planning prediction during fHRC which represents a largely unexplored problem that falls both into the categories of human posture prediction and physical human-robot collaboration.

Bio-informed physical human-robot collaboration: is a recent topic in robotics that integrates biomechanics methods to improve human-robot interaction through a better understanding of the influence of forces over the musculoskeletal system, e.g., Milner 2002; Tanaka et al. 2015; Saul et al. 2015. In our previous work Chen, L. F. Figueredo, et al. 2018, we devised an optimization-based planning strategy taking the muscle activation estimation from Tanaka et al., Tanaka et al. 2015, and peripersonal safety from Roncone et al. 2016. From a more comprehensive musculoskeletal model described in Saul et al. 2015, Peternel et al., Peternel, Fang, et al. 2018, focused on fatigue estimation—extending techniques from biomechanics literature Alibeji et al. 2017 to fHRC framework. More recently, this work was extended in Peternel, Fang, et al. 2019 to allow control of the task force direction, i.e., the relative pose attitude. The robot-tool attitude varied accordingly to muscle-activity-based fatigue estimation w.r.t. a set of predefined task-dependent muscle groups. The robot pose was however planned by assessing an ergonomics cost function based on the overloading joint-torque profile from centre of pressure and ground reaction forces, Peternel, Kim, et al. 2017; Kim, J. Lee, Tsagarakis, et al. 2017. Similar optimization-based planning strategies are also found in Kim, J. Lee, Peternel, et al. 2018; Kim, Lorenzini, et al. 2019.

Our work, on the other hand, presents an optimization-based planning strategy fully based

on the 6-DoF wrench mapping to muscle activation. In this sense, this work is similar to our previous efforts in Chen, L. F. Figueredo, et al. 2018. Yet, herein we unfold a more general comfort paradigm—with different musculoskeletal models. We also take a thorough experimental assessment addressing different comfort metrics and biosignals from EMGs. Furthermore, another novelty presented is the experimental assessment of the KMEA minimum-effort assumption—that underlies our biomechanics-based results during fHRC tasks and defines the redundancy resolution for most pHRC literature. To the best of the authors' knowledge, there are no other studies capable of both predicting and planning for human comfort, especially if we take forceful interaction into account. This is also the most complete pHRC work in terms of assessing muscle activity with 9 simultaneous biofeedback readings from EMGs.

Other works on ergonomics and comfort for HRC: Ergonomic concepts as RULA (rapid upper limb assessment) and REBA (rapid entire body assessment) were also exploited and extended to assess human-robot interaction comfort level in Busch et al. 2018; Busch 2018. Nonetheless, although ergonomic concepts are well-posed for high-level rapid task-planning, they fail to address the impact and magnitude of larger forces and dynamic constraints in fHRC.

There has also been a considerable amount of research on comfort analysis concerning HRI for object hand-over, Aleotti et al. 2012; Cakmak, Srinivasa, M. K. Lee, Forlizzi, et al. 2011; Cakmak, Srinivasa, M. K. Lee, Kiesler, et al. 2011, yet solutions neglect any forceful interaction and mostly rely on the geometry of interaction, physiological evaluation Dehais et al. 2011, object attitude Pandey et al. 2012, or at most learning transfer stability and corresponding wrist wrenches Medina et al. 2016; Chan et al. 2013.

5.2.4 Problem Formulation

To better illustrate the interaction context, consider the forceful task of drilling on an object held by the robot in a shared environment, as shown in Figure 5.3-C. The proposed planning strategy takes as prior knowledge the input set $\left(\boldsymbol{x}_{\mathrm{h}}, \boldsymbol{g}_{\mathrm{h}}, {}^{\mathrm{o}}\boldsymbol{x}_{\mathrm{t}}, m_t, {}^{\mathrm{o}}\boldsymbol{f}\right)$ (shown in Figure 5.3-A) given by[3]:

- Human-positioning, $\boldsymbol{x}_{\mathrm{h}}$, more specifically, their shoulder pose w.r.t. the robot frame $\sum_{\mathrm{r}}$;

[3]We use top-left superscripts to distinguish the coordinate frames with respect to which the variable is expressed. For simplicity, superscripts will be omitted for world (robot) coordinate frame $\sum_{\mathrm{r}}$.

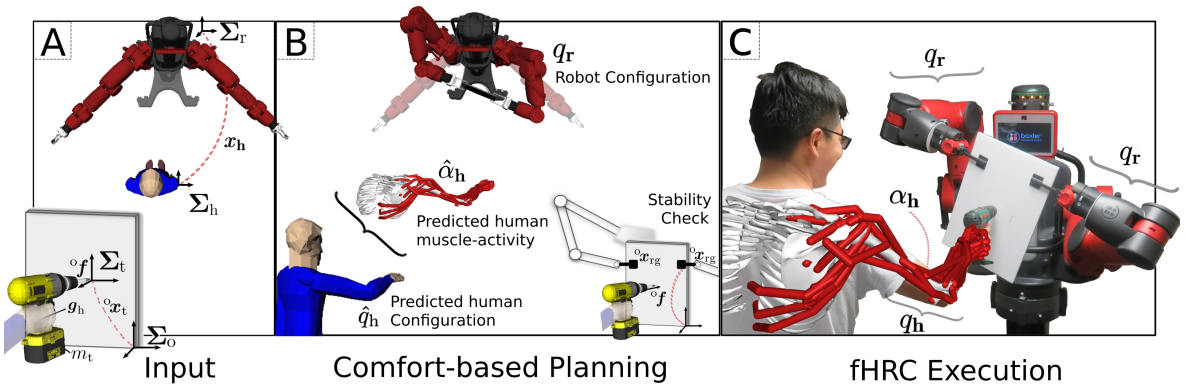


Figure 5.3: **Overview of the comfort-based forceful human-robot collaborative planning**: On the left, (**A**) shows the input information on human-robot positioning $\boldsymbol{x}_{\mathrm{h}}$, task tool (human grasp $\boldsymbol{g}_{\mathrm{h}}$ and mass m_{t}), and force operation (tooltip on the workpiece ${}^{\mathrm{o}}\boldsymbol{x}_{\mathrm{t}}$ and wrench ${}^{\mathrm{o}}\boldsymbol{f}$); (**B**) presents the planning overview as described by (5.1), illustrating the geometric, force and biomechanics constraints and the predicted human kinematics (5.9) and muscle-activity (5.7)-(5.8); and (**C**) shows the task-execution based on the planner output ($\boldsymbol{q}_{\mathrm{r}}^{\mathrm{opt}}$,${}^{\mathrm{o}}\boldsymbol{x}_{\mathrm{rg}}^{\mathrm{opt}}$) and the real human kinematics and muscle-activity response (available only for evaluation).

- Human grasp on the tool $\boldsymbol{g}_{\mathrm{h}}$, which also gives the tooltip pose ${}^{\mathrm{w}}\boldsymbol{x}_t$ w.r.t. the wrist frame $\sum_{\mathrm{w}}$;
- The pose ${}^{\mathrm{o}}\boldsymbol{x}_{\mathrm{t}}$ of the tooltip w.r.t. the object frame $\sum_{\mathrm{o}}$, e.g., the drill point on the board;
- The mass (and center of mass) of the tool m_{t};
- And, the generalized applied force ${}^{\mathrm{o}}\boldsymbol{f}$ at the tooltip w.r.t. to the object, e.g., drilling force.

With this input, the robot then plans its arms configuration in joint-space, $\boldsymbol{q}_{\mathrm{r}}$, and the robot grippers pose, ${}^{\mathrm{o}}\boldsymbol{x}_{\mathrm{rg}}$, to grasp the object, given in the object frame $\sum_{\mathrm{o}}$. These define the object pose and, consequently, where in the cooperative-task space the forceful interaction takes place.

Given the above inputs, our human-comfort-based planner aims at finding the robot configuration and grasp that minimizes muscular effort whilst satisfying robot kinematic and grasp stability constraints (as shown in Figure 5.3-B). We assume biological comfort is related to the generated forces and muscle activity during the execution of motor tasks, that is, we aim at lightening the human muscular load during interaction. More specifically, we aim to minimize the ratio of the applied muscle-tendon forces with respect to the maximum force capability per muscle involved in the motion/force output. More details about muscle activity are given in Section 5.2.5. Using this comfort-metric, we define the *comfort-based planning* as the following optimization problem:

$$\boldsymbol{q}_{\mathrm{r}}^{\mathrm{opt}}, {}^{\mathrm{o}}\boldsymbol{x}_{\mathrm{rg}}^{\mathrm{opt}} = \arg\min_{\boldsymbol{q}_{\mathrm{r}}, {}^{\mathrm{o}}\boldsymbol{x}_{\mathrm{rg}}} \left\{ \mathrm{muscleAct}\left(\hat{\boldsymbol{q}}_{\mathrm{h}}, {}^{\mathrm{o}}\boldsymbol{f}\right) \right\} \tag{5.1a}$$

$$s.t. \ \mathrm{biomecConstraints}\left(\hat{\boldsymbol{q}}_{\mathrm{h}}, {}^{\mathrm{o}}\boldsymbol{f}\right), \tag{5.1b}$$

$$\mathrm{graspStability}\left(\boldsymbol{q}_{\mathrm{r}}, {}^{\mathrm{o}}\boldsymbol{x}_{\mathrm{rg}}, {}^{\mathrm{o}}\boldsymbol{x}_{\mathrm{t}}, {}^{\mathrm{o}}\boldsymbol{f}\right), \tag{5.1c}$$

$$\mathrm{geomConstraints}\left(\boldsymbol{q}_{\mathrm{r}}, {}^{\mathrm{o}}\boldsymbol{x}_{\mathrm{rg}}, \boldsymbol{x}_{\mathrm{h}}, {}^{\mathrm{w}}\boldsymbol{x}_{t}, {}^{\mathrm{o}}\boldsymbol{x}_{\mathrm{t}}\right), \tag{5.1d}$$

where *muscleAct* is a comfort metric based functional that computes the summed muscle activity of different muscles involved in a task. Details on the functional and the biomechanics constraints, *biomecConstraints,* mapping task-space variables to predicted muscular-activity are given in Section 5.2.5. Additionally, the *graspStability* summarizes the robot grasp stability conditions (described in Section 5.2.7) for the given force operation and robot configuration, while the *geomConstraints* is described below.

geomConstraints: checks geometric and kinematic constraints ensuring the tightly coupled human-robot configuration is within human and the robot joint-limits range $(\mathbb{Q}_{\mathrm{h,lim}}, \mathbb{Q}_{\boldsymbol{r},\mathrm{lim}})$. Furthermore, assuming quasi-static human-robot interaction the *geomConstraints* defines where the interaction will take place by means of the tooltip pose $\boldsymbol{x}_{\mathrm{t}}$,

$$\boldsymbol{x}_{\mathrm{h}} \odot {}^{\mathrm{h}}\boldsymbol{x}_{\mathrm{w}} \odot {}^{\mathrm{w}}\boldsymbol{x}_{t} = \boldsymbol{x}_{\mathrm{t}}, \tag{5.2a}$$

$$\boldsymbol{x}_{\mathrm{rg}} \odot {}^{\mathrm{o}}\boldsymbol{x}_{\mathrm{rg}}^{-1} \odot {}^{\mathrm{o}}\boldsymbol{x}_{\mathrm{t}} = \boldsymbol{x}_{\mathrm{t}}, \tag{5.2b}$$

where $\odot$ is the rigid-body group operation, $\boldsymbol{x}_{\mathrm{rg}} \triangleq \mathrm{RFKM}(\boldsymbol{q}_{\mathrm{r}})$ are the robot end-effectors (grippers) pose based on robot forward kinematics model (RFKM), ${}^{\mathrm{o}}\boldsymbol{x}_{\mathrm{rg}}^{-1}$ is the pose of the object w.r.t. to the grippers (the inverse transformation of ${}^{\mathrm{o}}\boldsymbol{x}_{\mathrm{rg}}$), and ${}^{\mathrm{h}}\boldsymbol{x}_{\mathrm{w}}$ is the human wrist pose w.r.t. to human arm base (shoulder) given by the human forward kinematics model, HFKM:

$${}^{\mathrm{h}}\boldsymbol{x}_{\mathrm{w}} \triangleq \mathrm{HFKM}(\boldsymbol{q}_{\mathrm{h}}). \tag{5.3}$$

From (5.2)-(5.3), the robot can tailor human response in order to complete the task with the least amount of force and muscle activity (5.1a) based on human biomechanics models (5.1b), whilst satisfying robot kinematic and stability constraints.

Nonetheless, there is often an infinite number of arm configurations that satisfy (5.3). In this manner, the robot through (5.2) in fact shapes the set of all feasible human arm configurations $\mathcal{Q}_{\text{h}}(\boldsymbol{q}_{\mathbf{r}}, {}^{\text{o}}\boldsymbol{x}_{\text{rg}}, \boldsymbol{x}_{\text{h}}, {}^{\text{w}}\boldsymbol{x}_{t}, {}^{\text{o}}\boldsymbol{x}_{\text{t}})$. This reflects human flexibility (redundancy) to choose different configurations given kinematics constraints and raises the question of how the human will choose their arm configuration based on (5.2a) and (5.3). To solve this redundancy in a consistent manner, in the rest of this work, we assume the existence of a unique mapping function that predicts the human arm configuration $\hat{\boldsymbol{q}}_{\text{h}} \in \mathcal{Q}_{\text{h}}$ satisfying (5.2)-(5.3)—throughout this work, we will always use$\hat{}$ to distinguish predicted from real variables. Further details on this redundancy resolution strategy are given in Section 5.2.6.

5.2.5 Predicting the Muscle Effort: Task- to Muscle-Space Mapping

This section provides model descriptions for the human kinematics and biomechanics, as well as different methodologies for predicting muscular activity, human comfort and arm-configuration. These concepts shape the backbone of this work, and are crucial for the automatic reasoning and planning over human biological motor properties. In Subsection 5.2.5.1, we begin by defining the comfort metric used in muscleAct in Eq. 5.1a. We then describe the transformation that takes human task-space force and torques (see Figure 5.3-A) to human joint-space torques in Subsection 5.2.5.2. The torque values are thereafter mapped to muscle-space actuation by means of two fundamentally different paradigms in Subsections 5.2.5.3 and 5.2.5.4.

To keep the presentation simple, in this Section, we assume we know the human arm configuration at joint-level, $\boldsymbol{q}_{\text{h}}$, that the human will take during task execution. Nonetheless, as previously stressed, arm configuration can only be predicted by our planner. Details of this prediction will be explained later in Section 5.2.6.

5.2.5.1 Muscular Effort

To minimize the summed activation of all muscles involved with the task-space force application, we need to assess human effort from muscle-space variables. Similarly to Tanaka et al. 2015; Chen, L. F. Figueredo, et al. 2018; Khatib et al. 2009, we adopt the concept of **muscle activity effort** ($\|\hat{\boldsymbol{\alpha}}\|_{\mathbb{M}^m}$), and explicitly define the comfort metric functional in (5.1) as

$$\|\hat{\boldsymbol{\alpha}}\|^2_{\mathbb{M}^m} \triangleq \underset{\boldsymbol{\alpha}\in\mathbb{M}^m}{\text{muscleAct}} = \boldsymbol{\alpha}^T\boldsymbol{\alpha}, \tag{5.4}$$

where $\boldsymbol{\alpha}$ is the vector of activation level of the $m-$muscles involved in the force operation. The activation denotes the muscle-tendon force normalized by the maximum force a muscle can generate, that is, $\alpha_i \in [0,1]$, $i=\{1,\ldots,m\}$. Hence,

$$\boldsymbol{\alpha} \in \mathbb{M}^m, \text{ with } \mathbb{M}=\{\alpha \in \mathbb{R} \,|\, 0 \leq \alpha \leq 1\}. \tag{5.5}$$

We predict muscle activation and forces indirectly, first estimating the related joint-variables, i.e. human joint torques, and then mapping the joint torques to muscle activation. In Subsection 5.2.5.2, we present the mapping from task- to joint-space wrenches. One additional challenge is that there are many more DoFs in a musculoskeletal system than in joint-space (i.e., redundancy), De Groote et al. 2016 which leads to an indeterminacy w.r.t. muscle activation and forces. To solve this redundancy, we estimate $\hat{\boldsymbol{\alpha}}$ from biomechanics models (*biomecConstraints)* which often relies on either musculoskeletal-model-based optimization strategies or model-reduction techniques based on simulation or human-based experiments, Tanaka et al. 2015; Peternel, Fang, et al. 2018. In Subsections 5.2.5.3 and 5.2.5.4, we present these two different estimation paradigms for the *biomecConstraints* which shapes different comfort criteria with (5.1).

5.2.5.2 Task to Joint-Space Modeling for the Human Arm

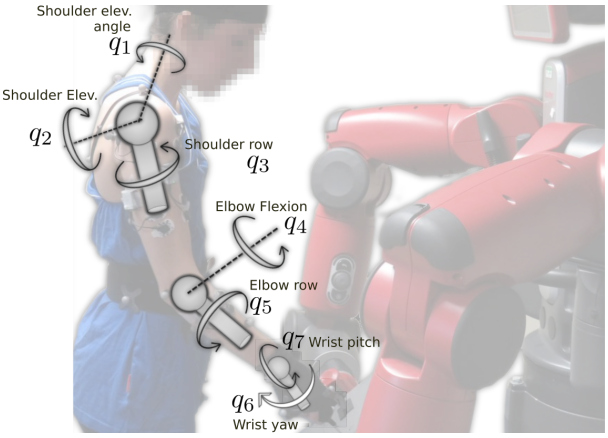


Figure 5.4: **Human-joints kinematics used in Subsection 5.2.5.3**

To reason over human biomechanics, we begin by recalling that similar to a robot manipulator, human limbs can be represented by kinematic chains. Indeed, the upper limb is often modeled[4]

[4]The HFKM of the human upper limb deployed in Subsection 5.2.5.4 is defined in accordance to Figure 5.4, and to the musculoskeletal model of Saul Holzbaur et al. 2005, whereas in Subsection 5.2.5.4, a standard spherical-revolute-spherical model is employed to satisfy the non-redundant transformation used in Tanaka et al. 2015;

as a 7-DOF serial chain system with the shoulder defined as the base frame, as shown in Figure 5.4. From the human kinematics and the geometric constraints, the pose of the tooltip $\boldsymbol{x}_{\mathrm{t}}$ can be computed as in (5.2a). Consequently, generalized velocities and wrenches exerted at this tooltip can be locally mapped to the joint-space manifold, at configuration $\boldsymbol{q}_{\mathrm{h}}$, through the geometric Jacobian $\boldsymbol{J}_{\mathrm{h}}$, that is,

$$\boldsymbol{\tau}_{\mathrm{h}} = \boldsymbol{J}_{\mathrm{h}}^{T}\left(\boldsymbol{f} + \boldsymbol{\rho}_{\mathrm{t}}\right) + \boldsymbol{\tau}_{\rho}, \tag{5.6}$$

where $\boldsymbol{\tau}_{\mathrm{h}}$ is the required joint-space torque and $\boldsymbol{f}$ is the exerted wrench represented in world frame—note that, for the sake of clarity, we are omitting arguments whenever possible. The wrench $\boldsymbol{f}$ is computed by means of norm-preserving object to tooltip and tool to world-frame transformations, i.e., ${}^{\mathrm{o}}\boldsymbol{x}_{\mathrm{t}}$ and $\boldsymbol{x}_{\mathrm{t}}(\boldsymbol{q}_{\mathrm{r}}, {}^{\mathrm{o}}\boldsymbol{x}_{\mathrm{rg}})$, applied to the known wrench at the tooltip in object-frame ${}^{\mathrm{o}}\boldsymbol{f}$. In (5.6), we can also account for joint-torque contributions from the arm and tool weights. The gravitational torques from the arm are given by $\boldsymbol{\tau}_{\rho}(\boldsymbol{q}_{\mathrm{h}})$, while $\boldsymbol{\rho}_{\mathrm{t}}({}^{\mathrm{h}}\boldsymbol{x}_{\mathrm{w}}, m_{\mathrm{t}})$ denotes the wrenches at end-pose stemming from the tool weight.[5]

5.2.5.3 Muscular Activity Prediction based on Static Optimization ($\hat{\boldsymbol{\alpha}}_{\mathbf{SO}}$)

To address the muscle redundancy and estimate the muscle activation level $\hat{\boldsymbol{\alpha}}\left(\boldsymbol{q}_{\mathrm{h}}, \boldsymbol{\tau}_{\mathrm{h}}\right)$, biomechanics solutions often rely on the observation that humans resolve this redundancy in a relatively consistent Lacquaniti and Soechting 1982 and optimal manner Anderson and Pandy 2001; Stanev and Moustakas 2019. Optimality, in this case, refers to minimizing energy expenditure by means of the motor control system optimization of the constrained norm of the muscular activity (5.5).

Existing muscle-effort optimization techniques are usually classified into static or dynamic—w.r.t. muscle activation and contraction dynamics. Static optimization neglects the nonlinear activation/contraction muscle dynamics which in turn eliminates the time-dependency from optimization and yields a bounded least-square problem Pedotti et al. 1978; Tsirakos et al. 1997. Compared to dynamic methods, they are less complex and time-consuming. Among classes of

Chen, L. F. Figueredo, et al. 2018. In general, the choice of HFKM will be dependent on the musculoskeletal model deployed for analysis as the torque to muscle mapping inherently relies on the HFKM and the mapping in (5.6).

[5] We assume quasi-static interaction, yet extension to dynamics can be obtained directly, e.g., by means of the Lagrangian method Spong et al. 2006, $\boldsymbol{M}_{\mathrm{h}}\ddot{\boldsymbol{q}}_{\mathrm{h}} + \boldsymbol{C}_{\mathrm{h}}\dot{\boldsymbol{q}}_{\mathrm{h}} = \boldsymbol{\tau}_{\mathrm{h}} - \boldsymbol{J}_{\mathrm{h}}^{T}(\boldsymbol{f} + \boldsymbol{\rho}_{\mathrm{t}}) - \boldsymbol{\tau}_{\rho}$, where $\boldsymbol{f}$ is the end-pose wrench, and $\boldsymbol{M}_{\mathrm{h}}$ and $\boldsymbol{C}_{\mathrm{h}}$ the inertia and centrifugal-Coriolis forces.

dynamic optimizers, direct shooting De Groote et al. 2016 and, computed muscle control Thelen et al. 2003 are the most widely used strategies that concern neural excitation and contraction dynamics while integrating muscle activation. Nonetheless, despite requiring more elaborate solvers, dynamic methods have only shown improvements in very narrow cases, e.g., long-term activity or fatigue estimation Alibeji et al. 2017, which are not the case in this work. We deploy static optimization strategy since we are focused on highly forceful but short interactions. In this sense, joint-torques are defined by muscle-tendon force and the moment-arm connecting the joint to the antagonistic pair of muscles. The optimization then focuses in providing the muscle activation vector that yields least muscular activity effort satisfying biomechanics constraints, that is, *biomecConstraints*:

$$\hat{\boldsymbol{\alpha}}_{\text{SO}} = \arg\min_{\boldsymbol{\alpha}\in\mathbb{M}^m} \left\{\boldsymbol{\alpha}^T\boldsymbol{\alpha}\right\} \tag{5.7a}$$

$$s.t.\ \boldsymbol{\Gamma}_{\text{h}}(\boldsymbol{q}_{\text{h}})\boldsymbol{F}_{\text{h}}(\boldsymbol{q}_{\text{h}})\boldsymbol{\alpha} = \boldsymbol{\tau}_{\text{h}}, \tag{5.7b}$$

where $\hat{\boldsymbol{\alpha}}_{\text{SO}}$, obtained from static optimization, gives the predicted muscle activity and provides an equality constraint to (5.1b). The diagonal matrix $\boldsymbol{F}_{\text{h}} = \text{diag}\,(f_1^{\max}, \ldots, f_m^{\max}) \in \mathbb{R}^{m\times m}$ depicts the maximum isometric muscle forces, and $\boldsymbol{\Gamma}_{\text{h}} \in \mathbb{R}^{7\times m}$ is a matrix-transformation that maps muscle forces to joint torques. $\boldsymbol{\Gamma}_{\text{h}}$ contains $\gamma_{ij} \in \mathbb{R}$ elements representing the moments-arms between the $i-$th muscle and the $j-$th joint. Hence, each i-th muscle contributes to the torque generated at the j-th joint by means of the muscle-force generated (activation level α_i times its maximum isometric force $f_i^{\max}$) and its moment-arm about the joint γ_{ij}, that is, $\tau_j = \sum_i^m \gamma_{ij}\,(f_i^{\max}\alpha_i)$.

The matrices $\boldsymbol{F}_{\text{h}}$ and $\boldsymbol{\Gamma}_{\text{h}}$ depend on the human joint-configuration $\boldsymbol{q}_{\text{h}}$ (we explain how to predict $\boldsymbol{q}_{\text{h}}$ in Section 5.2.6) and the corresponding musculoskeletal model. For the model, we take parameters from the seminal work of Saul et al, Saul et al. 2015, through the OpenSim simulator Delp et al. 2007, where $m = 50$.

Remark 1. The optimization (5.7) as well as the resulting $\boldsymbol{\alpha}_{\text{SO}}$ defining the *biomecConstraints* in (5.1b) satisfies the muscle-activation set definition in (5.5), i.e, $\boldsymbol{\alpha} \in \mathbb{M}^m$. This positive constraint makes it impossible to take an unconstrained optimization directly over the induced norm (as $\mathbb{M}^m$ is not a vector space) nor to device standard performance characterization metrics

as in Tanaka et al. 2015; Khatib et al. 2009,

$$\begin{aligned} E = \hat{\boldsymbol{\alpha}}^T \hat{\boldsymbol{\alpha}} &= \boldsymbol{\tau}_{\mathrm{h}}^T \left(\boldsymbol{\Gamma}_{\mathrm{h}} \boldsymbol{F}_{\mathrm{h}}^2 \boldsymbol{\Gamma}_{\mathrm{h}}^T \right)^{-1} \boldsymbol{\tau}_{\mathrm{h}} \\ &= (\boldsymbol{J}_{\mathrm{h}}^T (\boldsymbol{f} + \boldsymbol{\rho}_{\mathrm{t}}) + \boldsymbol{\tau}_{\rho})^T \left(\boldsymbol{\Gamma}_{\mathrm{h}} \boldsymbol{F}_{\mathrm{h}}^2 \boldsymbol{\Gamma}_{\mathrm{h}}^T \right)^{-1} (\boldsymbol{J}_{\mathrm{h}}^T (\boldsymbol{f} + \boldsymbol{\rho}_{\mathrm{t}}) + \boldsymbol{\tau}_{\rho}). \end{aligned}$$

The solution above is ill-conditioned as it neglects $\boldsymbol{\alpha}$ positiveness, i.e., it assumes the possibility of negative activation of muscles, which is physiologically unfeasible.

5.2.5.4 Muscular Activity Prediction based on Model Reduction ($\hat{\boldsymbol{\alpha}}_{\mathrm{MR}}$)

In addition to musculoskeletal optimization techniques, an alternative approach proposed by Tanaka et al. 2015 relies on directly measuring human upper-limb joint-torques resulting from task-space forces. In other words, it experimentally evaluates the transformation between end-point force capabilities w.r.t. joint-torques bypassing the muscle- to joint-torques transformation. To reduce the dimensionality of the original problem, Tanaka et al. Tanaka et al. 2015 constrained the study on the most relevant agonist muscles per joint motion-dynamics. Recording muscle activation and joint-torques, generated by both uniarticular movements (positive and negative motions) at different joint-vector ($\boldsymbol{q}_{\mathrm{h}}$) configurations, the authors devised a method to compute the activation level of the agonist (most relevant) muscles given the joint posture, direction of motion (e.g., flexion or extension), and torque. Hence, for a given $\boldsymbol{q}_{\mathrm{h}}$, a unique muscular activation is associated for each joint-torque (given its uniarticular direction). In this sense, the redundancy concerning muscle and joint-torques is removed.

With this mapping, for a given $\boldsymbol{q}_{\mathrm{h}}$ and joint-direction, we can compute the maximum possible torque at the i-th joint, τ_i^{max} (based on maximum absolute values under maximum voluntary contraction). This leads to a bijective mapping based on the matrix transformation $\boldsymbol{\Pi}(\boldsymbol{q}_{\mathrm{h}}, \boldsymbol{\tau}_{\mathrm{h}}) = \mathrm{diag}\left(\tau_1^{max}(\boldsymbol{q}_{\mathrm{h}}, \boldsymbol{\tau}_{\mathrm{h}}), \ldots, \tau_7^{max}(\boldsymbol{q}_{\mathrm{h}}, \boldsymbol{\tau}_{\mathrm{h}})\right)$—a diagonal matrix composed of human upper-limb maximum torque elements—that can be used to compute the muscle activation as follows *biomecConstraints* ($\boldsymbol{\alpha}_{\mathrm{MR}}$):

$$\hat{\boldsymbol{\alpha}}_{\mathrm{MR}} = \boldsymbol{\Pi}^{-1}(\boldsymbol{q}_{\mathrm{h}}, \boldsymbol{\tau}_{\mathrm{h}}) \boldsymbol{\tau}_{\mathrm{h}}, \tag{5.8}$$

where $\hat{\boldsymbol{\alpha}}_{\mathrm{MR}} = [\alpha_1, \ldots, \alpha_7]^T \in \mathbb{M}^7$ provides the predicted muscle activation, and an equality constraint to (5.1b).

Note however $\boldsymbol{\Pi}(\boldsymbol{q}_{\text{h}}, \boldsymbol{\tau}_{\text{h}})$ has a nonlinear dependency to the joints positions and torques, particularly torque direction. This is because each functional $\tau_i^{max}(\boldsymbol{q}_{\text{h}}, \boldsymbol{\tau}_{\text{h}})$ approximates the muscle-dynamics linearized at given joint posture and expected motion/torque direction. That is to say, the maximum torque for each joint depends not only on its position but also on its motion and torque direction (particularly, the torque which implicitly defines extension/flexion of antagonistic muscles). Hence, $\hat{\boldsymbol{\alpha}}_{\text{h}}^T \hat{\boldsymbol{\alpha}}_{\text{h}}$ is non-symmetrical w.r.t. $\boldsymbol{\tau}_{\text{h}}$.[6]

Equipped with joint configurations and sign/directions of the torques, we can build the matrix of maximum torque elements $\boldsymbol{\Pi}(\boldsymbol{q}_{\text{h}}, \boldsymbol{\tau}_{\text{h}})$ and compute the muscular activation (5.8). The main advantage of the solution (5.8) compared to (5.7) is the reduced computational complexity obtained from removing the redundancy.

Other Methods for Muscular Activity Estimation

In addition to optimization and model-reduction based strategies, it is worth mentioning the work Peternel, Fang, et al. 2018 which similarly to (5.8) also presents an efficient and fast solution to output muscular activity estimation based on the user configuration and external forces. In contrast to previous methods, the work in Peternel, Fang, et al. 2018 addresses the problem from a machine learning point of view by means of a GPR-based learning algorithm combined with a simulated dataset of arm joint configurations, endpoint forces and resulting muscular forces from Saul et al. musculoskeletal model Saul et al. 2015 and the OpenSim simulator Delp et al. 2007. In this context, the resulting metric provides approximate, but faster results compared to (5.7), and could be straightforwardly used with our comfort-based planning without loss of generality. Notice that, if well-trained, any similar strategy will lead to the same results as in (5.7).

5.2.6 Predicting the Human Kinematic Configuration: The Kinematic Minimum-Effort Assumption

For a given forceful task, our goal is to plan robot joints and grasp configurations, and an object pose that optimizes human comfort according to *muscleAct* in (5.4). However, as stressed in the problem definition, Section 5.2.4, the robot can only shape the set of all feasible human configurations $\mathcal{Q}_{\text{h}}(\boldsymbol{q}_{\mathbf{r}}, {}^{\text{o}}\boldsymbol{x}_{\text{rg}}, \boldsymbol{x}_{\text{h}}, {}^{\text{w}}\boldsymbol{x}_t, {}^{\text{o}}\boldsymbol{x}_{\text{t}})$, which in turn raises the question of how the human

[6] Experimental data to compute the maximum torque matrix $\boldsymbol{\Pi}(\boldsymbol{q}_{\text{h}}, \boldsymbol{\tau}_{\text{h}})$ in (5.8) is found in Tanaka et al. 2015. Proportions for maximum joint-torques follow a similar pattern across individuals and, even for different body weights, differing only in magnitude.

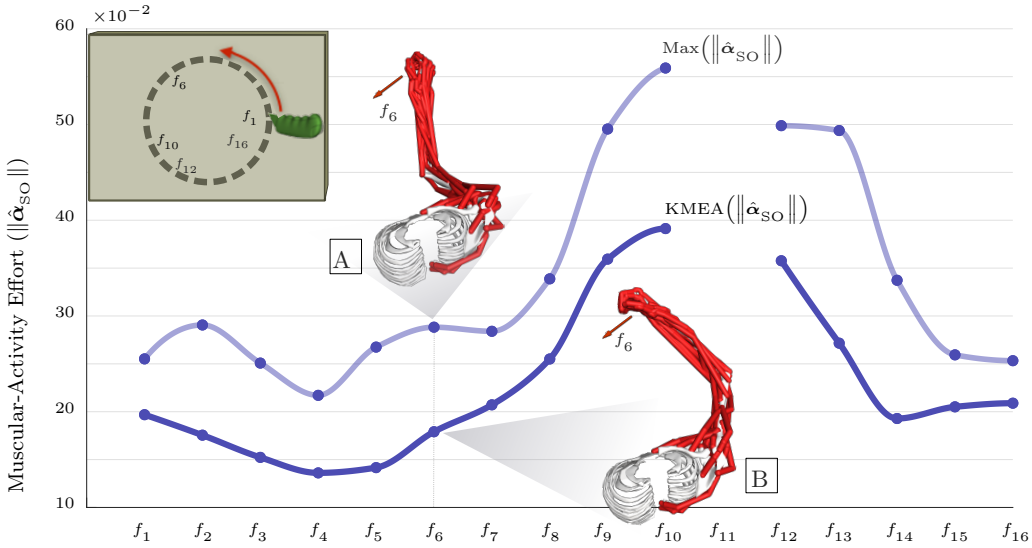


Figure 5.5: **Muscle effort variation within human's kinematic redundancy**: worst-case for $\boldsymbol{q}_{\mathrm{h}}$ (light-blue) compared to KMEA configuration for same end-pose and force. Two different arm postures for cutting force f_6 (with direction shown by the red arrows) are shown in [A] and [B] for worst-case and KMEA, respectively.

will choose their configuration and if that will satisfy our comfort metric.

In biomechanics literature, e.g., Kang et al. 2005; Khatib et al. 2009; Anderson and Pandy 2001; Thelen et al. 2003, it is often assumed that humans resolve this redundancy consistently in the most efficient manner in terms of minimizing the muscle activation required to transmit a given task-space force. We call this the Kinematics Minimum Effort Assumption (KMEA) and adopt this assumption in this work.

In other words, KMEA relies on human's innate self-motion optimization scheme in the integrated joint-muscle nullspace, that is, the nullspace projection from task-space to muscle-space. The self-motion optimization can therefore be described by

$$\begin{aligned} \hat{\boldsymbol{q}}_{\mathrm{h}} = \arg \min_{\boldsymbol{q}_{\mathrm{h}} \in \mathbb{Q}_{\mathrm{h,lim}}} & \left\{ \hat{\boldsymbol{\alpha}}^T \left(\boldsymbol{q}_{\mathrm{h}}, \boldsymbol{\tau}_{\mathrm{h}}(\boldsymbol{q}_{\mathrm{h}}) \right) \hat{\boldsymbol{\alpha}} \left(\boldsymbol{q}_{\mathrm{h}}, \boldsymbol{\tau}_{\mathrm{h}}(\boldsymbol{q}_{\mathrm{h}}) \right) \right\} \\ s.t. \quad & \hat{\boldsymbol{\alpha}} \leftarrow \mathrm{biomecConstraints} \left(\boldsymbol{q}_{\mathrm{h}}, {}^{\mathrm{o}}\boldsymbol{f} \right), \\ & \boldsymbol{q}_{\mathrm{h}} \in \mathcal{Q}_{\mathrm{h}}({\boldsymbol{q}_{\mathrm{r}}}, {}^{\mathrm{o}}\boldsymbol{x}_{\mathrm{rg}}, \boldsymbol{x}_{\mathrm{h}}, {}^{\mathrm{w}}\boldsymbol{x}_t, {}^{\mathrm{o}}\boldsymbol{x}_{\mathrm{t}}), \\ & \hat{\boldsymbol{\alpha}} \in \mathbb{M}^m, \end{aligned} \tag{5.9}$$

where *biomecConstraints* refers to the equality constraint defined either by (5.7), for static optimization solutions, i.e., $\hat{\boldsymbol{\alpha}}_{\mathrm{SO}}$, or by (5.8), for model-reduction approaches, $\hat{\boldsymbol{\alpha}}_{\mathrm{MR}}$. The constraint $\boldsymbol{\alpha} \in \mathbb{M}^m$ also ensures the optimal result is well posed. The set $\mathcal{Q}_{\mathrm{h}}$ is defined over (5.2a) and $\boldsymbol{\tau}_{\mathrm{h}}$ is obtained in (5.6) based on the joint configuration.

To better understand KMEA, take for example a task of cutting off a circular piece off a board, shown in Figure 5.5. The board configuration is pre-set and the circle is divided into 16 discrete (also) pre-set points and forces (15 N along the cutting direction). We computed feasible IK solutions for such task satisfying the constraints in (5.9) with (5.7b). The dark blue curve depicts the optimization following (5.9), that is, when human is at the most comfortable configuration (KMEA), whilst the light blue depicts the worst (most uncomfortable) configuration—i.e., the arg max from (5.9) which yields the highest muscular activity. For two possible configurations Figure 5.5, A and B, our experience is that configuration [B] is much more comfortable than [A], which coincides with the comfort metric assessment and experiments in Section 5.2.9. Moreover, at the proximity of joint-limits (position f_{11} has no feasible IK solution), we observe the soaring muscular activity cost (degradation in comfort) as expected. Also, note the consistency of the metric at the circular closing (positions f_{16} to f_1). Figure 5.5 also shows the importance of planning and control strategies in shaping the human feasible response to comfortable configurations.

5.2.7 Ensuring Grasp and Robot Stability

From the robot's point of view, quasi-static forceful interaction imposes constraints over reachability in terms of coupled kinematics and stability in terms of static equilibrium. The former ensures the existence of a joint configuration $\boldsymbol{q}_{\mathrm{r}}$ satisfying (5.2) within the joint limits, that is, $\boldsymbol{q}_{\mathrm{r}} \in \mathbb{Q}_{\boldsymbol{r},\mathrm{lim}}$. On the other hand, the grasp stability constraint describes the relationship between the force applied on the object and its counterpart at joint-space with respect to the robot capability to resist it. Given our assumption of a bimanual cooperative robot, $\boldsymbol{q}_{\mathrm{r}} = [\boldsymbol{q}_{\mathrm{r}}^T[1] \;\; \boldsymbol{q}_{\mathrm{r}}^T[2]]^T \in \mathbb{R}^n$, where $\boldsymbol{q}_{\mathrm{r}}[1], \boldsymbol{q}_{\mathrm{r}}[2]$ refer to the left and right arm configuration, the grasp stability can be computed from the symmetric formulation from Uchiyama and Dauchez 1988. This formulation, however, leaves the forces at the grip contacts unconstrained. Herein, we are also interested in checking the stability against insufficient forces at the gripper contacts (e.g., if the frictional forces between fingers can prevent the object from sliding) and deformation due to contact compliance. Imposing this additional constraint onto the symmetric formulation Uchiyama and Dauchez 1988, the robot stability against human exerted forces is checked by

graspStability:

$$\begin{aligned} \boldsymbol{W}_{\mathrm{r}}\boldsymbol{f}_{\mathrm{r}} &= -\boldsymbol{f}, \\ \boldsymbol{J}_{\mathrm{r}}^{T}\boldsymbol{f}_{\mathrm{r}} &= \boldsymbol{\tau}_{\mathrm{r}}, \\ |\boldsymbol{\tau}_{\mathrm{r}}| &\leq \boldsymbol{\tau}_{\mathrm{r}}^{\max}, \\ |\boldsymbol{f}_{r}| &\leq \boldsymbol{f}_{r}^{max} \end{aligned} \tag{5.10}$$

where $\boldsymbol{f}_{\mathrm{r}}=[\boldsymbol{f}_{\mathrm{r}}^{T}[1], \boldsymbol{f}_{\mathrm{r}}^{T}[2]]^{T} \in \mathbb{R}^{12}$ is wrench vector at each robot gripper, and $\boldsymbol{W}_{\mathrm{r}} \in \mathbb{R}^{6\times 12}$ is the grasp matrix that maps the wrenches at the grippers to the reactive resultant task-space force and torques on the object, that is, $\boldsymbol{f}$—this refers to the human applied force in the world frame, which depends on the input force task ${}^{\mathrm{o}}\boldsymbol{f}$ and the planned object pose $\boldsymbol{x}_{\mathrm{o}}$.

Similarly, $\boldsymbol{J}_{\mathrm{r}} \in \mathbb{R}^{12\times n}$ is a block diagonal matrix with both arms geometric Jacobians used to map the wrenches at robot grippers into the joint-space manifold yielding the augmented joint-torque value $\boldsymbol{\tau}_{\mathrm{r}}=[\boldsymbol{\tau}_{\mathrm{r}}^{T}[1], \boldsymbol{\tau}_{\mathrm{r}}[2]^{T}]^{T} \in \mathbb{R}^{n}$. The robot cooperative stability is thus secured if the required joint-torque, $\boldsymbol{\tau}_{\mathrm{r}}$, and wrench at gripper point, $\boldsymbol{f}_{r}$, are respectively within the torque limits $\boldsymbol{\tau}_{\mathrm{r}}^{\max} \in \mathbb{R}^{n}$ and gripper force limits $\boldsymbol{f}_{r}^{max} = [\boldsymbol{f}_{r_1}^{max}, \boldsymbol{f}_{r_2}^{max}]^{T} \in \mathbb{R}^{12}$. We skip further details on the mathematical formulation as they lie beyond the scope of this work, yet can be found in our previous work Chen, L. F. C. Figueredo, et al. 2018.

5.2.8 Planning – Quantitative Analysis

This section explores quantitative aspects of the proposed comfort-based planning strategies under different scenarios (exerted force (${}^{\mathrm{o}}\boldsymbol{f}$), human-robot positioning ($\boldsymbol{x}_{\mathrm{h}}$), tool transformation (${}^{\mathrm{w}}\boldsymbol{x}_{t}$), weight (m_{t}) and tooltip position on the object, ${}^{\mathrm{o}}\boldsymbol{x}_{\mathrm{t}}$). In all scenarios, the simulated Baxter Robot needs to plan to grasp and to position an object in the human's workspace to perform a fHRC task, as shown in Figure 5.3. Planning decisions were made according to the following planners:

- **Random-planner**: Given a forceful operation, the robot randomly picks an object pose within the reachable human-robot space (5.2) and only checks for static stability (5.10) and cooperative geometric constraints (5.2). This planner acts as a baseline;
- **SO-Comf-Planner**: Our comfort-based planner from (5.1) with muscular activity effort ($\|\hat{\boldsymbol{\alpha}}_{\mathrm{SO}}\|$) computed from static optimization (5.7);

- **MR-Comf-Planner**: Similarly, this planner optimizes (5.1) but with muscular activity effort ($\|\hat{\boldsymbol{\alpha}}_{\text{MR}}\|$) computed from the model-reduction strategy (5.8);

In addition to the above planners, we also defined a **fixed-pose** configuration inbetween human and robot (more specifically, 40 cm in front of the shoulder)—and, the robot plans grasps such that both geometric and stability constraints are satisfied for all scenarios.

The scenarios included the human performing puncturing, pulling and cutting operations with the aid of the robot. The force directions for puncturing and pulling were taken normal to the board in opposite directions, while for the cutting task, it was aligned with the cutting direction. For each forceful task, we also designed different simulations based on varying the force magnitude (${}^{\text{o}}\boldsymbol{f}$), human-robot positioning ($\boldsymbol{x}_{\text{h}}$) and tool weight ($m_{\text{t}}$) and length (which gives way different poses of the tooltip w.r.t. the wrist frame, i.e., ${}^{\text{w}}\boldsymbol{x}_t$). To obtain a realistic representation of the required forces during planning stage, before the experiments, we estimated force magnitudes using a force-torque sensor. For quantitative purposes, planning algorithms were executed in Matlab using multistart SQP-solver and scatter-search-based surrogate Ugray et al. 2007 for global optimization. For the muscular effort assessment with $\|\hat{\boldsymbol{\alpha}}_{\text{SO}}\|$ and computing the biomechanics constraints (5.7), we also exported musculoskeletal model parameters from Saul et al. 2015 using OpenSim simulator Delp et al. 2007.

Table 5.1: **Average muscular activity effort** (lower the better) normalized with Random-Planner (RndP) results for 45 puncturing, 45 pulling and 45 cutting operations.

	Musc. Act. Effort ($\|\hat{\boldsymbol{\alpha}}_{\text{MR}}\|$)			Musc. Act. Effort ($\|\hat{\boldsymbol{\alpha}}_{\text{SO}}\|$)		
	RndP	Fixed-Pose	MR-Comf-Planner	RndP	Fixed-Pose	SO-Comf-Planner
puncturing	1	$.920 \pm .310$	$\mathbf{.606 \pm .342}$	1	$1.279 \pm .517$	$\mathbf{.341 \pm .145}$
Pulling	1	$1.189 \pm .445$	$\mathbf{.371 \pm .141}$	1	$1.073 \pm .336$	$\mathbf{.262 \pm .087}$
Cutting	1	$1.164 \pm .434$	$\mathbf{.817 \pm .205}$	1	$2.340 \pm .953$	$\mathbf{.610 \pm .193}$

5.2.8.1 Optimization Performance

This subsection illustrates the comfort gains, in terms of reduced muscle-activity, from both comfort-based planners in contrast to random and fixed-pose configurations. To this aim, we devised 135 different scenarios for each planner—involving 45 puncturing, 45 cutting and 45 pulling tasks with

- Three different force magnitudes $\{7.5, 15, 30\}$ N;
- Three human-robot positioning ($\boldsymbol{x}_{\text{h}}$): $\{[0, 1.2], [0.2, 1.4], [-0.2, 1.0]\}$ m along the floor

plane with constant height and orientation (human-robot facing each other);

- Five tools (weight (kg), length (m) $\in \{[.35, .1], [.1, .1], [.7, .1], [.35, .5], [.35, .15]\}$).

Table 5.1 shows the statistics of the three planners and the fixed-pose results for the puncturing, pulling and cutting forceful tasks. For each output, we computed the muscular activity effort from $\|\hat{\boldsymbol{\alpha}}_{\text{SO}}\|$ and $\|\hat{\boldsymbol{\alpha}}_{\text{MR}}\|$ using KMEA based on the corresponding muscle-activity prediction criteria.

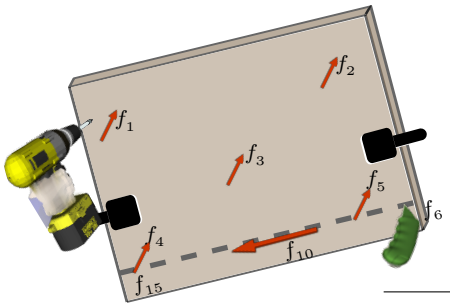
For the first part of the table (first three columns), we computed the human kinematics that minimize (5.9) according to $\hat{\boldsymbol{\alpha}}_{\text{MR}}$, i.e., *biomecConstraints* defined in (5.8) and compute the corresponding muscular activity effort according to $\|\hat{\boldsymbol{\alpha}}_{\text{MR}}\|$. The same steps are taken for the second part (last three columns), i.e., we computed KMEA and muscular activity effort according to $\|\hat{\boldsymbol{\alpha}}_{\text{SO}}\|$. To improve readability, results from the random-planner were used as baseline to normalize the results of other planners.

As expected, SO-Comf-Planner outperforms others for comfort-metric based on $\|\hat{\boldsymbol{\alpha}}_{\text{SO}}\|$, while MR-Comf-Planner yields superior results when using $\|\hat{\boldsymbol{\alpha}}_{\text{MR}}\|$. In a practical application this implies that, for $\|\hat{\boldsymbol{\alpha}}_{\text{SO}}\|$, the random-planner and fixed-pose configuration compared to our comfort-planner respectively demand in average up to 2.9× and 3.8× more muscular activity for puncturing, 3.8× and 4.1× more for pulling; and 1.6× and 3.8× for cutting tasks. This corroborates with our argument and validates the performance both comfort-based planners. Another point to highlight is that the improvements from the SO-Comf-Planner are more noticeable w.r.t. to other planners.

On the other end, the fixed-position often yields worst results with large uncertainty—reflected in the large standard deviation. This is due to the fact that a simple pose as intuitive as it is (a board positioned in front of a user) cannot cover all different interaction possibilities comfortably which calls for an optimization method that guarantees reduced muscular requirements.

The consistency of our approach and results, particularly for the static optimization, is reflected by the lower standard deviation. While one limitation is the required planning time. To compute one solution, the SO-Comf-Planner took 32.2 seconds on average while the MR-Comf-Planner took 23.9 seconds.

Table 5.2: **Muscular activity effort (lower the better) for min-max optimization** over 5 puncturing and 10 sequential cutting operations normalized with Random-Planner (RndP) results.



	$\|\hat{\boldsymbol{\alpha}}_{\text{MR}}\|$	$\|\hat{\boldsymbol{\alpha}}_{\text{SO}}\|$
RndP	1	1
Fixed-Pose	0.785	0.504
MR-Comf-Planner	**0.344**	0.425
SO-Comf-Planner	0.465	**0.300**

5.2.8.2 Optimization Performance: Multiple-Tasks

We also assessed planning performance to address multiple tasks producing a configuration that minimizes the worst muscular activity effort among those tasks. This is done by extending the comfort-based planner from one task in (5.1) to a min-max optimization-based planner, that is,

$$\boldsymbol{q}_{\mathbf{r}}^{\text{opt}}, {}^{\text{o}}\boldsymbol{x}_{\text{rg}}^{\text{opt}} = \arg\min_{\boldsymbol{q}_{\mathbf{r}}, {}^{\text{o}}\boldsymbol{x}_{\text{rg}}} \max_{\ell \in \{1,\ldots,|\ell|\}} \left\{ \underset{\ell}{\text{muscleAct}} \left(\hat{\boldsymbol{q}}_{\text{h},\ell}, {}^{\text{o}}\boldsymbol{f}_{\ell} \right) \right\}$$

$$s.t. \text{ same constraints from (5.1b)} - \text{(5.1d) for each task } \ell.$$

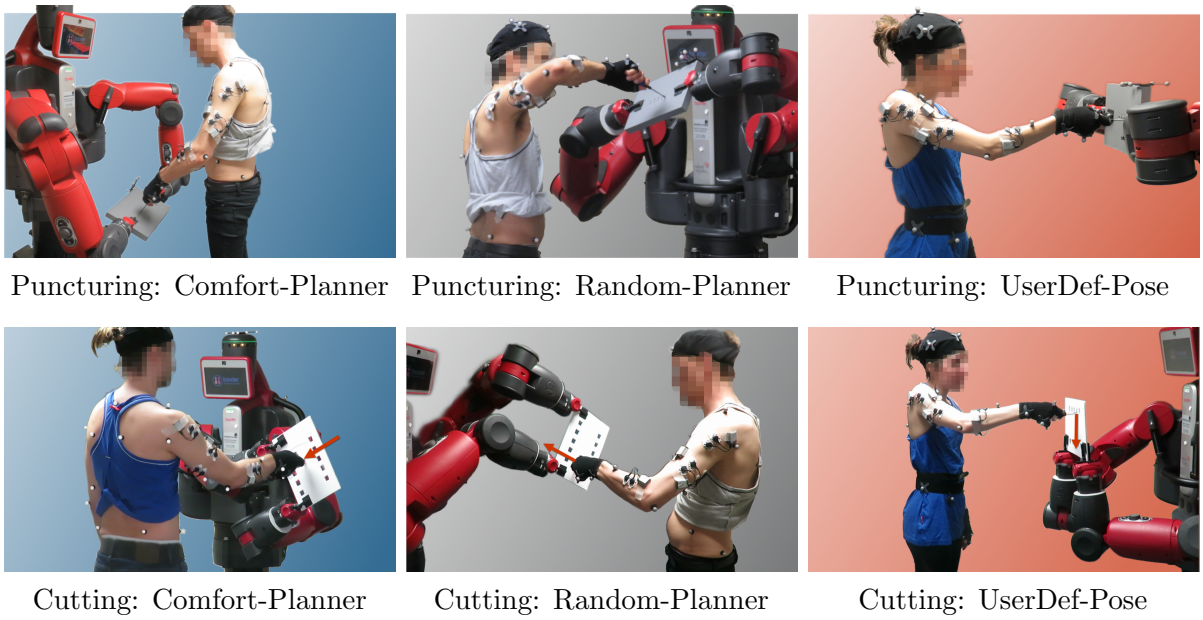
Here, we considered fifteen sequential tasks, i.e., $|\ell|$=15, involving 5 puncturing operations followed by a straight line cutting divided in 10 discrete operations, as shown in the top-left figure in Table 5.2.

Similarly to the previous analysis, both comfort-based planners produced a robot response capable of reducing the muscular-activity of the human counterpart. Particularly, SOComf-Planner outperforms others for $\|\hat{\boldsymbol{\alpha}}_{\text{SO}}\|$ comfort-metric, whilst MRComf-Planner for $\|\hat{\boldsymbol{\alpha}}_{\text{MR}}\|$. The values in gray corresponds to one comfort-based planner with a different assessment metric, e.g., evaluating the SOComf-Planner with $\|\hat{\boldsymbol{\alpha}}_{\text{MR}}\|$. The Random-Planner yields the worst results and demands up to 3.3× more muscular activity compared to SOComf-Planner. The fixed pose scheme, in this case, provides better results compared to the purely Random-Planner, yet it demands at least 1.7× more muscle activation than our comfort-based planners. This highlights that it is possible to plan for multiple operations with human comfort in mind, ensuring no operation demands too much muscular activity. This result paves the way for integrating more elaborate motion/task planners that consider continuous and/or sequential forceful interactions,

e.g., Chen, L. F. Figueredo, et al. 2020; Chen, L. F. C. Figueredo, et al. 2019, while minimizing the total muscular activity required from the human co-worker.

5.2.9 Human-Robot Experiments

This section presents a series of human-robot experiments focused on validating comfort assumptions and evaluating the performance of the proposed comfort-based planning scheme during forceful cooperative motor tasks in unconstrained real-world scenarios with the Baxter robot. The experimental setup[7] used in our study is illustrated in Figure 5.6.



Puncturing: Comfort-Planner | Puncturing: Random-Planner | Puncturing: UserDef-Pose

Cutting: Comfort-Planner | Cutting: Random-Planner | Cutting: UserDef-Pose

Figure 5.6: **Experiments showing forceful human-robot collaborative puncturing (top row) and cutting (bottom figures with cutting direction indicated by the red arrows) and robot configurations** established by the Comfort-Planner, Random-Planner, and UserDef-Pose.

Healthy Participants (A to E, 5, 1 female) of an average age of (30.5 $\pm$ 6.5) were recruited. All participants but one was right hand dominant. Participant A was used to conduct the pilot studies, and the data is not included here. To reduce stress of interacting with the robot participants, on arrival, were suggested to actively engage with the Baxter robot to familiarize them with it. This commonly involved the participants manipulating Baxter's arms and exploring its gravity compensation mode. Participants were then briefed on the two fHRC tasks they would conduct:

[7]Experiments were approved by the ethics committee of the University of Leeds (ID: MEEC 17-034) respecting the Declaration of Helsinki. An exclusion criteria was applied, ensuring that people with known neurophysiological disorders or injuries were not selected. All participants were in good physical condition, followed experimental guidelines (e.g., use of sports gear, avoid caffeine or exercise in both days prior to the experiment) and provided their full consent towards the experiments.

- **Puncturing (Figs. 5.2 and 5.6)**:
  - A hard foam board (2.5 cm depth), designed for resisting puncturing actions, was prepared for each of the participants;
  - Equidistant locations are marked on each board, representing puncturing targets;
  - The participant begins the task by moving their dominant arm towards the target while holding the puncturing tool in a power grip;
  - The participant then proceeds to puncture the target, and subsequently removing the tool from the board, lowering their arm to a neutral position close to the body;
- **Cutting (Figs. 5.2 and 5.6)**:
  - A craft foam board (0.5 cm depth) is prepared for the participants to cut through;
  - Similar to the puncturing task, a target cut pattern is designed for each trial and board, by preparing the board with two hollow squares per trial. Each square indicates the start and finish location for the cut line. For safety, participants do not cut across the board;
  - With a precision grip, the participants initiate the task by raising their dominant arm towards the "Start" square of the indicated trial;
  - The participant then proceeds to cut the board, within the space between the hollow squares, until he/she reaches the "End" square;
  - The participant then removes the cutting tool from the board and returns their arm to a neutral, close to body position;

For planning purposes, we assumed a puncturing force, normal into the board, with magnitude 15 N, and a cutting force, aligned with the cutting direction, with maximum magnitude 10 N.

Prior to beginning the task, the participants positioned themselves in the work space in their desired position. This position was marked on the floor, to ensure in each trial a quasi equal positioning of the participant. To mitigate any possible effects of fatigue (Trossman and Li 1989; Green et al. 2014), adequate rest periods of 2 minutes was ensured between trials. The tasks were designed to measure different levels of comfort in three distinct conditions as defined by the robot planner strategy. Each participant completed a minimum of 42 trials in all (7

trials per condition). The three different configurations were offered in a random order to avoid any bias:

- **Comfort-Planner**: Our comfort-based planner from (5.1) with muscular activity effort ($\|\hat{\boldsymbol{\alpha}}_{\text{SO}}\|$) was computed from static optimization (5.7). [8] The planned object pose and robot configuration are shown in Figure 5.6 (left) for the two operations.
- **Random-planner**: Similar to the Random-Planner defined in Section 5.2.8. Yet, all users had the same human to board pose transformation, which was selected randomly prior to the start of the experiments. The robot planned grasps and configurations accordingly. This was done to maintain consistency between participants' performance across the experiments. This object pose and robot configuration can be seen in Figure 5.6 (centre), for the two operations.
- **UserDef-Pose**: Similar to the fixed-pose in Section 5.2.8, but different for puncturing and cutting. Also, instead of taking a heuristic-based approach, the configurations were selected based on previous human-robot experiments where six different participants were asked to identify preferred (comfortable) positions for both operations. The userDef-Pose was built on the mean pose of the board w.r.t. the human, after outliers removal. Similar to the Random-Planner, for consistency, all users had the same human to board pose transformation. This object pose and robot configuration can be seen in Figure 5.6 (right), for the two operations.

In addition to the above operations, participants performed similar tasks at maximum voluntary contraction (MVC) before and after the experiments which served as a baseline assessment of forces and to confirm that there were no changes in the force capability during the experiment. For the human kinematics tracking, we used Optitrack system (at 120 Hz) synchronized with the force acquisition (at 1 KHz) from the robot and the electromyography (EMG) recording system (Noraxon wireless DTS sensors, model 546 with 10 Hz high-pass filter and low-pass at 1.5 KHz). Recorded data were further processed with Spike2 and Matlab. Each individual muscle activity was normalized against the summed muscle activity and generated force of each trial. The resulting database was also manually scrutinised to ensure quality and experiments with data loss were removed, e.g. camera occlusion and EMG noise.

[8] Given the forceful nature of the tasks, it was seen in the pilot experiments that participants were fatigued when performing too many trials. Hence, only one comfort-based planner was implemented which suffices to illustrate its advantages.

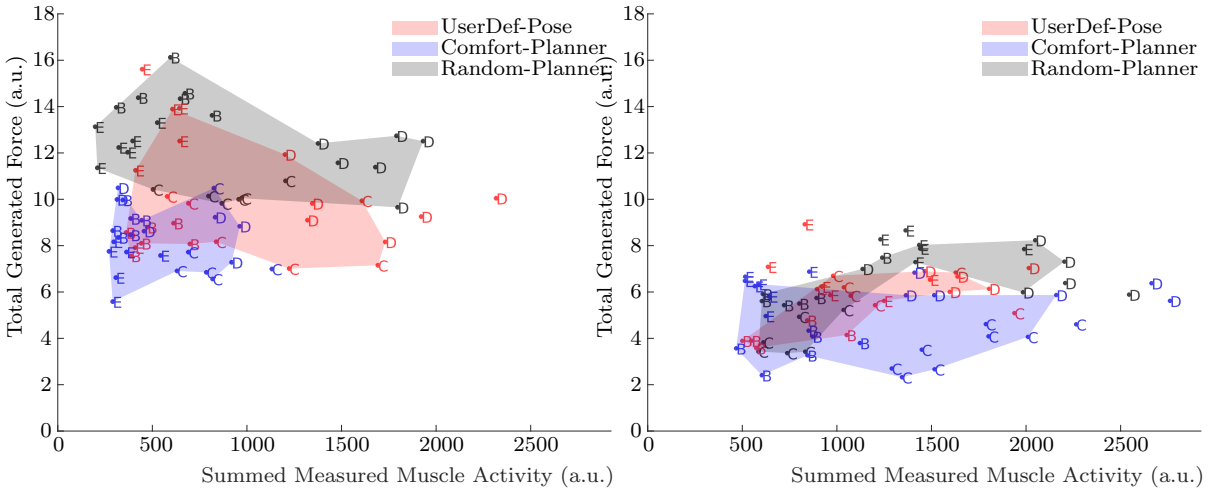
The wireless EMG-sensors were anatomically placed over 9 different muscles selected to include the main muscular actuators for the corresponding motor tasks across the shoulder, elbow and wrist joints. Tables 5.4 and 5.5, both in Section 5.2.13, detail the muscles description, body functions, and relevance to the forceful tasks.

Finally, for clarity, the following definitions will be used hereafter.

Predicted Muscle Activation Level refers to the estimated muscle activation level $\hat{\boldsymbol{\alpha}} \in \mathbb{M}^m$, for the musculoskeletal model with 50-muscles from Saul et al. 2015;

Predicted Muscle Force refers to the estimated muscle force $\hat{f}_{i,m}{=}\hat{\alpha}_i F_i$, that is, the force at the $i-$th muscle given by the predicted activation $\hat{\alpha}_i$ scaled by its maximum isometric force F_i;

Measured Muscle Activity refers to the muscle activity measured from EMG recordings from muscles, which is related to the force generated by selected muscles.



Task: Puncturing Task: Cutting

Figure 5.7: **Measured summed muscle activity (lower the better) and respective task-space force values**; each marker represents a trial from the corresponding subject. The colour shaded areas represents a cluster of trials with similar characteristics under the same condition—as established by the Comfort-Planner, Random-Planner, and UserDef-Pose—without the outliers (defined as those over 3 scaled median absolute deviations from the remaining points). For simplicity, units are displayed as arbitrary units (a.u.).

5.2.10 Comfort Performance from EMGs Biofeedback

As expected, the different configurations—established by the Comfort-Planner, Random-Planner, and UserDef-Pose—invoked different muscle recruitment patterns from the subjects, generating varying levels of force and muscle activity for each trial and condition. In this section, our objective is to analyze if, during the above experiments, the comfort-planning strategy consis-

Table 5.3: The **Summed Muscle Activity of each subject presented as the Mean ± Standard Deviation for both Puncturing and Cutting tasks**. Comparison across planners is thus possible and highlights subjects' preference to the planners. The values for Comfort-Planner for the Puncturing task were consistently the lowest, highlighting its role in reducing muscle effort to complete the task. For the Cutting Task, such a relationship is not as clear, with cases like Subjects C and D presenting a higher values for the Comfort-Planner.

		Subject B	Subject C	Subject D	Subject E
Puncturing	UserDef	495.6 ± 132.8	1105.0 ± 475.9	1639.7 ± 430.7	526.7 ± 116.2
	Comfort	$\mathbf{361.7 \pm 54.8}$	$\mathbf{813.7 \pm 173.9}$	$\mathbf{633.5 \pm 304.1}$	$\mathbf{345.1 \pm 102.0}$
	Random	577.5 ± 182.2	883.2 ± 231.5	1675.8 ± 210.2	$\mathbf{336.8 \pm 123.4}$
Cutting	UserDef	$\mathbf{696.3 \pm 242.3}$	1037.0 ± 114.0	$\mathbf{1698.9 \pm 209.4}$	942.7 ± 251.2
	Comfort	$\mathbf{696.4 \pm 194.5}$	1568.5 ± 280.7	1925.6 ± 600.6	$\mathbf{574.4 \pm 53.3}$
	Random	725.1 ± 124.8	$\mathbf{713.2 \pm 110.9}$	1882.2 ± 508.4	1380.04 ± 100.6

tently reduced muscular effort, when compared with the Random-Planner and the UserDef-Pose strategies.

We present the data we collected in our experiments in Figure 5.7 and in Table 5.3.

Figure 5.7 presents all the trials by all the subjects. Each point is a trial. We plot the measured summed muscle activity and their respective task-space force values for puncturing (left) and cutting (right). Each point is labelled with the human subject (B to E) performing that trial. Each point is colored according to the planner used for the trial, i.e. the Comfort-Planner (blue), Random-Planner (grey) or UserDef-Pose (red). To make visual comparison between planners easier, a condition area is drawn for each planner using the boundary data points from trials of that planner, excluding outliers (i.e. those over 3 scaled median absolute deviations from the remaining points).

Table 5.3 presents the data focusing on each subject separately. For each subject (B to E), we present the mean and standard deviation of the 7+ trials under each planner, for puncturing and cutting. The lowest mean muscle activity of each subject is emphasized in bold.

Below, we discuss the data separately for puncturing and cutting. We also perform statistical significance tests, to test for our claim that the comfort planner produces consistently lower muscle activity when compared to the other planners.

Puncturing. For the puncturing task, the data indicates a reduction in the muscular effort when the Comfort-Planner is used. In Figure 5.7, the resulting blue condition area presents

the lowest summed muscle activity and force values. It also presents a narrower area than the remaining conditions, as expected. The Random-Planner yields the worst results (least comfortable), while the highly scattered UserDef-Pose results reveals that general (one-fits-all) solutions do not sufficiently constrain the forceful operation to a comfort area. This leads to a larger variability amongst participants which in turn yields both comfortable and uncomfortable executions (even for the same participant on different trials). The smaller variation in the Comfort-planner trials (when compared with the variations of the UserDef and Random planners) may be suggesting that while the UserDef and Random data points are sampled from a larger underlying distribution, the Comfort-Planner results are sampled from the smaller subset that requires less muscular activity. Overall, the centroid of the UserDef-Pose and Random-Planner condition areas respectively yield muscular-activity 69.5% and 72.5% larger compared to the Comfort-Planner condition area, and similarly 29.8% and 60.2% larger forces.

Table 5.3 also supports our claim that the comfort planner produces lower muscle activity at the subject level. The comfort planner has the lowest mean muscle activity for three of the four subjects. For the fourth subject (E), while the Random Planner mean muscle activity is lower, the Comfort Planner value is extremely close.

To test our hypothesis, we have performed a repeated measures ANOVA to compare the effect of planner-type on each subject's performance in terms of muscle activity. Significant difference in means was assessed posthoc, and a Bonferroni-Holm correction applied (P_h). This was all performed using the JASP software (JASP 0.14.1.0., University of Amsterdam). Overall, the mean measured muscle activity was different for the puncturing task (F = 18.45, p¡ .001, df= 2) significantly different between Comfort-planner (F = 10.07, df =3, p ¡ .001) and Userdef (P_h ¡ .001) and also with Random (P_h ¡ .001). The means of Userdef and Random were not (P_h = 0.39) significantly different. In other words, our hypothesis that the comfort planner produces consistently lower muscle activity is indeed valid and statistically significant.

Cutting. Results for the cutting task are less clear. In Figure 5.7, different planners reveal smaller differences when looking at the overall area per condition.

The subject-specific evaluation in Table 5.3 is also not completely convincing, but for two of the four subjects (B and E) the Comfort-Planner produces minimal muscle activity. An exceptional case was Subject-C response for the cutting task. Subject-C data shows lowest mean muscle activity for the Random-Planner, whereas the Comfort-Planner performs worst

(This result agrees with the responses of Subject-C to the questionnaire, which we will present in Section 5.2.11). There are two possible scenarios to explain this: either the musculoskeletal model didn't properly cope with the real muscle activity model from Subject-C or the muscle-nullspace response was not optimized for the specific task-space. For the second possibility, it is relevant to highlight that Subject C has expressed in the Questionnaire additional comments to be unfamiliar with DIY tasks. In this sense, and taking note that the cutting was a harder task to understand and perform compared to the puncturing, it is possible that the unfamiliarity prevented a proper optimization in the nullspace. In other words, the motor control system was not aware of which forces to expect and therefore did not respond as predicted (shown in Figure 5.8). From this perspective, additional executions would likely improve the overall expected response. Yet, it is worth noticing that this effect could also be mitigated by taking uncertainties related to human response into consideration.

There is another important difference between the Puncturing task and Cutting task: The Puncturing task was much shorter (both in terms of the time it takes and the distance the tool needs to travel) than the Cutting task. This has negative consequences for the Cutting results in two ways. First, during cutting, there were more opportunities for the subject to change body posture, or the grasp on the tool. Since our model assumes a fixed human body posture, this represented a larger deviation from our assumptions, when compared with the Puncturing case. Second, the length of the Cutting tasks also meant more dynamic activity of the muscles which in general results in less reliable and more noisy readings with the EMG biosensors. These aspects of the task might have contributed to the weaker results we observe with Cutting.

Statistical significance tests (including Subject-C) produce inconclusive results for the Cutting task. The mean of the measured muscle activity was not significantly different for the planners across subjects for cutting (F =0.39, p = 0.68, df =2). There was no difference in means across the three planners - Comfort-planner to Userdef ($P_h = 1$) and with Random ($P_h = 1$). Also means of Userdef and Random were not ($P_h = 1$) significantly different. Still, we note that, if we exclude Subject-C, UserDef-Pose and Random-Planner condition areas in Figure 5.7 respectively yield muscular-activity 26.6% and 58.6% larger compared to the Comfort-Planner condition area.

Muscle-Activity Prediction:

We also analyzed the prediction capabilities of the comfort metric $\|\hat{\boldsymbol{\alpha}}_{\text{SO}}\|$. Figure 5.8 presents the predicted summed muscle forces from the musculoskeletal model Saul et al. 2015, i.e., the norm of the force generated by the m=50 muscles. The values were computed by taking the measured human kinematics, i.e., $\boldsymbol{q}_{\text{h}}$ and measured task-space force ${}^{\text{o}}\boldsymbol{f}$ (vertical axis in Figure 5.8).

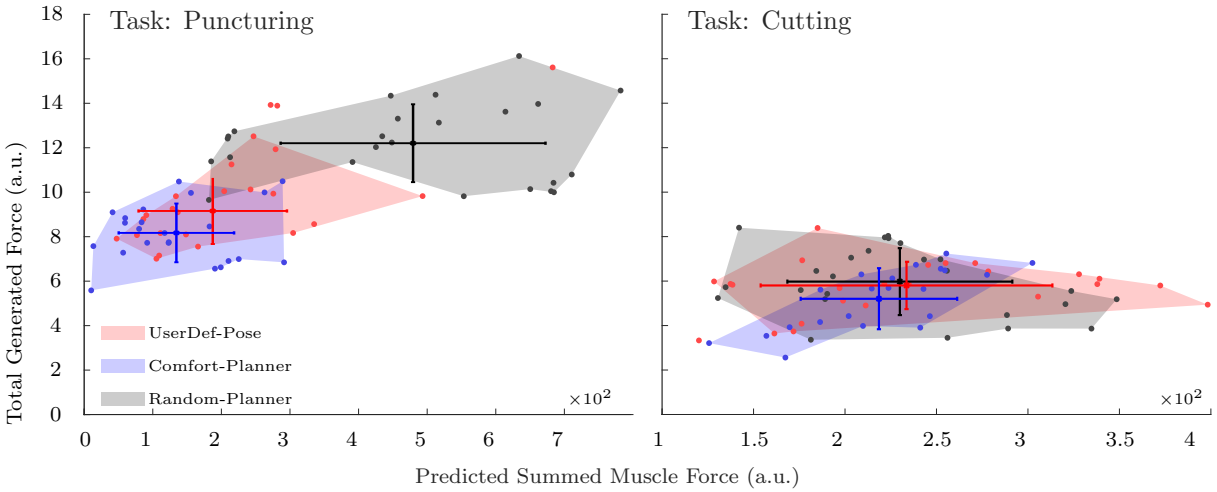


Figure 5.8: **Predicted muscle forces from musculoskeletal model and corresponding task-space forces** condition areas were constructed as in Figure 5.7

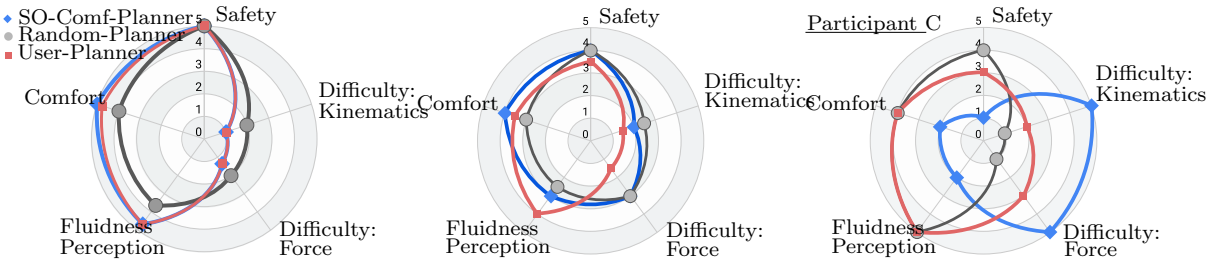
The predicted condition areas are consistent with the measured values in Figure 5.7, particularly for the puncturing task. The cutting task presented larger differences with respect to the measured data. This reflects participants perception of puncturing being an easier to understand/ implement task (see Subsection 5.2.11).

The puncturing task also presented a linear behaviour w.r.t. to the task-space force to predicted muscle activation and forces, as expected by combining (5.6) with (5.7b). That is, a linear increase in task-space force should reflect a linear increase in muscular activation. Similar behaviour is also observed for the cutting task based on the Comfort-Planner scenario.

5.2.11 Participants' perception of comfort

After the experiments, for each forceful task and robot configuration, participants were asked to complete a psychometric questionnaire. Participants were asked to grade (1 to 5) the following questions (in addition to providing further comments on the experiments):

1. How safe have you felt during the robot interaction?
2. How difficult was the task for you, in terms of the kinematics (reaching for the task)?



(a) Puncturing (b) Cutting (c) Cutting-C

Figure 5.9: **Average response from participants according to questions in Subsection 5.2.11** for (a) puncturing; (b) cutting (excluding subject C); and (c) individual cutting task for Subject C

3. How difficult was the task for you, in terms of the required force?

4. How natural/fluid was the interaction for you? (How likely were you to choose the board-/robot pose?)

5. Overall, how comfortable was the task for you?

The scores are summarized in Figure 5.9. For questions 1, 4 and 5, the higher the grade the better the user perception about the interaction while questions 2-3 work the other way around.

From Figures 5.9(a-b), it is clear that participants agreed the puncturing task was more comfortable, safer and easier to execute (both in terms of their body posture as well as in terms of the required forces) compared with the cutting task. For the puncturing task, participants' perception of the Comfort-Planner and UserDef-Pose configurations were similar with a small improved comfort perception to our planner. Performance for the Random-Planner was considerably worse, as predicted by both musculoskeletal model and the measured muscle activity shown in Figures 5.75.8.

For the cutting task, participants expressed the robot behaviour w.r.t. the Comfort-Planner to be more comfortable and safe, yet less intuitive than the UserDef-Pose. Participants graded the UserDef-Pose response to be the less difficult (w.r.t. the kinematics) which corroborate with participants general comments on intuitiveness. Curiously, participants also graded the UserDef-Pose to be less force demanding which contradicts the readings from task-space force sensors and EMGs data, shown in Figure 5.7.

An exceptional case was Subject C's responses for the cutting task, as shown in Figure 5.9(c). The participant expressed the Random-Planner resulting configuration as the best both in terms

of safety and comfort as well as in terms of being less difficult, whilst considered the Comfort-Planner the worst in all questions. The results for this participant differed completely from the other participants in this task, yet participant's consideration was also captured from the EMGs response as discussed previously.

All participants reported that the cutting task was more difficult to execute than the puncturing—which agrees with the general response in Figure 5.9. Subjects C-D also commented they needed to increase their force during task as the task was not as fluid. Subject C has additionally expressed to have never done DIY tasks. Subject D was the only participant to have performed HRI experiments prior to this work, yet all participants reported to have enjoyed the experience and have found the fHRC to be safe.

5.2.12 Quantitative Analysis of KMEA

During fHRC experiments, participants were free to perform the tasks in the way they felt more comfortable, which in turn implied slightly different human kinematic configurations compared to the ones predicted and therefore different musculoskeletal response.

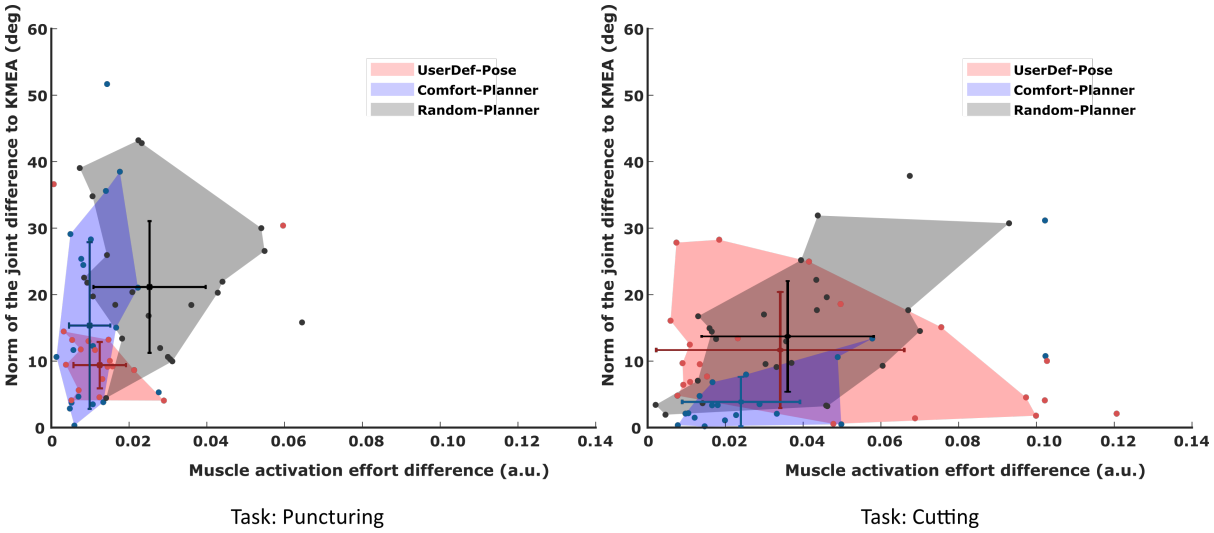


Figure 5.10: **Norm of the kinematics error between predicted KMEA and measured joints**, that is, $\left\|\hat{\boldsymbol{q}}_{\mathrm{h}} - \boldsymbol{q}_{\mathrm{h}}\right\|$, and corresponding predicted muscle activity effort error norm $\left\|\hat{\boldsymbol{\alpha}}_{\mathrm{h}}\left(\hat{\boldsymbol{q}}_{\mathrm{h}}\right) - \hat{\boldsymbol{\alpha}}_{\mathrm{h}}\left(\boldsymbol{q}_{\mathrm{h}}\right)\right\|$. The coloured condition areas were constructed as in Figures 5.7 and 5.8.

To quantitatively analyze KMEA, for each trial, we computed the KMEA kinematics and corresponding predicted muscle activity effort and compared the outputs with participants' results. The difference between predicted and real data is shown in Figure 5.10. The $y-$axis shows the kinematics error norm in term of joint values from predicted KMEA ($\hat{\boldsymbol{q}}_{\mathrm{h}}$) and real measured

joints ($\boldsymbol{q}_{\text{h}}$)—that is, $\left\|\hat{\boldsymbol{q}}_{\text{h}} - \boldsymbol{q}_{\text{h}}\right\|$. The $x-$axis depicts the predicted muscle activity effort from all trials $\hat{\boldsymbol{\alpha}}\left(\boldsymbol{q}_{\text{h}}\right)$—computed from (5.7)—compared to the values associated with the KMEA configuration, that is, the muscle activity prediction error norm due to the KMEA, $\left\|\hat{\boldsymbol{\alpha}}\left(\hat{\boldsymbol{q}}_{\text{h}}\right) - \hat{\boldsymbol{\alpha}}\left(\boldsymbol{q}_{\text{h}}\right)\right\|$. In this sense, a zero kinematics error, i.e., $\hat{\boldsymbol{q}}_{\text{h}} = \boldsymbol{q}_{\text{h}}$ implies zero predicted muscle-activity error, i.e., $\hat{\boldsymbol{\alpha}}\left(\hat{\boldsymbol{q}}_{\text{h}}\right) = \hat{\boldsymbol{\alpha}}\left(\boldsymbol{q}_{\text{h}}\right)$. The closer to 0, the better is the KMEA prediction.

In both puncturing (left) and cutting (right) tasks, the muscular effort, as shown in Figure 5.10, remained close to predicted muscular minimum effort value. Yet, the puncturing task allowed for a larger kinematic redundancy from participants while maintaining small variations of the muscular effort value. This is particularly clear for configurations based on the Comfort-Planner (blue cluster) which were able to accommodate larger joint-deviations without undermining muscle-activity. Configurations based on the Random-Planner forced participants to larger deviations from the KMEA assumption for both puncturing and cutting scenarios. Such behaviour may be associated with the difficulty of visualizing the task from such non-intuitive random configurations (as highlighted by participants). The muscular effort variation is also higher in the cutting task compared to the puncturing and more liable to increase even with small kinematic changes.

5.2.13 Individual Muscle Selection and Assessment

Table 5.4: **Selection of muscles and their respective functions associated with the upper-limb** Biel 2010.

Code	Name	Function
PM	Pectoralis Major	Flex and medially rotate shoulder joint, horizontally adduct humerus towards opposite shoulder
AD	Anterior Deltoid	Flex, medially rotate and horizontally adduct the shoulder
PD	Posterior Deltoid	Extend, laterally rotate and horizontally abduct the shoulder
LD	Latissimus Dorsi	Extend, medially rotate and adduct the shoulder joint
BB	Biceps Brachii	Flex the elbow, supinate the forearm, assist to flex the shoulder
LT	Triceps B. (Lateral head)	Extend the elbow
MT	Triceps B. (Medial head)	Extend the elbow, extend the shoulder, assist to adduct the shoulder
FR	Flexor Carpi Radialis	Extend the wrist, abduct the wrist, assist to flex the elbow
ER	Extensor Carpi Radialis	Flex the wrist, abduct the wrist, may assist to flex the elbow

This section presents an additional discussion about the muscle selection, their relevance to the task, and a thorough assessment of measured activity of individual muscles.

Table 5.5: **The ratio between the predicted least summed muscular force** $\left\|\hat{\boldsymbol{f}}_m\right\|$ from the selected muscles compared to the 50 muscle segments in Saul et al. 2015.

	Comfort-Planner	Random-Planner	UserDef-Pose
Puncturing	0.780	0.896	0.855
Cutting	0.654	0.609	0.537

5.2.13.1 Muscle Selection

For all experiments in Section 5.2.9, the wireless sensors were placed in 9 different anatomical positions selected to include the main actuators for the corresponding motor tasks across the shoulder, elbow and wrist joints. Table 5.4 details the muscle code used and their body functions. It is important to highlight that the 9 EMGs sensors are in fact covering 16 individual muscle segments from the model in Saul et al. 2015. This is due to the fact that it is difficult to fully isolate muscle segments activities from certain muscles in real-world unconstrained applications—e.g., although BIClong and BICshort presented in Saul et al. 2015 have different contributions, anatomically, they belong and are considered just segments of the BB. The 16 corresponding muscle segments from the musculoskeletal system Saul et al. 2015 are PECM{1,2,3} DELT{1,3}, LAT{1,2,3}, BIClong, BICshort, TRIlat, TRIlong, TRImed, FCR, ECRB, and ECRL—muscle code from OpenSim Delp et al. 2007.

To better understand the relevance of the muscle selection and validate their importance prior to the real experiments to the planning results, we also computed the expected muscular force for the 50–muscles model in Saul et al. 2015. The ratio between the predicted muscle force stemming from the selected muscles compared to the total muscle force of the upper-limb (generated by the 50-muscle segments) is shown in Table. 5.5. As expected the selected muscles cover most of the total force generated—about 78% to 90% of the total muscle-force for puncturing and 54% to 65% for cutting.

5.2.13.2 Individual Muscle Assessment

In this subsection, we explore specificities of the muscle activation and analyze whether the musculoskeletal model can predict which muscles are being activated during the fHRC.

Figure 5.11 presents the individual muscle recruitments against the total generated force, for all puncturing trials (different vertical lines) performed under the comfort-planner strategy. From the results, it is clear how each participant employs different muscle configurations to

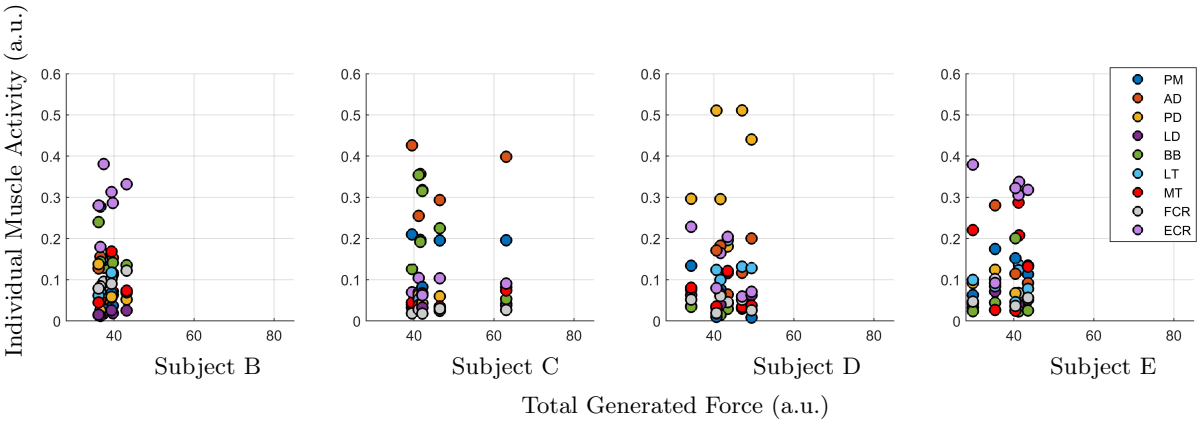


Figure 5.11: **Puncturing task dataset for the comfort-planner**: compilation of the force generated and individual measured muscle force data for all subjects and individual trials. Vertical lines represent individual trials, populated with the measured data of each muscle recorded

complete the tasks, with AD, ECR, PD and BB generally being the most active muscles for the puncturing task (for the cutting task, the most activated muscles were PM, PD, MT and FCR, yet for brevity we will focus on puncturing). The muscle codes are described in Table 5.4.

The experiment was designed with a fixed human grasp per operation, yet there was no constraint on the human while executing the task. An unforeseen degree of freedom rose from the hand grip the subjects were adopting while holding the tools. While in the puncturing task there is a fairly limited number of possible grips (typically a diagonal volar grip is used), for the cutting, we have noticed two distinct grips (internal precision grip and the diagonal volar grip). The immediately noticeable effect of these distinct grip modes is on the FCR and ECR muscles, altering the subject's grasp force on the tool itself. This grasp force does not contribute directly towards the generated force at the end-effector of the tool. At this stage, the impact towards our algorithm development and model verification is minimal and the individual measured muscle force normalized by the summed force is in most cases well distributed. Still, these different grips pose an interesting new question to solve at a later stage.

5.2.14 Conclusion and Future-Work

This work provides a human-comfort-based planner that improves robot decision making capabilities in shaping human musculoskeletal response during a fHRC. Our planner relies on predictions of the human-arm configuration and muscle to task-space mapping in order to deploy robot grasps and configurations that tailor human collaborative action towards a less muscular demanding interaction area.

The proposed comfort planning framework, agnostic to muscular activity estimation paradigms, enables the robot to shape human kinematics and musculoskeletal response. Effectiveness of our algorithm were first analyzed through different simulation scenarios. Furthermore, extensive experiments on two distinct motor tasks (drilling and cutting) have validated our comfort and kinematic response hypotheses. Most importantly, results demonstrated the efficiency of the proposed Comfort-Planner which is able to identify and plan collaborative actions leading humans to exert smaller muscular forces. Experimental results have also shown that both random and user defined poses fail to ensure satisfactory behavior for different participants which highlights the importance of user-tailored planning solutions in order to improve fHRC acceptance. Results also reveal the practical potential of the proposed strategy to reduce muscular load in manufacturing and other industries through intelligent collaborative robots.

Among possible directions the proposed framework can lead to future findings, we highlight a few. First, possible improvements w.r.t. muscle-activity prediction. Possible research focus would either include online learning strategies, relying on musculoskeletal model calibration, or adding robustness to the optimization to mitigate model uncertainties. The latter is more suitable for practical applications due to the constraints in measuring biofeedback signals outside a laboratory environment. In future works, we aim to assess additional human factors (e.g., safety-perception Chen, L. F. Figueredo, et al. 2018; Mansfeld et al. 2018) and task-specific execution (e.g., visibility criterion) to improve even further human experience during a collaborative action. We are also currently investigating methods based on precomputing a comfort map from KMEA for the human reachable space to speed up the comfort assessment, particularly for real-time control applications. Finally, we will also explore fHRC positioning influence over the human grasp. For instance, taking the human grasp clustering in Feix et al. 2016; Sburlea and Müller-Putz 2018, we may explore if the robot can modify the human grasp for a given task.

5.2.15 Acknowledgements

This project has received funding from the European Union's Horizon 2020 research and innovation programme under the Marie Sklodowska-Curie grant agreement No 746143 and 795714, the AI4EU project (agreement No 825619) and from the UK Engineering and Physical Sciences Research Council under grant EP/P019560/1. This work was also partially funded by the Lighthouse Initiative Geriatronics by StMWi Bayern (Project X, grant no. 5140951), LongLeif

GaPa gGmbH (Project Y, grant no. 5140953), and Universal-CNPq (grant no. 429550/2016-2).

5.2.16 References

Ajoudani, A., Zanchettin, A. M., Ivaldi, S., Albu-Schäffer, A., Kosuge, K., and Khatib, O. (2018). "Progress and prospects of the human–robot collaboration". In: *Autonomous Robots* 42.5, pp. 957–975. ISSN: 1573-7527. DOI: 10.1007/s10514-017-9677-2.

Albu-Schäffer, A., S., H., Ott, C., Stemmer, A., Wimbock, T., and Hirzinger, G. (2007). "The DLR lightweight robot: design and control concepts for robots in human environments". In: *Industrial Robot* 34.5, pp. 376–385. DOI: 10.1108/01439910710774386.

Aleotti, J., Micelli, V., and Caselli, S. (2012). "Comfortable robot to human object hand-over". In: *The 21st IEEE International Symposium on Robot and Human Interactive Communication (RO-MAN)*, pp. 771–776. DOI: 10.1109/ROMAN.2012.6343845.

Alibeji, N., Kirsch, N., and Sharma, N. (2017). "An adaptive low-dimensional control to compensate for actuator redundancy and FES-induced muscle fatigue in a hybrid neuroprosthesis". In: *Control Engineering Practice* 59, pp. 204–219. DOI: 10.1016/J.CONENGPRAC.2016.07.015.

Anderson, F. C. and Pandy, M. G. (2001). "Static and dynamic optimization solutions for gait are practically equivalent". In: *Journal of Biomechanics* 34.2, pp. 153–161. ISSN: 0021-9290. DOI: https://doi.org/10.1016/S0021-9290(00)00155-X.

Australian Bureau of Statistics (2010). *Work-related injuries, Australia.* Tech. rep. Technical Report. Australia: Australian Bureau of Statistics.

Baptista, R. d. S., Bó, A. P. L., and Hayashibe, M. (2017). "Automatic Human Movement Assessment With Switching Linear Dynamic System: Motion Segmentation and Motor Performance". In: *IEEE Transactions on Neural Systems and Rehabilitation Engineering* 25.6, pp. 628–640. ISSN: 1558-0210.

Biel, A. R. (2010). *Trail Guide to the Body: A Hands-on Guide to Locating Muscles, Bones, and More.* 4th ed. Books of Discovery, p. 440. ISBN: 0982663404.

Busch, B., Toussaint, M., and Lopes, M. (2018). "Planning Ergonomic Sequences of Actions in Human-Robot Interaction". In: *2018 IEEE International Conference on Robotics and Automation (ICRA)*, pp. 1916–1923. DOI: 10.1109/ICRA.2018.8462927.

Busch, B. (2018). "Optimization techniques for an ergonomic human-robot interaction". PhD thesis, p. 105.

Cakmak, M., Srinivasa, S. S., Lee, M. K., Forlizzi, J., and Kiesler, S. (2011). "Human preferences for robot-human hand-over configurations". In: *IEEE/RSJ International Conference on Intelligent Robots and Systems*. DOI: 10.1109/IROS.2011.6094735.

Cakmak, M., Srinivasa, S. S., Lee, M. K., Kiesler, S., and Forlizzi, J. (2011). "Using spatial and temporal contrast for fluent robot-human hand-overs". In: *2011 6th ACM/IEEE International Conference on Human-Robot Interaction (HRI)*, pp. 489–496. DOI: 10.1145/1957656.1957823.

Chan, W. P., Parker, C. A., Van der Loos, H. M., and Croft, E. A. (2013). "A human-inspired object handover controller". In: *The International Journal of Robotics Research* 32.8, pp. 971–983.

Chen, L., Figueredo, L. F. C., and Dogar, M. (2018). "Manipulation Planning Under Changing External Forces". In: *2018 IEEE/RSJ International Conference on Intelligent Robots and Systems (IROS)*, pp. 3503–3510. DOI: 10.1109/IROS.2018.8593555.

Chen, L., Figueredo, L. F., and Dogar, M. R. (2018). "Planning for Muscular and Peripersonal-Space Comfort During Human-Robot Forceful Collaboration". In: *2018 IEEE-RAS 18th International Conference on Humanoid Robots (Humanoids)*, pp. 1–8. DOI: 10.1109/HUMANOIDS.2018.8624978.

Chen, L., Figueredo, L. F. C., and Dogar, M. (2019). "Manipulation Planning Using Environmental Contacts to Keep Objects Stable under External Forces". In: *2019 IEEE-RAS 19th International Conference on Humanoid Robots (Humanoids)*, pp. 417–424. DOI: 10.1109/Humanoids43949.2019.9034998.

Chen, L., Figueredo, L. F., and Dogar, M. R. (2020). "Manipulation planning under changing external forces". In: *Autonomous Robots* 44.7, pp. 1249–1269.

Damsgaard, M., Rasmussen, J., Christensen, S. T., Surma, E., and Zee, M. de (2006). "Analysis of musculoskeletal systems in the AnyBody Modeling System". In: *Simulation Modelling Practice and Theory* 14.8. SIMS 2004, pp. 1100–1111. ISSN: 1569-190X. DOI: https://doi.org/10.1016/j.simpat.2006.09.001.

De Groote, F., Kinney, A. L., Rao, A. V., and Fregly, B. J. (2016). "Evaluation of Direct Collocation Optimal Control Problem Formulations for Solving the Muscle Redundancy Problem". In: *Annals of Biomedical Engineering* 44.10, pp. 2922–2936. ISSN: 1573-9686. DOI: 10.1007/s10439-016-1591-9.

Dehais, F., Sisbot, E. A., Alami, R., and Causse, M. (2011). "Physiological and subjective evaluation of a human–robot object hand-over task". In: *Applied ergonomics* 42.6, pp. 785–791.

Delp, S. L., Anderson, F. C., Arnold, A. S., Loan, P., Habib, A., John, C. T., Guendelman, E., and Thelen, D. G. (2007). "OpenSim: Open-Source Software to Create and Analyze Dynamic Simulations of Movement". In: *IEEE Transactions on Biomedical Engineering* 54.11, pp. 1940–1950. ISSN: 0018-9294. DOI: 10.1109/TBME.2007.901024.

Demircan, E., Kulić, D., Oetomo, D., and Hayashibe, M. (2015). "Human Movement Understanding [TC Spotlight]". In: *IEEE Robotics Automation Magazine* 22.3, pp. 22–24. ISSN: 1558-223X. DOI: 10.1109/MRA.2015.2452171.

Dimeas, F. and Aspragathos, N. (2016). "Online Stability in Human-Robot Cooperation with Admittance Control". In: *EEE Trans. Haptics* 9.2, pp. 267–278. ISSN: 1939-1412. DOI: 10.1109/TOH.2016.2518670.

Feix, T., Romero, J., Schmiedmayer, H.-B., Dollar, A. M., and Kragic, D. (2016). "The GRASP Taxonomy of Human Grasp Types". In: *IEEE Transactions on Human-Machine Systems* 46.1. DOI: 10.1109/THMS.2015.2470657.

Green, L. A., Parro, J. J., and Gabriel, D. A. (2014). "Beneficial effects of serial contractions on muscle performance after a brief period of rest". In: *European Journal of Applied Physiology* 114.8, pp. 1657–1665. DOI: 10.1007/s00421-014-2896-8.

Haddadin, S. and Croft, E. (2016). "Physical Human–Robot Interaction". In: *Springer Handbook of Robotics*. Ed. by B. Siciliano and O. Khatib. Cham: Springer International Publishing, pp. 1835–1874. ISBN: 978-3-319-32552-1. DOI: 10.1007/978-3-319-32552-1_69.

Kang, T., He, J., and Tillery, S. I. H. (2005). "Determining natural arm configuration along a reaching trajectory". In: *Experimental Brain Research* 167, pp. 352–361.

Khatib, O., Demircan, E., Sapio, V. D., Sentis, L., Besier, T., and Delp, S. (2009). "Robotics-based synthesis of human motion". In: *Journal of Physiology-Paris* 103.3. Neurorobotics, pp. 211–219. ISSN: 0928-4257. DOI: https://doi.org/10.1016/j.jphysparis.2009.08.004.

Kim, W., Lee, J., Peternel, L., Tsagarakis, N., and Ajoudani, A. (2018). "Anticipatory Robot Assistance for the Prevention of Human Static Joint Overloading in Human–Robot Collaboration". In: *IEEE Robotics and Automation Letters* 3.1, pp. 68–75. ISSN: 2377-3766. DOI: 10.1109/LRA.2017.2729666.

Kim, W., Lee, J., Tsagarakis, N., and Ajoudani, A. (2017). "A real-time and reduced-complexity approach to the detection and monitoring of static joint overloading in humans". In: *2017 International Conference on Rehabilitation Robotics (ICORR)*. DOI: 10.1109/ICORR.2017.8009351.

Kim, W., Lorenzini, M., Balatti, P., Nguyen, P. D. H., Pattacini, U., Tikhanoff, V., Peternel, L., Fantacci, C., Natale, L., Metta, G., and Ajoudani, A. (2019). "Adaptable Workstations for Human-Robot Collaboration: A Reconfigurable Framework for Improving Worker Ergonomics and Productivity". In: *IEEE Robotics Automation Magazine* 26.3, pp. 14–26. DOI: 10.1109/MRA.2018.2890460.

Kragic, D., Gustafson, J., Karaoguz, H., Jensfelt, P., and Krug, R. (July 2018). "Interactive, Collaborative Robots: Challenges and Opportunities". In: *Proceedings of the Twenty-Seventh International Joint Conference on Artificial Intelligence, IJCAI-18*. International Joint Conferences on Artificial Intelligence Organization, pp. 18–25. DOI: 10.24963/ijcai.2018/3.

Kulić, D., Venture, G., Yamane, K., Demircan, E., Mizuuchi, I., and Mombaur, K. (2016). "Anthropomorphic Movement Analysis and Synthesis: A Survey of Methods and Applications".

In: *IEEE Transactions on Robotics* 32.4, pp. 776–795. ISSN: 1941-0468. DOI: 10.1109/TRO.2016.2587744.

Lacquaniti, F. and Soechting, J. F. (1982). "Coordination of arm and wrist motion during a reaching task". In: *The Journal of neuroscience* 2.4, pp. 399–408. DOI: 10.1523/JNEUROSCI.02-04-00399.

Lasota, P. A., Rossano, G. F., and Shah, J. A. (2014). "Toward Safe Close-Proximity Human-Robot Interaction with Standard Industrial Robots". In: *IEEE Intern Conf on Automation Science & Engineering*.

Mansfeld, N., Hamad, M., Becker, M., Marin, A. G., and Haddadin, S. (2018). "Safety Map: A Unified Representation for Biomechanics Impact Data and Robot Instantaneous Dynamic Properties". In: *IEEE Robotics and Automation Letters* 3.3, pp. 1880–1887. ISSN: 2377-3766. DOI: 10.1109/LRA.2018.2801477.

Medina, J. R., Duvallet, F., Karnam, M., and Billard, A. (2016). "A human-inspired controller for fluid human-robot handovers". In: *2016 IEEE-RAS 16th International Conference on Humanoid Robots (Humanoids)*. IEEE, pp. 324–331.

Milner, T. E. (2002). "Contribution of geometry and joint stiffness to mechanical stability of the human arm". In: *Experimental Brain Research* 143.4, pp. 515–519. ISSN: 1432-1106. DOI: 10.1007/s00221-002-1049-1.

Pandey, A. K., Saut, J. P., Sidobre, D., and Alami, R. (2012). "Towards planning Human-Robot Interactive manipulation tasks: Task dependent and human oriented autonomous selection of grasp and placement". In: *IEEE International Conference on Biomedical Robotics and Biomechatronics (EMBS BioRob)*, pp. 1371–1376. DOI: 10.1109/BioRob.2012.6290776.

Pedotti, A., Krishnan, V., and Stark, L. (1978). "Optimization of muscle-force sequencing in human locomotion". In: *Mathematical Biosciences* 38.1, pp. 57–76. ISSN: 0025-5564. DOI: https://doi.org/10.1016/0025-5564(78)90018-4.

Peternel, L., Fang, C., Tsagarakis, N., and Ajoudani, A. (2018). "Online Human Muscle Force Estimation for Fatigue Management in Human-Robot Co-Manipulation". In: *2018 IEEE/RSJ*

International Conference on Intelligent Robots and Systems (IROS), pp. 1340–1346. DOI: 10.1109/IROS.2018.8593705.

Peternel, L., Kim, W., Babic, J., and Ajoudani, A. (2017). "Towards ergonomic control of human-robot co-manipulation and handover". In: *IEEE-RAS 17th International Conference on Humanoid Robotics (Humanoids)*, pp. 55–60. DOI: 10.1109/HUMANOIDS.2017.8239537.

Peternel, L., Fang, C., Tsagarakis, N., and Ajoudani, A. (2019). "A selective muscle fatigue management approach to ergonomic human-robot co-manipulation". In: *Robotics and Computer–Integrated Manufacturing* 58, pp. 69–79. ISSN: 0736-5845. DOI: https://doi.org/10.1016/j.rcim.2019.01.013.

Roncone, A., Hoffmann, M., Pattacini, U., Fadiga, L., and Metta, G. (2016). "Peripersonal space and margin of safety around the body: Learning visuo-tactile associations in a humanoid robot with artificial skin". In: *PLoS ONE* 11.10, pp. 1–32. ISSN: 19326203. DOI: 10.1371/journal.pone.0163713.

Santis, A. D., Siciliano, B., Luca, A. D., and Bicchi, A. (2008). "An atlas of physical human-robot interaction". In: *Mechanism and Machine Theory* 43.3, pp. 253–270. ISSN: 0094-114X. DOI: https://doi.org/10.1016/j.mechmachtheory.2007.03.003.

Saul, K. R., Hu, X., Goehler, C. M., Vidt, M. E., Daly, M., Velisar, A., and Murray, W. M. (2015). "Benchmarking of dynamic simulation predictions in two software platforms using an upper limb musculoskeletal model Benchmarking of dynamic simulation predictions in two software platforms using an upper limb musculoskeletal model". In: *Computer Methods in Biomechanics and Biomedical Engineering* 18.13, pp. 1445–1458. DOI: 10.1080/10255842.2014.916698.

Saul Holzbaur, K. R., Murray, W. M., and Delp, S. L. (2005). "A Musculoskeletal Model Of The Upper Extremity For Surgical Simulation And Neurocontrol Applications". In: *Annals of BIomedical Engineering* 6.33, pp. 829–840.

Sburlea, A. I. and Müller-Putz, G. R. (2018). "Exploring representations of human grasping in neural, muscle and kinematic signals". In: *Nature - Scientific Reports* 8.16669. DOI: 10.1038/s41598-018-35018-x.

Spong, M., Hutchinson, S., and Vidyasagar, M. (2006). *Robot modeling and control*. John Wiley & Sons. ISBN: 0471649902.

Stanev, D. and Moustakas, K. (2018). "Simulation of Constrained Musculoskeletal Systems in Task Space". In: *IEEE Transactions on Biomedical Engineering* 65.2, pp. 307–318. DOI: 10.1109/TBME.2017.2764630.

Stanev, D. and Moustakas, K. (Jan. 2019). "Modeling musculoskeletal kinematic and dynamic redundancy using null space projection". In: *PLOS ONE* 14.1, pp. 1–26. DOI: 10.1371/journal.pone.0209171.

Tanaka, Y., Nishikawa, K., Yamada, N., and Tsuji, T. (2015). "Analysis of Operational Comfort in Manual Tasks Using Human Force Manipulability Measure". In: *IEEE Transactions on Haptics* 8.1, pp. 8–19. ISSN: 1939-1412. DOI: 10.1109/TOH.2014.2371025.

Thelen, D., Anderson, F., and Delp, S. L. (2003). "Generating dynamic simulations of movement using computed muscle control." In: *Journal of Biomechanics* 36.3, pp. 321–328.

Trossman, P. B. and Li, P.-W. (1989). "The effect of the duration of intertrial rest periods on isometric grip strength performance in Young Adults". In: *The Occupational Therapy Journal of Research* 9.6, pp. 362–378. DOI: 10.1177/153944928900900604.

Tsirakos, D., Baltzopoulos, V., and Bartlett, R. (1997). "Inverse optimization: functional and physiological considerations related to the force-sharing problem". In: *Critical reviews in biomedical engineering* 25.4, pp. 371–407. ISSN: 0278-940X.

Uchiyama, M. and Dauchez, P. (1988). "A symmetric hybrid position/force control scheme for the coordination of two robots". In: *IEEE International Conference on Robotics and Automation (ICRA)*, pp. 350–356. DOI: 10.1109/ROBOT.1988.12073.

Ugray, Z., Lasdon, L., Plummer, J., Glover, F., Kelly, J., and Martí, R. (2007). "Scatter Search and Local NLP Solvers: A Multistart Framework for Global Optimization". In: *Informs Journal on Computing* 19.3. DOI: 10.1287/ijoc.1060.0175.

Wan, W., Igawa, H., Harada, K., Onda, H., Nagata, K., and Yamanobe, N. (2018). "A Regrasp Planning Component for Object Reorientation". In: *Autonomous Robots*.

5.3 Appendix

5.3.1 Potential Application Towards Rehabilitation Assistive Technologies

In addition to this study's discussion and future directions, a new interesting application scenario has been envisioned. A new project aims to create an intelligent robotic physiotherapist assistant that focuses on efficacy and safety for individuals in stroke patient rehabilitation, particularly for impaired upper limbs. Making use of our optimisation algorithm, the robot is informed about the patient through MAPs, biomechanics, and our metric of task efficacy, which may also be used to evaluate task performance. This approach allows for person-tailored therapy plans to maximise individual recovery.

This new project's objectives are supported by four main components: Objective 1 involves data collection from healthy and non-healthy individuals during prescribed arm motions to develop a biomechanical model; Objective 2 is the development of a robot system to assist patients in performing therapeutic motions with varying stiffness, based on targeted muscles/pathways' accuracy and activation. The robot corrects deviations and gradually reduces assistance to promote patient involvement; Objective 3 focuses on optimising the path itself for each patient using trajectory optimisation methods, comparing data from healthy subjects to effectively activate the target muscles/pathways on the non-healthy individuals; Lastly, Objective 4 entails testing both robotic systems on healthy and stroke patients in collaboration with therapists to evaluate their effectiveness.

This comprehensive approach to intelligent robot-assisted physiotherapy has the potential to significantly improve stroke patient rehabilitation by providing high-intensity, personalised, and safe assistance in relearning motor skills and restoring functional abilities in the impaired upper limb.

5.4 Short Summary

Results from the study demonstrate the intended optimisation in the efficacy of each task for the subject. Even when comparing results from the User-Defined and the Comfort conditions, the efficacy levels are highest with the algorithm's predictions. This establishes a new metric to evaluate a task's efficacy, in comparative studies.

In some cases though, there is an overlap on the performance of the subject in both Comfort

and User-Defined conditions, suggesting that, for these subjects, their self-assessed efficacy configuration is already maximised. As well, for the case of the cutting task, one subject presented more "efficacious" results in the supposedly least efficacious configuration. This highlights that not every individual will have the same response to a certain configuration. Tailoring these estimations further, with individual MAPs, and taking into consideration the subject's self-assessment and background is of utmost importance. Future iterations of this work will require an improved understanding over these outlier cases, and what distinguishes these individuals from a broader, shared population response in terms of MAPs and efficacy.

With the combination of all 3 variables discussed in Chapter 1, this last study explored all the different relationships between physiology and biomechanics we defined. Using these relationships a new metric for efficacy was established. The results highlight the subject variability and the value in application of different tools to investigate human motor control. To further expand this work, addition of the previously presented neural pathways analysis (see Chapter 3) can clarify the impact of the different conditions with the recruitment strategies from the CNS.

Chapter 6

General Discussions

6.1 Identifying MAPs in ADLs

Following the principles presented in Chapter 1 and the methodology in Chapter 2, a series of muscle activity patterns were identified in the tasks presented in Articles 3, 4 and 5. Investigated as the mean of RMS values per muscle, MAPs were computed in each experiment, and exhibit a repertoire of different patterns depending on the experiment, motor task and subject.

Unlike typical constrained motor control studies, where subjects are conditioned to perform a motor task in a specific repeatable manner, we here explored less constrained ADLs. We argue that to better understand the hierarchy and modularity of our CNS in terms of volitional motor control, we need to understand the nuances and sources of variability in individual motor control systems. Extreme care should be taken though in isolating this variability, accounting for any external sources outside of the physiology that may be contributing to the individual variability of a subject in terms of MAPs.

To ensure the collection of meaningful data in ADLs, MAPs should be extracted synchronously with the biomechanical features of the subject and task, providing validation mechanisms for any possible recorded variability. With a focus on ADLs and the importance of investigating human motor control in natural scenarios, a push towards wearable technologies is discussed in Article 4. Ideally, data collection technologies and sensors should ensure a minimal distraction source to the subject, to ensure a completely unbiased recording. Considerations on sensor location, weight and impact on mobility are key elements to investigate prior to any study.

While biomechanics technologies already provide exciting solutions for ADLs recordings (please refer to Prasanth et al. 2021), the sEMG acquisition systems are still limited in recording ADLs, in terms of sensor battery duration, interference and portability. In Articles 4 and 5 especially, we highlight the important links of the kinematic and force recordings with the sEMG data.

Exploring MAPs in ADLs scenarios does not replace in any way the crucial work done in appropriately controlled motor experiments in clinical or lab settings. Although, controlling a subject to conduct a task in a fixed manner may condition their muscle recruitment strategies and, consequently, the identified MAPs. We argue in our presented articles that observing only the shared features in motor control mechanisms, across a population in constrained experiments, does not provide the individual dynamics and adaptability of our motor control system. The key to progress further in understanding volitional human motor control and the modular subsystems integrated within is to link MAPs collected in naturalistic environments with those collected in higher controlled experiments.

6.1.1 Significant inter-subject variability

Discussed in the articles that comprise this project we often reiterate the versatility and variability of the human control mechanisms. This variability endows the subjects with characteristic individual manners to conduct the explored motor tasks. Article 3 presents the MAPs and force profiles during a static motor task, and highlight this inter-subject variability. Distinct MAPs were identified among subjects, even when following the same guidelines to complete the task. Some subjects present higher shoulder muscles activity, while others present higher elbow muscles activity.

A bias towards a certain muscle group may be indicative of an estimated optimal response of the motor control system to solve the task at hand, based on previous experience on similar tasks. Subjects were formally enquired about their sports practices and activity levels. Interestingly, subjects who mentioned to be active swimmers demonstrated a higher muscle activity levels in shoulder muscles, while subjects that were used to weightlifting and maintained gym habits presented a higher muscle activity levels in elbow muscles. This bias towards a certain group of muscles demonstrates the importance of the subjects' previous experience with similar motor tasks, suggesting that background has an equally relevant effect on the recruitment strategy for the MAPs and associated biomechanics.

Noticeable differences are also found in the force profiles of each of the subjects. Three distinct groups were found, based on response time to reach the maximum force level and the fluctuations of force at the start of the static contractions. These witnessed behaviours are comparable to a PID (Proportional, Integrative, Derivative) Controller (see Ogata et al. 2010 for further details), often used in robotics to control actuators. These behaviours can be described as:

- Underdamped: the subject's force level overshoots their mean force level at the start of the trial, creating a ripple effect on the force profile until stabilising as the trial progresses.
- Overdamped: the subject's force level slowly but progressively increases throughout the trial, until reaching a maximum force.
- Critically damped: the subject's force level rises and stabilises right at the start of the trial and maintains little variation until the trial is completed.

These terms refer to typical engineering controllers, where an output, in this case the force level, is maximised to match a desired level, while ensuring a certain temporal response and the system's stability. This variability in the different force profiles, considering the type of response to a desired stimulus or action, may be indicative of a possible motor control mechanism scheme employed by the individual.

Interestingly, within the same subject, trial results in terms of MAPs are fairly similar. In a few cases, labelled initially as missed trials due to abnormally low produced forces, the MAPs present similarity, but divided by an amplitude factor, suggesting lower contraction levels but with the same muscle pattern. Per trial, further temporal segmentation was conducted, defining 3 equally timed windows: early, mid and late. The MAPs of each of the temporal segments were computed and little variation was found between early, mid and late stages of a trial. There is a small discrepancy of few percentile points found in a few muscles, but in the remainder muscle activity levels present little to no alteration within the trial. While MAPs remain fairly constant, the force profile does not, presenting over 10% fluctuation within a trial.

Inter-subject variability is further explored in the higher complexity dynamic motor tasks of Article 5. In this experiment, higher biomechanical variability was expected beforehand, as no restrictions were imposed on the subjects regarding the planes of motion to conduct the task. Instead, three different conditions were used to guide the subjects initially towards a certain biomechanical configuration of their posture and upper-limb. First, the mechanical variability

is witnessed easily through the limb trajectories that subjects take when completing a trial. Every successful trial is unique in terms of limb trajectory, for any of the subjects. Similarly, for the generated forces, even per condition, there is noticeable shifts in the force levels used to complete the task.

Considering the initial diagram presented in Figure 2.4, and building upon the dynamic scenarios we have explored, it becomes evident that defining the relationships between variable kinematics, MAPs, and force profiles is exponentially complex. When considering even a simple reach-and-grasp motion, limb trajectories and respective kinematics (limb segment velocities, joint angles, etc.) will present a near infinite number of solutions for MAPs to "solve" this determined task. This problem is further expanded when considering motor tasks with limb trajectories involving a high number of joints, where the coordinated variation between individual joints may not be identifiable when looking at too short or too long temporal windows of muscle activity.

Both the kinematic configurations and force variability can be easily explained through the redundancy argument: for a similar motor task, in this case focusing on the trials of the puncturing task, the subjects employed significantly varied limb configurations to solve the task. Each subject's posture, the angles of the shoulder, elbow, and wrist joints, and especially the way they would grip the tool had a clear effect on the identified MAPs.

Traditional methods of MAPs analysis, which do not account for these individual variations in forces, torques, joint angles, and limb dynamics, may lead to biased or insufficient conclusions. Using the traditional dimensionality reduction tools, finding a common shared drive across the small experiment population would disregard these varied limb configuration differences and provide inconclusive or incomplete MAPs.

To advance our understanding of this variability and relationship, it is essential to combine in-vivo and in-silico assessments. For example, we can expand further on our work in Chapter 5 with the findings of York et al. 2022; Osborne et al. 2021; De Kamps et al. 2008. By integrating new findings in MAPs with models of motor control structures and their organisation, as well as existing biomechanical models, we can further expand our understanding of coordinated muscle recruitment.

Furthermore, interesting new developments in parallel factorisation (e.g., Scano et al. 2022) allow for dimensionality reduction informed by simultaneous synchronised variables, ensuring

MAPs are extracted directly with correlated kinematics. This interdisciplinary approach will enable us to gain deeper insights into human movement, optimise the design of interventions, and ultimately enhance our comprehension of biomechanics and motor control.

In our study of Article 5, we are able to explore this variability, at an individual level instead of the whole population, by segmenting the motor tasks in windows of relevant activity per trial and subject. Using key motor event detection through biomechanics, discussed further, we are able to segment the motor task and isolate a window to extract MAPs using simpler algorithms, while still encompassing the individual variability information.

6.1.2 sEMG spectral features for neural pathway discrimination

An important discussion we present in Article 3 is the possibility to infer on neural pathway activity, by analysing non-invasive physiological recordings. Corticomuscular coherence, observed in EEG-EMG coherence studies (e.g., Liu et al. 2019; Dideriksen et al. 2018) demonstrate possible bands at which neural signals operate. In (Conway et al. 1995), evidence suggests that the corticospinal tract operates within the frequency band of 15 to 35 Hz (beta band). In more recent studies, Richards 2018 and Oya et al. 2020 explored further possible links between descending pathways and the extracted frequency bands of sEMG signals. These studies, using stimulation at cortical and spinal levels, conducted static and cyclical motor tasks in mammals: human subjects in Richards 2018 and monkeys in Oya et al. 2020. Operation of the reticulospinal tract at a low-gamma (35-60 Hz) band is suggested. Results from Richards 2018 further indicate the possibility that local spinal interactions may operate at high-gamma (60 - 100 Hz).

In Article 3 we have investigated, through spectral analysis, possible evidence to corroborate the estimated links between frequency bands and the different pathways involved in motor control. We have explored, through power spectrum analysis and filtering, at different stages of the motor task, what changes occurred in the estimated activity levels of each corticospinal, reticulospinal and spinal loops. Although promising, we believe that this analysis requires further evidence to support this characterisation of bands to different pathways.

Nevertheless, the preliminary results demonstrate an interesting frequency oscillating behaviour per predicted pathway, even when MAPs show little variation in the static motor task of Article 3. A constant adaptation of the neural signal, in each of the classified bands, is witnessed

throughout the trial and subjects. Force was witnessed to vary within a trial, which prompts the question that there is a possible link between the force levels, in the investigated static tasks, with specific neural pathways, even when MAPs are constant within the task duration. This may indicate a neural reinforcement mechanism at play, to ensure that the force levels are maintained in the isometric contraction, and indicate a constantly updating, adaptive recruitment loop. Further studies, based on our findings and the work of Richards 2018 and Oya et al. 2020 should clarify the mechanisms at play and the interactions between the different active pathways and the motor task variables. Through the integration of these findings with the neuronal population models presented in De Kamps et al. 2008 and Osborne et al. 2021, we may be able to model the impact of the pathways on physiology and biomechanics of the subject, and assess possible implications if the pathways are disturbed, as in stroke or spinal cord injury scenarios.

6.2 MAPs and Biomechanics in Motor Control

6.2.1 Kinematics or Force for motor event detection

Investigating muscle activity alone is often not sufficient to identify relevant event windows of a motor task. Using, for example, the sEMG signal's energy levels (e.g., Tabie and Kirchner 2013) or sample entropy (e.g., Zhang and Zhou 2012), allows for the detection of the onset and offset of a muscle's activity, but not the sequence of motor actions involved within a task. In the case of fixed, non-fatiguing cyclical tasks, where repeats of muscle activity are expected, some studies had success in identifying the associated MAPs, using classifiers and machine learning. Nevertheless, when conducting more complex and non-cyclical movements, while recording from several muscles at the same time, these methods are compromised and an accurate window of relevant activity over the different muscles is hard to estimate through EMG alone.

When investigating motor tasks, besides recording the muscles with sEMG, we here highlight the importance of having additional recorded variables related to the task being conducted, as kinematics or force. In Article 4, we discuss in detail the use of accelerometry, as a kinematic variable, to detect gait events and segment the sEMG activity into the different gait cycles. Regardless of possible unexpected changes in the sEMG activity, or even the change of gait modality, having characteristic and easily identifiable acceleration events allows for a more robust and accurate windowing mechanism to detect relevant muscle activity. This is demonstrated in our protocol (Article 4), where the same gait event detection algorithm, using

acceleration as a basis, works with different subjects and each of the walking modalities: ramp up/down, staircase up/down and level ground walking. With adjustments slight adjustments to the modality characteristics (e.g., expected cadence), accuracy of our algorithm is further improved, without the need to retrain the detection tool per subject. As each subject presents different MAPs across their gait cycle, the use of sEMG to segment the relevant activity would entail an individual calibration and setup to each individual for the accurate extraction of the the gait cycle MAPs.

In Article 3, another interesting case for motor event detection is presented with the static task. Due to the unconstrained nature of this task, subjects required to produce as much force as possible against a pulley system, in the defined configuration described in the article. Priming is a known mechanism that the CNS employs, prior to recruiting muscles to conduct a task (Kayser 2003; Stoykov and Madhavan 2015). In order words, before the muscle fibres are recruited, the CNS makes sure that the fibres are at a state to be recruited and ready to fire. This potentially generates vestigial sEMG activity, interfering with the clear detection of the onset of the muscle activity. In addition, even in a static task, there is a lag between the start of the contraction and the effective start of the relevant portion of the task. This is clear in the case of Article 3, where subjects would lift the pulley into the desired kinematic configuration of their upper limb and then start the static portion on the task.

The subject force profiles presented in Article 3 present a loading and unloading phase, before and after the respective static hold task being executed. In this case, as the temporal duration of these loading and unloading segments would vary greatly, between trials and subjects, attempting to segment sEMG activity into the static hold via sEMG onset estimation would not be viable. Instead, by analysing the force profiles, two key events were detected, at the start and end of the static portion of the task. These detected force timepoints are what allowed for an accurate and relevant window of sEMG activity to be isolated in each trial. Similarly, for the case of Article 5, a window of relevant activity to validate the efficacy prediction algorithm was generated around the timepoint of maximal generated force, relating to the puncturing moment of the motor task. By segmenting the sEMG activity within this window, including a temporal safety margin, we were able to identify the MAPs witnessed in the results.

Recording the activity of a muscle alone, or a small group of muscles, is insufficient to understand the recruitment strategy and motor task characteristics. In motor recruitment studies, involving

sEMG, we here reiterate the importance of multiple muscle recordings and further task variables, synchronously recorded, not only to simplify the windowing and analysis of the MAPs, but to ensure accuracy and relevance of the physiological data being collected.

6.2.2 Linking MAPs, Force and Kinematics: creating a biomarker

The efficacy of a task can be improved by evaluating its mechanical requirements and the impact on the subject's biomechanics and muscle recruitment. In Article 5 we take into account the relationship between the biomechanical constraints of the human and the robot, the forces generated by the human on workspace, and the physiological variables recorded as EMG signals. Through the kinematics and kinetics estimation of the human subject, and a prediction of muscle activity levels, the robot computes an ideal configuration to position the workspace for the human to interact with. However, relying solely on predictions to minimise muscular effort and force based on biomechanical and physical properties of the human system is not sufficient to make a task more efficacious for the individual. The subject's self-perception of efficacy may not always equate to the most efficacious way of doing the task, especially when individual variability is taken into consideration. This assessment of efficacy is witnessed especially in the analysed motor task of cutting in Article 5, where subjects were inquired about their task preferences. Conditions that forced some subjects into individually awkward body configurations were found to be the most efficacious, and perceived as such, for others.

The individual preferences, physical condition, sports activity, and familiarity with the task all impact the subject's biomechanics and the extracted MAPs. Only by acknowledging these requirements and linking these to the efficacy optimisation algorithm we were able to define a biomarker for efficacy. The relationship between a subject's overall muscle activity, with the generated forces and their own assessment of the task allowed for the definition of our measure of efficacy: the least amount of muscle activity and force required to successfully complete a motor task. Promising results are demonstrated for all subjects of the drilling task in Article 5. But interestingly, even with the considerations mentioned, the efficacy optimisation algorithm performed awkwardly for the assessment of the cutting task. Not all subject's performance under the "Comfort" condition in the cutting task was identified as efficacious, where some subjects' "Random" and "User-Defined" conditions rendered more efficacious results according to our measurement scheme. To improve upon this, factors can be considered and integrated into the optimisation algorithm, along with an initial calibration, that take into account the

subject's preferences and performance.

In addition to the measure of efficacy, an interesting finding was the overlap of the "Comfort" and "User-Defined" conditions, suggesting a potential task familiarity mechanism at play as well. If a subject is familiar with a motor task, variability in both biomechanics and MAPs may be reduced, has the human motor control architecture have attained an optimal solution for the completion of the task. Increasing the number of subjects to verify this, under the same experimental conditions, may render interesting results on the effects of learning on efficacy and the perception of it.

The creation and use of biomarkers is common in motor control studies. Athlete performance assessments, work-environment ergonomics and the investigation of fatigue through RMS and frequency analysis of EMG signals are but a few of the employed solutions. Nevertheless, when considering any biomarker solution or system to aid an individual to complete a task, it is imperative to not only compute the mechanical or physiological estimates, but to enquire the individual on their own mechanisms to achieve the task.

6.3 Summary of study outcomes

Our discussed research explores muscle activity patterns (MAPs) in less constrained activities of daily living (ADLs) to better understand the hierarchy and modularity of the human central nervous system in terms of volitional motor control. The identified MAPs exhibit a repertoire of different patterns depending on the experiment, motor task, and subject. To collect meaningful data in ADLs, MAPs should be extracted synchronously with the biomechanical features of the subject and task. Wearable technologies are discussed as promising solutions for the recording of MAPs in ADLs, but considerations on sensor location, weight, and impact on mobility are essential. We argue that exploring MAPs in ADLs scenarios complements but does not replace the crucial work done in appropriately controlled motor experiments in clinical or lab settings. The key to further understanding volitional human motor control and modular subsystems is to link MAPs collected in naturalistic environments with those collected in higher controlled experiments.

The variability of human control mechanisms is a crucial factor in individual differences in conducting motor tasks. Our articles shed light on the complexity of these mechanisms, highlighting

the importance of considering multiple variables in physiological data collection to improve accuracy and relevance. The studies presented explored different types of motor tasks and analysed the variability of muscle activation patterns, force profiles, limb trajectories and force levels among subjects. Moreover, the possibility of inferring neural pathway activity through non-invasive physiological recordings was discussed, highlighting the potential for future research to improve our understanding of the interactions between different active pathways and motor task variables. Overall, the integration of these findings with neuronal population models may help model the impact of pathways on the physiology and biomechanics of subjects and assess possible implications if the pathways are disturbed. These studies contribute to our understanding of the complexity of human control mechanisms and the importance of considering multiple variables in physiological data collection to improve accuracy and relevance.

We discuss as well the limitations of using muscle activity alone to characterise motor tasks, especially in complex movements. The importance of task-related variables, such as kinematics or force, is highlighted. Biomechanics and generated forces are discussed as useful variables for detecting key motor events and segmenting sEMG activity. The importance of recording multiple muscles and task variables simultaneously is reiterated to ensure accurate and relevant physiological data collection. The synchronised and correlated analysis of MAPs, kinematics and force allows for the design of biologically informed mechanisms to improve motor task assessments, diagnose neurological disorders and classify motor tasks more accurately.

Chapter 7

General Conclusions

7.1 Concluding Remarks and Applications

As demonstrated in our studies, variable synchronisation not only is beneficial to better correlate physiology to anatomical features, but critical if we want to understand how movement is encoded and how muscles are coordinated at different stages of a task. When analysed in isolation, either MAPs or biomechanics may be misrepresented due to insufficient information on how the task was completed.

To ensure we have the right tools to link then MAPs with biomechanics, we have presented in our report the modularity features of the CNS. Care should be taken though on how MAPs are extracted or how synergies are identified. Currently used methods for MAPs identification may condition data depending on the employed dimensionality reduction algorithms, as these often are not designed with physiology in mind. There is a clear risk that typical dimensionality reduction methods are neglecting potential critical individual variability and adaptability information of each subject, as they are only applied and valid if looking at a population. Combination of the population shared motor control features and the individualised MAPs of a subject should provide clearer understanding on how a task is being coordinated and executed. We have adapted simpler tools then to identify patterns in muscle activity, without losing the unique variability of the subject, and taking into consideration human physiology and biomechanics alike. These solutions are easier as well to adapt to current diagnostic tools, offering lower processing requirements and, consequently, faster outputs.

Studying MAPs and biomechanics in unconstrained settings is also beneficial to best explore the motor control mechanisms of an individual. Subjecting a person to conduct a motor task in a limited or constrained configuration will bias their muscle recruitment strategies. With slight adjustments in posture, or the manner to approach the task, characteristic of the individual, results demonstrate that inter-subject MAPs variability is extremely low, within and between trials. This suggests that even if no supervision or tight control is given to the subject, there are identifiable natural MAPs and biomechanical configurations that are repeatable and unique to the subject.

Among subjects, some MAPs similarities are found as well, but not enough to establish a genuine comprehensive mean of a fully generic control pattern. Nevertheless, there is an observable clustering in different subjects' MAPs, which may be based on the person's background, manner to conduct the task and timing. This clustering or characterisation towards a certain bias, be it a group of muscles or a certain profile in terms of biomechanics or force, is already valuable towards a first level diagnosis of motor control mechanisms. Creation of a repertoire of possible MAPs for specific ADLs, collected from healthy individuals, will further explore these clustering effects and may serve as a benchmark to diagnose unhealthy MAPs. In addition, using spectral analysis, we can now estimate changes in neural drive, while a subject conducts ADLs. This possibility to investigate the activity of neural pathways, in a non-invasive manner, gives us a new tool to look at the impact on movement when structures of the CNS are disrupted. Previously, this was only possible using invasive methods, and in heavily controlled and confined scenarios.

With current events in regards of world health (Covid-19 pandemic), an exponential advancement in wearable technologies over the past decades, and an increasing number of mobility impaired patients, interest is shifting towards a tele-health environment. To monitor a patient's performance in their daily-lives, and more easily generate data to diagnose and assess their condition, is of high value for clinician's and therapists. Personalising rehabilitation strategies, and providing more reliable, natural information, of a patient's performance through ADLs, may drastically increase the effectiveness of therapies and reduce the time needed for improvements to be met. Care nevertheless should be taken in a number of factors: data protection, technology misuse and data validity should all be well considered and strategies should be devised to tackle these issues.

Rehabilitation has long been driven by different scientific fields, mixing knowledge from biology and engineering. Integrating our findings of MAPs in ADLs in neuro-rehabilitation scenarios will allow for more individuality tailored therapies, potentially improving the outcome and reducing time of recovery. Application of identified MAPs simplifies the integration of physiology data into computerised systems, to inform and guide external devices. Benefits in human-robot-collaborations, with lower processing constraints and faster responses, were explored here. Richer information over the motor control scheme provided by the MAPs can be integrated into robotics, providing ad-hoc adaptable rehabilitation tools that are constantly informed of a subject's muscle activity while they conduct a certain therapy. Not only does this benefit the area explored here of human-robot-interaction, but may also improve current neuro-prosthetic devices. Typical neuro-prosthetic classifiers available rely on the vestigial activity of muscles in the affected limb. These classifiers often rely on the training of the subject to perform unnatural muscle contractions to drive a prosthetic joint, e.g., flexing your Biceps Brachii and Triceps muscles will generate a open/close hand motion. Instead, increasing slightly the number of muscles recorded from, and looking at MAPs instead of the activity of 1 or 2 remaining muscles on the stump, may provide a richer signal, that can be more easily classified into joint motions, and based on a more natural activity pattern for the subject. Not only would this reduced the training times of the subject to learn how to drive the neuro-prosthetic device, adapting it to the individual's MAPs, but would ensure a more reliable and robust control signal, less prone to individual muscle noise.

7.2 Future Work

There are estimated differences in muscle recruitment strategies depending on the nature of the task. The typical analytical tools and experiments in literature mainly focus in static tasks. The complexity of dynamic tasks, with higher amounts of varying information, both in biomechanics and MAPs, complicates the analysis of the motor control mechanisms in these scenarios. To address these issues, an experiment had been designed to look at gradual muscle recruitment strategies, involving both static and dynamic sections. In this experiment, subjects would lift objects of different weights, hold them stationary for a period of time, and lower the weights back down to a platform. A sequence of "Loading", "Hold" and "Unloading" task sections was devised, where both static and dynamic contractions would be elicited. The weight of the

object would be gradually increased after a set number of trials. A set of pilots were conducted for this experiment, and initial results demonstrated an amplitude adjustment in MAPs, with increasing weights. The comparison between the static and dynamic contractions of the task was the following analysis. Unfortunately, due to the Covid-19 pandemic, not enough data was collected to complete the experiment. This would be the immediate next order of work, to better link the presented studies in this report.

For the completed experiments, it would be interesting to extend the repertoire of analysed ADLs, and increase in mass the numbers of subjects investigated. Repeating these experiments with patients presenting known neurological disorders (e.g., stroke, PD, SCI), will allow us to investigate what changes occur in the MAPs, via spectral pathways analysis, in the pathological cases, compared to the healthy scenarios.

Although the ADL scenario is proven to be extremely valuable, a strategy needs to be created to validate such data. Unconstrained movement is the goal for motor control studies, but data consistency and care for noise and unwanted variability needs to be accounted for. For this scenario, it is imperative to have the most information collected in terms of biomechanics and MAPs. Significance, robustness, reliability and validity are all features that need to be supervised when making the transition of clinic bound protocols and diagnosis to ADL assessments. Based on our presented work, it would be interesting to build a new framework for rehabilitation therapies, that would address patient individuality, while still maintaining the level of rigour of in-clinic patient data collections.

7.3 Reflective Summary

This concluding section presents a reflection of my PhD program, experiences, articles, critiques and future work. The transition from a purely engineering field into a neuroscience environment was an incredible challenge, accompanied by an equally exciting steep learning curve. My previous background before this project provided me an application driven mindset, disregarding perhaps the key component of this work: human variability. One solution definitely does not fit all when considering biological systems. The exploratory nature of neuroscience, especially in human motor control, instilled new ways of thinking about control mechanisms, and more important, how to ask and formulate the right questions to advance my knowledge of human motor control.

At the start of this program, several more experiments and applications were planned. The driving factor that brought me to the project was the integration of machine learning algorithms, to more effectively classify physiological signals directly into motor actions, enriching the dexterity of prosthetic devices. This "engineer" idea was quickly overturned by the realisation that simply applying complex computational tools and artificial intelligence does not, as a matter of fact, improve directly our understanding of the human motor control mechanism. Instead this just creates another black-box scenario that fails to address the most basic understanding of how a neural signal package travels from our motor cortex to our muscles to generate a seemingly simple hand wave. Application of high-end tools will always render exciting results: the question is, can they be interpreted and validated, are they meaningful or are they just another rabbit hole waiting to happen, leaving another unanswered question? Correlations are easily found everywhere but associated causation is seldom explored.

An unexpected challenge was presented as well in the disconnect between the fields that explore motor control. Deficiencies were found in published studies in understanding simple employed tools, without questioning validity and applicability, and even generating erroneous results. Arguments for and against tools that impose completely different interpretations, as with the case of sEMG rectification, are still poorly addressed and perhaps disregarded. One must take great care when drawing unquestioned conclusions over the use of new technologies. Both Delorme 2023 and McClelland et al. 2012a discuss this in interesting detail, for the cases of EEG methodologies and the mathematical tools and impact of rectification over power spectrum analysis. Question and critique of any methods and their application should be a basis for any researcher. Clear issues lie as well in countless different terminologies for the same concepts across disciplines and the lack of communication between experts of each area. As with MAPs and biomechanics, neuroscientists, sports scientists, clinicians and engineers in isolation won't be able to solve the mechanisms of motor control. A collaboration between fields and creation of translational methodologies and results is the necessary approach to ensure meaningful advances in our understanding of volitional human control.

Regarding my project, due to Covid-19 restrictions, several designed experiments were unfortunately cancelled due to our inability to work with human participants. We designed and piloted an experiment that explores the differences between static and dynamic motor control: "Graded recruitment of muscles with increasing loads: static to dynamic transitions". Ethics

was approved for this experiment and initial results were promising. We aimed to design a prediction tool that estimates dynamic behaviours based only on static task information. As demonstrated in our project, the relationship between muscle contraction levels and generated forces in not linear, and still poorly understood. With the graded recruitment investigation, we hoped to define this MAPs and force relationship and to explore the clear differences of force generation between isometric and eccentric/concentric contractions.

As expected, at the end of this PhD, we are happily left with more questions than those which we started with. To improve upon the spectral analysis of neural pathways, it would be exciting to compare data from healthy subjects with pathological cases, as stroke patients. The integration of spinal circuit models in our protocols would allow for the validation of the impact of these neurological disorders in our neural pathways. By analysing stroke patients sEMG data and MAPs differences, the goal would be to identify the affected pathways in a fully non-invasive manner. Another exciting application which I will follow through is the integration of MAPs as a control signal for external devices. Current prosthetic solutions still rely on an "on-off" approach, using physiological signals from 1 or 2 muscles alone to control the device. This control mechanism not only is inefficient and prone to quickly lose calibration parameters, but also not intuitive for the users as it relies on the activity of muscles disconnected from the desired motor task. Instead, adaptation of MAPs, previously identified to be associated with a desired motor task, could reduce the disconnect from the human to the prosthetic control systems. Improvements over the classification accuracy of desired tasks, prosthetic device motion repertoire and quicker responses are some of the expected outcomes in application of our tools to these prosthetic systems.

References

Alessandro, C., Delis, I., Nori, F., Panzeri, S., and Berret, B. (2013). "Muscle synergies in neuroscience and robotics: from input-space to task-space perspectives". In: *Frontiers in Computational Neuroscience* 7.April, pp. 1–16. DOI: 10.3389/fncom.2013.00043. URL: http://journal.frontiersin.org/article/10.3389/fncom.2013.00043/abstract.

Amundsen Huffmaster, S. L., Van Acker, G. M., Luchies, C. W., and Cheney, P. D. (2018). "Muscle synergies obtained from comprehensive mapping of the cortical forelimb representation using stimulus triggered averaging of EMG activity". In: *The Journal of Neuroscience* 38.41, pp. 2519–17. ISSN: 0270-6474. DOI: 10.1523/JNEUROSCI.2519-17.2018. URL: http://www.jneurosci.org/lookup/doi/10.1523/JNEUROSCI.2519-17.2018.

Antuvan, C. W., Bisio, F., Marini, F., Yen, S.-C., Cambria, E., and Masia, L. (2016). "Role of Muscle Synergies in Real-Time Classification of Upper Limb Motions using Extreme Learning Machines". In: *Journal of NeuroEngineering and Rehabilitation* 13.1, p. 76. DOI: 10.1186/s12984-016-0183-0. URL: http://jneuroengrehab.biomedcentral.com/articles/10.1186/s12984-016-0183-0.

Armstrong, D. M. (1988). "The supraspinal control of mammalian locomotion." In: *The Journal of Physiology* 405.1, pp. 1–37. DOI: 10.1113/jphysiol.1988.sp017319.

Artoni, F., Pirondini, E., Panarese, A., and Micera, S. (2016). "Exploring neuro-muscular synergies of reaching movements with unified independent component analysis". In: *Proceedings of the Annual International Conference of the IEEE Engineering in Medicine and Biology Society, EMBS* 2016-Octob, pp. 3183–3186. DOI: 10.1109/EMBC.2016.7591405.

Bernstein, N. (1966). "The co-ordination and regulation of movements". In: *The co-ordination and regulation of movements*.

Bigland-Ritchie, B. (1981). "EMG/force relations and fatigue of human voluntary contractions". In: *Exercise and Sport Sciences Reviews* 9.1. DOI: 10.1249/00003677-198101000-00002.

Bizzi, E., d'Avella, A., Saltiel, P., and Tresch, M. (2002). "Book review: Modular organization of spinal motor systems". In: *The Neuroscientist* 8.5, pp. 437–442.

Bizzi, E. and Cheung, V. C. K. (2013). "The neural origin of muscle synergies". In: *Frontiers in Computational Neuroscience* 7.April, pp. 1–6. DOI: 10.3389/fncom.2013.00051. URL: http://journal.frontiersin.org/article/10.3389/fncom.2013.00051/abstract.

Boonstra, T. W. and Breakspear, M. (2012). "Neural mechanisms of intermuscular coherence: implications for the rectification of surface electromyography". In: *Journal of neurophysiology* 107.3, pp. 796–807.

Borzelli, D., d'Avella, A., Gurgone, S., and Gastaldi, L. (2022). "Unconstrained and constrained estimation of a linear EMG-to-force mapping during isometric force generation". In: *2022 IEEE International Symposium on Medical Measurements and Applications (MeMeA)*. DOI: 10.1109/memea54994.2022.9856461.

Brantley, J. A., Luu, T. P., Nakagome, S., Zhu, F., and Contreras-Vidal, J. L. (2018). "Full body mobile brain-body imaging data during unconstrained locomotion on stairs, ramps, and level ground". In: *Scientific Data* 5.1. DOI: 10.1038/sdata.2018.133.

Briggs, A. M. and Dreinhöfer, K. E. (2017). "Rehabilitation 2030: A Call to Action Relevant to Improving Musculoskeletal Health Care Globally". In: *Journal of Orthopaedic & Sports Physical Therapy* 47.5. PMID: 28459192, pp. 297–300. DOI: 10.2519/jospt.2017.0105. eprint: https://doi.org/10.2519/jospt.2017.0105. URL: https://doi.org/10.2519/jospt.2017.0105.

Britannica, T. E. o. E. (June 2023a). *gradient*. Encyclopedia Britannica. URL: https://www.britannica.com/science/gradient-mathematics (visited on 07/12/2023).

Britannica, T. E. o. E. (June 2023b). *root-mean-square voltage*. Encyclopedia Britannica. URL: https://www.britannica.com/technology/root-mean-square-voltage (visited on 07/12/2023).

Butterworth, S. et al. (1930). "On the theory of filter amplifiers". In: *Wireless Engineer* 7.6, pp. 536–541.

Carpenter, R. and Reddi, B. (2012). *Neurophysiology: a conceptual approach*. CRC Press.

Chen, L., Figueredo, L. F., and Dogar, M. R. (2020). "Manipulation planning under changing external forces". In: *Autonomous Robots* 44.7, pp. 1249–1269.

Cheung, V. C. K., Turolla, A., Agostini, M., Silvoni, S., Bennis, C., and Kasi, P. (2012). "Muscle synergy patterns as physiological markers of motor cortical damage". In: *PNAS* 109.36, pp. 1–5. DOI: 10.1073/pnas.1212056109. arXiv: pnas.1212056109 [10.1073].

Christensen, H., Søgaard, K., Jensen, B. R., Finsen, L., and Sjøgaard, G. (1995). "Intramuscular and surface EMG power spectrum from dynamic and static contractions". In: *Journal of Electromyography and Kinesiology* 5.1, pp. 27–36. DOI: 10.1016/s1050-6411(99)80003-0.

Chvatal, S. A. and Ting, L. H. (2013). "Common muscle synergies for balance and walking". In: *Frontiers in Computational Neuroscience* 7.May, pp. 1–14. DOI: 10.3389/fncom.2013.00048. URL: http://journal.frontiersin.org/article/10.3389/fncom.2013.00048/abstract.

Clark, D. J., Ting, L. H., Zajac, F. E., Neptune, R. R., and Kautz, S. A. (2010). "Merging of healthy motor modules predicts reduced locomotor performance and muscle coordination complexity post-stroke". In: *Journal of neurophysiology* 103.2, pp. 844–857.

Conway, B., Halliday, D., Farmer, S., Shahani, U., Maas, P., Weir, A., and Rosenberg, J. (1995). "Synchronization between motor cortex and spinal motoneuronal pool during the performance of a maintained motor task in man." In: *The Journal of physiology* 489.3, pp. 917–924.

D'Avella, A. (2014). "Muscle synergies and neuromotor recovery". In.

d'Avella, A., Saltiel, P., and Bizzi, E. (2003). "Combinations of muscle synergies in the construction of a natural motor behavior". In: *Nature neuroscience* 6.3, pp. 300–308.

Davis, P. J. (1975). *Interpolation and approximation*. Courier Corporation.

De Kamps, M., Baier, V., Drever, J., Dietz, M., Mösenlechner, L., and Van Der Velde, F. (2008). "The state of MIIND". In: *Neural networks* 21.8, pp. 1164–1181.

De Luca, C. (2006). "Electromyography". In: *Encyclopedia of Medical Devices and Instrumentation*. John Wiley & Sons, Ltd. ISBN: 9780471732877. DOI: https://doi.org/10.1002/0471732877.emd097.

De Luca, G. (2003). "Fundamental concepts in EMG signal acquisition". In: *Copyright Delsys Inc.*

Dehghani, S. and Bahrami, F. (2020). "How does the CNS control arm reaching movements?: Introducing a hierarchical nonlinear predictive control organization based on the idea of muscle synergies". In: *PLOS ONE* 15.2. DOI: 10.1371/journal.pone.0228726.

Delis, I., Hilt, P. M., Pozzo, T., Panzeri, S., and Berret, B. (2018). "Deciphering the functional role of spatial and temporal muscle synergies in whole-body movements". In: *Scientific Reports* 8.1, pp. 1–17. DOI: 10.1038/s41598-018-26780-z.

Delis, I., Panzeri, S., Pozzo, T., and Berret, B. (2014). "A unifying model of concurrent spatial and temporal modularity in muscle activity". In: *Journal of neurophysiology* 111.3, pp. 675–693.

Delorme, A. (2023). "EEG is better left alone". In: *Scientific Reports* 13.1, p. 2372.

Delp, S. L., Anderson, F. C., Arnold, A. S., Loan, P., Habib, A., John, C. T., Guendelman, E., and Thelen, D. G. (2007). "OpenSim: open-source software to create and analyze dynamic simulations of movement". In: *IEEE transactions on biomedical engineering* 54.11, pp. 1940–1950.

Desrochers, E., Harnie, J., Doelman, A., Hurteau, M.-F., and Frigon, A. (2018). "Spinal control of muscle synergies for adult mammalian locomotion". In: *The Journal of Physiology* 597.819 (1), pp. 1–34. DOI: 10.1113/JP277018. URL: http://doi.wiley.com/10.1113/JP277018.

Devarajan K., C. V. (2018). "On non-negative matrix factorization algorithms for signal- dependent noise with application to electromyography data". In: *Neural Comput.* 26.6, pp. 1128–1168. DOI: 10.1162/NECO. arXiv: 1803.01446. URL: http://arxiv.org/abs/1803.01446.

Dideriksen, J. L., Negro, F., Falla, D., Kristensen, S. R., Mrachacz-Kersting, N., and Farina, D. (2018). "Coherence of the surface EMG and common synaptic input to motor neurons". In: *Frontiers in Human Neuroscience* 12, p. 207.

Disselhorst-Klug, C., Schmitz-Rode, T., and Rau, G. (2009). "Surface electromyography and Muscle Force: Limits in semg–force relationship and new approaches for applications". In: *Clinical Biomechanics* 24.3, pp. 225–235. DOI: 10.1016/j.clinbiomech.2008.08.003.

Drew, T., Kalaska, J., and Krouchev, N. (2008). "Muscle synergies during locomotion in the cat: A model for motor cortex control". In: *Journal of Physiology* 586.5, pp. 1239–1245. DOI: 10.1113/jphysiol.2007.146605.

Eberle, H., Hayashi, Y., Kurazume, R., Takei, T., and An, Q. (2021). "Modeling of hyper-adaptability: From motor coordination to rehabilitation". In: *Advanced Robotics* 35.13-14, pp. 802–817. DOI: 10.1080/01691864.2021.1943710.

Ficuciello, F., Romano, A., Lippiello, V., Villani, L., and Siciliano, B. (2014). "Human Motion Mapping to a Robot Arm with Redundancy Resolution". In: *Advances in Robot Kinematics*. Ed. by J. Lenarčič and O. Khatib. Cham: Springer International Publishing, pp. 193–201. ISBN: 978-3-319-06698-1. DOI: 10.1007/978-3-319-06698-1_21. URL: https://doi.org/10.1007/978-3-319-06698-1_21.

Fitts, R. H., McDonald, K. S., and Schluter, J. M. (1991). "The determinants of skeletal muscle force and power: their adaptability with changes in activity pattern". In: *Journal of biomechanics* 24, pp. 111–122.

Frère, J. (2017). "Spectral properties of multiple myoelectric signals: New insights into the neural origin of muscle synergies". In: *Neuroscience* 355, pp. 22–35. DOI: 10.1016/j.neuroscience.2017.04.039.

Garcia-Aguilar, F., Caballero, C., Sabido, R., and Moreno, F. J. (2022). "The use of non-linear tools to analyze the variability of force production as an index of fatigue: A systematic review". In: *Frontiers in Physiology* 13, p. 1074652.

Gentner, R. and Classen, J. (2006). "Modular Organization of Finger Movements by the Human Central Nervous System". In: *Neuron* 52.4, pp. 731–742. DOI: 10.1016/j.neuron.2006.09.038.

Georgopoulos, A., Kalaska, J., and Caminiti, R. (1985). "Relations between two-dimensional arm movements and single-cell discharge in motor cortex and area 5: movement direction versus movement end point". In: *Experimental brain research*, pp. 175–183.

Georgopoulos, A. P., Schwartz, A. B., and Kettner, R. E. (1986). "Neuronal population coding of movement direction". In: *Science* 233.4771, pp. 1416–1419.

Gizzi, L., Nielsen, J. F., Felici, F., Ivanenko, Y. P., and Farina, D. (2011). "Impulses of activation but not motor modules are preserved in the locomotion of subacute stroke patients". In: *Journal of Neurophysiology* 106.1, pp. 202–210. DOI: 10.1152/jn.00727.2010. URL: http://jn.physiology.org/cgi/doi/10.1152/jn.00727.2010.

Hermens, H. J., Freriks, B., Merletti, R., Stegeman, D., Blok, J., Rau, G., Disselhorst-Klug, C., and Hägg, G. (1999). *Standards for suface electromyography: The European project Surface EMG for non-invasive assessment of muscles (SENIAM)*. oessingh Research and Development.

Hesam-Shariati, N., Trinh, T., Thompson-Butel, A. G., Shiner, C. T., and McNulty, P. A. (2017). "A longitudinal electromyography study of complex movements in poststroke therapy. 2: Changes in coordinated muscle activation". In: *Frontiers in Neurology* 8.JUL. DOI: 10.3389/fneur.2017.00277.

Hirano, K., Nishimura, S., and Mitra, S. (1974). "Design of Digital Notch Filters". In: *IEEE Transactions on Communications* 22.7, pp. 964–970. DOI: 10.1109/TCOM.1974.1092311.

Houk, J. C. (1989). "Cooperative control of limb movements by the motor cortex, brainstem and cerebellum". In: *Models of brain function*, pp. 309–325.

Houk, J. C. and Wise, S. P. (1995). "Feature article: Distributed modular architectures linking basal ganglia, cerebellum, and cerebral cortex: Their role in planning and controlling action". In: *Cerebral Cortex* 5.2, pp. 95–110. DOI: 10.1093/cercor/5.2.95.

Hu, G., Yang, W., Chen, X., Qi, W., Li, X., Du, Y., and Xie, P. (2018). "Estimation of Time-Varying Coherence Amongst Synergistic Muscles During Wrist Movements". In: *Frontiers in Neuroscience* 12.August, pp. 1–12. DOI: 10.3389/fnins.2018.00537. URL: https://www.frontiersin.org/article/10.3389/fnins.2018.00537/full.

Jensen, P., Frisk, R., Spedden, M. E., Geertsen, S. S., Bouyer, L. J., Halliday, D. M., and Nielsen, J. B. (2019). "Using corticomuscular and intermuscular coherence to assess cortical contribution to ankle plantar flexor activity during gait". In: *Journal of Motor Behavior* 51.6, pp. 668–680.

Kalaska, J. F. and Crammond, D. J. (1992). "Cerebral cortical mechanisms of reaching movements". In: *Science* 255.5051, pp. 1517–1523.

Kalmar, J. M. and Cafarelli, E. (1999). "Effects of caffeine on neuromuscular function". In: *Journal of Applied Physiology* 87.2, pp. 801–808. DOI: 10.1152/jappl.1999.87.2.801.

Kargo, W. J. and Giszter, S. F. (2008). "Individual premotor drive pulses, not time-varying synergies, are the units of adjustment for limb trajectories constructed in spinal cord". In: *Journal of Neuroscience* 28.10, pp. 2409–2425.

Kayser, B. (2003). "Exercise starts and ends in the brain". In: *European journal of applied physiology* 90, pp. 411–419.

Kerkman, J. N., Daffertshofer, A., Gollo, L. L., Breakspear, M., and Boonstra, T. W. (2018). "Network structure of the human musculoskeletal system shapes neural interactions on multiple time scales". In: *Science advances* 4.6, eaat0497.

Kieliba, P., Tropea, P., Pirondini, E., Coscia, M., Micera, S., and Artoni, F. (2018). "How are Muscle Synergies Affected by Electromyography Pre-Processing?" In: *IEEE Transactions on Neural Systems and Rehabilitation Engineering* 26.4, pp. 882–893. DOI: 10.1109/TNSRE.2018.2810859.

Krishnamoorthy, V., Latash, M. L., Scholz, J. P., and Zatsiorsky, V. M. (2003). "Muscle synergies during shifts of the center of pressure by standing persons". In: *Experimental Brain Research* 152.3, pp. 281–292. DOI: 10.1007/s00221-003-1574-6.

Kuriki, H. U., Mello, E. M., De Azevedo, F. M., Takahashi, L. S. O., Alves, N., and Faria Negrão Filho, R. de (2012). *The relationship between electromyography and muscle force*. Citeseer.

Kutch, J. J. and Valero-Cuevas, F. J. (2012). "Challenges and new approaches to proving the existence of muscle synergies of neural origin". In: *PLoS Computational Biology* 8.5. DOI: 10.1371/journal.pcbi.1002434. arXiv: NIHMS150003.

Latash, M. L., Scholz, J. P., and Schöner, G. (2007). "Toward a new theory of motor synergies". In: *Motor control* 11.3, pp. 276–308.

Lee, C.-L., Lu, S.-Y., and Wu, C.-Y. (2022). "Rest period and object load effects on upper limb muscle strength recovery for manual load transfer". In: *International Journal of Industrial Ergonomics* 89, p. 103274.

Lehman, G. J. (2002). "Clinical considerations in the use of surface electromyography: Three experimental studies". In: *Journal of Manipulative and Physiological Therapeutics* 25.5, pp. 293–299. DOI: 10.1067/mmt.2002.124423.

Lemon, R. N. (2008). "Descending pathways in motor control". In: *Annual Review of Neuroscience* 31.1, pp. 195–218. DOI: 10.1146/annurev.neuro.31.060407.125547.

Liu, J., Sheng, Y., and Liu, H. (2019). "Corticomuscular coherence and its applications: A review". In: *Frontiers in human neuroscience* 13, p. 100.

Macpherson, J. M. (1988). "Strategies that simplify the control of quadrupedal stance. II. Electromyographic activity". In: *Journal of neurophysiology* 60.1, pp. 218–231.

Masuda, K., Masuda, T., Sadoyama, T., Inaki, M., and Katsuta, S. (1999). "Changes in surface EMG parameters during static and dynamic fatiguing contractions". In: *Journal of Electromyography and Kinesiology* 9.1, pp. 39–46. DOI: 10.1016/s1050-6411(98)00021-2.

MATLAB (2020). *version 9.8.0 (R2020a)*. Natick, Massachusetts, USA: The MathWorks Inc.

McClelland, V. M., Cvetkovic, Z., and Mills, K. R. (2012a). "Rectification of the EMG is an unnecessary and inappropriate step in the calculation of corticomuscular coherence". In: *Journal of neuroscience methods* 205.1, pp. 190–201.

– (2012b). "Rectification of the EMG is an unnecessary and inappropriate step in the calculation of corticomuscular coherence". In: *Journal of Neuroscience Methods* 205.1, pp. 190–201. DOI: 10.1016/j.jneumeth.2011.11.001.

Merel, J., Botvinick, M., and Wayne, G. (2019). "Hierarchical motor control in mammals and machines". In: *Nature Communications* 10.1. DOI: 10.1038/s41467-019-13239-6.

Merkle, L., Layne, C., Bloomberg, J., and Zhang, J. (1998). "Using factor analysis to identify neuromuscular synergies during treadmill walking". In: *Journal of Neuroscience Methods* 82.2, pp. 207–214. DOI: 10.1016/S0165-0270(98)00054-5. URL: http://www.sciencedirect.com/science/article/pii/S0165027098000545.

Merletti, R. and Muceli, S. (2019). "Tutorial. surface EMG detection in space and time: Best practices". In: *Journal of Electromyography and Kinesiology* 49, p. 102363. DOI: 10.1016/j.jelekin.2019.102363.

Negro, F., Keenan, K., and Farina, D. (2015). "Power spectrum of the rectified EMG: When and why is rectification beneficial for identifying neural connectivity?" In: *Journal of Neural Engineering* 12.3, p. 036008. DOI: 10.1088/1741-2560/12/3/036008.

Neto, O. P. and Christou, E. A. (2010). "Rectification of the EMG signal impairs the identification of oscillatory input to the muscle". In: *Journal of Neurophysiology* 103.2, pp. 1093–1103. DOI: 10.1152/jn.00792.2009.

Noraxon (2013). *Noraxon DTS EMG Sensor User Manual, P-5428/5468 Rev A (Dec 2013)*. Scottsdale, Arizona: Noraxon U.S.A. Inc.

Ogata, K. et al. (2010). *Modern control engineering*. Vol. 5. Prentice hall Upper Saddle River, NJ.

Oppenheim, A. V. and Schafer, R. W. (1975). *Digital Signal Processing*. Prentice Hall. ISBN: 0-13-214635-5.

Oppenheim, A. V., Schafer, R. W., and Buck, J. R. (1999). *Discrete-Time Signal Processing*. Upper Saddle River, NJ: Prentice Hall.

Organization, W. H. (2020). *Rehabilitation 2030: a call for action: 6-7 February 2017, Executive Boardroom, WHO Headquarters, meeting report*. World Health Organization, vii, 45 p.

Osborne, H., Lai, Y. M., Lepperød, M. E., Sichau, D., Deutz, L., and Kamps, M. de (2021). "MIIND : A model-agnostic simulator of neural populations". In: *Frontiers in Neuroinformatics* 15. DOI: 10.3389/fninf.2021.614881.

Oya, T., Takei, T., and Seki, K. (2020). "Distinct sensorimotor feedback loops for dynamic and static control of primate precision grip". In: *Communications Biology* 3.1, p. 156.

Phinyomark, A., Phukpattaranont, P., and Limsakul, C. (2012). "Feature reduction and selection for EMG Signal Classification". In: *Expert Systems with Applications* 39.8, pp. 7420–7431. DOI: 10.1016/j.eswa.2012.01.102.

Phinyomark, A., Quaine, F., Charbonnier, S., Serviere, C., Tarpin-Bernard, F., and Laurillau, Y. (2014). "Feature extraction of the first difference of EMG time series for EMG Pattern Recognition". In: *Computer Methods and Programs in Biomedicine* 117.2, pp. 247–256. DOI: 10.1016/j.cmpb.2014.06.013.

Phinyomark, A., Thongpanja, S., Hu, H., Phukpattaranont, P., and Limsakul, C. (2012). "The Usefulness of Mean and Median Frequencies in Electromyography Analysis". In: *Computational Intelligence in Electromyography Analysis*. Ed. by G. R. Naik. Rijeka: IntechOpen. Chap. 8. DOI: 10.5772/50639. URL: https://doi.org/10.5772/50639.

Pierrot-Deseilligny, E. and Burke, D. (2005). *The circuitry of the human spinal cord: its role in motor control and movement disorders*. Cambridge university press.

Prasanth, H., Caban, M., Keller, U., Courtine, G., Ijspeert, A., Vallery, H., and Zitzewitz, J. von (2021). "Wearable Sensor-Based Real-Time Gait Detection: A Systematic Review". en. In: *Sensors* 21.8, p. 2727. ISSN: 1424-8220. DOI: 10.3390/s21082727. URL: https://www.mdpi.com/1424-8220/21/8/2727 (visited on 04/04/2022).

Prochazka, A. (1989). "Sensorimotor gain control: a basic strategy of motor systems?" In: *Progress in neurobiology* 33.4, pp. 281–307.

Reaz, M. B. I., Hussain, M. S., and Mohd-Yasin, F. (2006). "Techniques of EMG signal analysis: detection, processing, classification and applications". In: *Biological procedures online* 8.1, pp. 11–35.

Reed, J. and Bowen, J. D. (2008). "Principles of Sports Rehabilitation". In: *The Sports Medicine Resource Manual*. Saunders/Elsevier, pp. 431–436.

Richards, T. C. (2018). "Identifying Shared Pathways Across Multiple Muscle Groups of the Human Upper Limb". URL: https://etheses.whiterose.ac.uk/24138/.

Roh, J., Rymer, W. Z., Perreault, E. J., Yoo, S. B., and Beer, R. F. (2013). "Alterations in upper limb muscle synergy structure in chronic stroke survivors". In: *Journal of Neurophysiology* 109.3, pp. 768–781. DOI: 10.1152/jn.00670.2012. URL: http://jn.physiology.org/cgi/doi/10.1152/jn.00670.2012.

Sabatini, A. M. (2002). "Identification of neuromuscular synergies in natural upper-arm movements". In: *Biological Cybernetics* 86.4, pp. 253–262. DOI: 10.1007/s00422-001-0297-7.

Saltiel, P., Wyler-Duda, K., D'Avella, A., Tresch, M. C., and Bizzi, E. (2001). "Muscle Synergies Encoded Within the Spinal Cord: Evidence From Focal Intraspinal NMDA Iontophoresis in the Frog". In: *Journal of Neurophysiology* 85, pp. 605–619. DOI: 10.1152/jn.2001.85.2.605.

Santello, M., Baud-Bovy, G., and Jörntell, H. (2013). "Neural bases of hand synergies". In: *Frontiers in computational neuroscience* 7, p. 23.

Saul, K. R., Hu, X., Goehler, C. M., Vidt, M. E., Daly, M., Velisar, A., and Murray, W. M. (2014). "Benchmarking of dynamic simulation predictions in two software platforms using an upper limb musculoskeletal model". In: *Computer Methods in Biomechanics and Biomedical Engineering* 18.13, pp. 1445–1458. DOI: 10.1080/10255842.2014.916698.

Saul Holzbaur, K. R., Murray, W. M., and Delp, S. L. (2005). "A Musculoskeletal Model Of The Upper Extremity For Surgical Simulation And Neurocontrol Applications". In: *Annals of BIomedical Engineering* 6.33, pp. 829–840.

Scano, A., Mira, R. M., and d'Avella, A. (2022). "Mixed matrix factorization: A novel algorithm for the extraction of kinematic-muscular synergies". In: *Journal of Neurophysiology* 127.2, pp. 529–547.

Scott, S. H. and Kalaska, J. F. (1997). "Reaching movements with similar hand paths but different arm orientations. I. Activity of individual cells in motor cortex". In: *Journal of neurophysiology* 77.2, pp. 826–852.

Scott, S. H. (2004). "Optimal feedback control and the neural basis of volitional motor control". In: *Nature Reviews Neuroscience* 5.7, pp. 532–545. DOI: 10.1038/nrn1427.

Semprini, M., Cuppone, A. V., Delis, I., Squeri, V., Panzeri, S., and Konczak, J. (2017). "Biofeedback Signals for Robotic Rehabilitation: Assessment of Wrist Muscle Activation Patterns in Healthy Humans". In: *IEEE Transactions on Neural Systems and Rehabilitation Engineering* 25.7, pp. 883–892. DOI: 10.1109/TNSRE.2016.2636122.

Shadmehr, R. and Krakauer, J. W. (2008). "A computational neuroanatomy for Motor Control". In: *Experimental Brain Research* 185.3, pp. 359–381. DOI: 10.1007/s00221-008-1280-5.

Sherrington, C. S. (1910). "Flexion-reflex of the limb, crossed extension-reflex, and reflex stepping and standing". In: *The Journal of Physiology* 40.1-2, pp. 28–121. DOI: 10.1113/jphysiol.1910.sp001362.

Sidek, S. N. and Haja Mohideen, A. J. (2012). "Mapping of EMG signal to hand grip force at varying wrist angles". In: *2012 IEEE-EMBS Conference on Biomedical Engineering and Sciences*. DOI: 10.1109/iecbes.2012.6498069.

Sjøgaard, G., Jensen, B. R., Hargens, A. R., and Søgaard, K. (2004). "Intramuscular pressure and EMG relate during static contractions but dissociate with movement and fatigue". In: *Journal of Applied Physiology* 96.4, pp. 1522–1529. DOI: 10.1152/japplphysiol.00687.2003.

Spuler, M. and Sanz, A. S. (2016). "Extracting Muscle Synergy Patterns from EMG Data Using Autoencoders". In: *Lecture Notes in Computer Science (including subseries Lecture Notes in Artificial Intelligence and Lecture Notes in Bioinformatics)*. Vol. 9887, pp. 533–534. DOI: 10.1007/978-3-319-44781-0. arXiv: 1604.02313.

Stålberg, E., Dijk, H. van, Falck, B., Kimura, J., Neuwirth, C., Pitt, M., Podnar, S., Rubin, D. I., Rutkove, S., Sanders, D. B., and al., et (2019). "Standards for quantification of EMG and neurography". In: *Clinical Neurophysiology* 130.9, pp. 1688–1729. DOI: 10.1016/j.clinph.2019.05.008.

Stevens, J. C. and Cain, W. S. (1970). "Effort in isometric muscular contractions related to force level and duration". In: *Perception & Psychophysics* 8.4, pp. 240–244.

Stoykov, M. E. and Madhavan, S. (2015). "Motor priming in neurorehabilitation". In: *Journal of neurologic physical therapy: JNPT* 39.1, p. 33.

Tabie, M. and Kirchner, E. A. (2013). "EMG Onset Detection - Comparison of Different Methods for a Movement Prediction Task based on EMG". In: *Proceedings of the International Conference on Bio-inspired Systems and Signal Processing - Volume 1: BIOSIGNALS, (BIOSTEC 2013)*. INSTICC. SciTePress, pp. 242–247. ISBN: 978-989-8565-36-5. DOI: 10.5220/0004250102420247.

Takei, T., Confais, J., Tomatsu, S., Oya, T., and Seki, K. (2017). "Neural basis for hand muscle synergies in the primate spinal cord". In: *Proceedings of the National Academy of Sciences* 114.32, pp. 8643–8648. DOI: 10.1073/pnas.1704328114. URL: http://www.pnas.org/lookup/doi/10.1073/pnas.1704328114.

Tankisi, H., Burke, D., Cui, L., Carvalho, M. de, Kuwabara, S., Nandedkar, S. D., Rutkove, S., Stålberg, E., Putten, M. J. van, Fuglsang-Frederiksen, A., and al., et (2020). "Standards of instrumentation of EMG". In: *Clinical Neurophysiology* 131.1, pp. 243–258. DOI: 10.1016/j.clinph.2019.07.025.

Ting, L. H. and Macpherson, J. M. (2005). "A limited set of muscle synergies for force control during a postural task". In: *Journal of neurophysiology* 93.1, pp. 609–613.

Torres-Oviedo, G. (2006). "Muscle Synergy Organization Is Robust Across a Variety of Postural Perturbations". In: *Journal of Neurophysiology* 96.3, pp. 1530–1546. DOI: 10.1152/jn.00810.2005. URL: http://jn.physiology.org/cgi/doi/10.1152/jn.00810.2005.

Tresch, M. C., Cheung, V. C., and d'Avella, A. (2006). "Matrix factorization algorithms for the identification of muscle synergies: evaluation on simulated and experimental data sets". In: *Journal of neurophysiology* 95.4, pp. 2199–2212.

Tresch, M. C. and Jarc, A. (2009). "The case for and against muscle synergies". In: *Current opinion in neurobiology* 19.6, pp. 601–607.

Viitasalo, J. T. and Komi, P. V. (1981). "Effects of fatigue on isometric force-and relaxation-time characteristics in human muscle". In: *Acta Physiologica Scandinavica* 111.1, pp. 87–95.

Wærsted, M. (2000). "Human muscle activity related to non-biomechanical factors in the workplace". In: *European Journal of Applied Physiology* 83.2–3, pp. 151–158. DOI: 10.1007/s004210000273.

Woods, J. and Bigland-Ritchie, B. (1983). "Linear and non-linear surface EMG/force relationships in human muscles: an anatomical/functional argument for the existence of both". In: *American Journal of Physical Medicine & Rehabilitation* 62.6, pp. 287–299.

Yakovenko, S., Gritsenko, V., and Olesh, E. (2018). "A novel method of identifying motor primitives using wavelet decomposition". In: *Int Conf Wearable Implant Body Sens Netw.* 131.20, pp. 1796–1803. DOI: 10.1161/CIRCULATIONAHA.114.010270.Hospital. arXiv: 15334406.

Yakovenko, S., Sobinov, A., and Gritsenko, V. (2018). "Analytical CPG model driven by limb velocity input generates accurate temporal locomotor dynamics". In: *PeerJ* 6, e5849.

York, G., Osborne, H., Sriya, P., Astill, S., Kamps, M. de, and Chakrabarty, S. (2022). "The effect of limb position on a static knee extension task can be explained with a simple spinal cord circuit model". In: *Journal of Neurophysiology* 127.1, pp. 173–187.

Zhang, X. and Zhou, P. (2012). "Sample entropy analysis of surface EMG for improved muscle activity onset detection against spurious background spikes". In: *Journal of Electromyography and Kinesiology* 22.6, pp. 901–907.

Zhao, K., Wen, H., Zhang, Z., Atzori, M., Müller, H., Xie, Z., and Scano, A. (2022). "Evaluation of methods for the extraction of spatial muscle synergies". In: *Frontiers in neuroscience* 16, p. 732156.